5-2020

The Autoimmune System: The Effect of Physiological Stressors on Autoantibody Glycosylation and Fidelity of Autoantibody Profiles

Rahil Kheirkhah
Rowan University

THE AUTOIMMUNE SYSTEM:

THE EFFECT OF PHYSIOLOGICAL STRESSORS ON AUTOANTIBODY GLYCOSYLATION AND FIDELITY OF AUTOANTIBODY PROFILES

Rahil Kheirkhah, B.S.

A Dissertation submitted to the Graduate School of Biomedical Sciences, Rowan University in partial fulfillment of the requirements of the Ph.D. Degree.

Stratford, New Jersey 08084

May 2020

Table of Contents

ACKNOWLEDGEMENTS

It's hard to put into words how the last three years have helped me grow into the person that I am today, but I know that this has been one of the best experiences of my life. When I was working as a teaching assistant in college, my professor said, "Getting a Ph.D. is like contributing your piece to the fountain of knowledge." I understand that better now, and can only hope that my humble contribution stands the test of time; but getting a Ph.D. for me has been so much more than that and for that, I have the people below to thank.

Firstly, I'd like to thank my thesis advisor, Dr. Nagele. Being your student has been a great privilege. Over the last three years, I have watched you overcome one challenge after another – always steadfast in your resolve that if we are just creative enough, we can get through anything. There are many things I've learned from you, but perhaps the most important is to try and find a career that I'm as passionate about as you are about yours. You have helped me find confidence in my voice, to recognize my own capacity, and to laugh a lot at the same time. It will be a lot harder to pay personal visits after every email now, but I still expect to hear back from you in 0.4 seconds.

I would like to thank my family for their unconditional support. You have been a centering force in my life, helping me find my balance time and time again. I love you all very much and feel very lucky to have you in my corner.

To my mentors, Dr. Spur, Dr. Yin, Dr. Goldberg, and Dr. Forsberg: thank you for your time and wisdom. My thesis project would not be what it is today without the unique perspective and experience that you each contributed. My gratitude cannot extend further, but I'll still buy you lunch as a small token.

I would also like to thank my lab family has been the soul of this experience. George, thank you for always having my back and being the most reliable person I know. Hana, for being an incredible friend and seeing more in me than I do in myself at times. Mary, for all the unforgettable one-liners and for all the times you stayed at work later, just to make sure that I would be ok. Abhi, for keeping me on my toes with our everyday banter but also for helping me stay calm by just being calm yourself. Lastly, my lab partner-in-crime Cassie, you have been with me every hour of every day and you have become one of my closest friends. I thank you for being someone I could talk to about anything and for just being you. Whoever that I end up working with next will have very big shoes to fill.

Finally, I have to thank all the friends that have supported me throughout this process. My longest friend Devon, for having seen me through all of my adventures so far. Ashley, Jenna and Joe for proving that we don't always have to stay on the same

path to remain close and supportive of each other. Zahara, for giving me a reason to laugh every day. My classmates Claire, Sara, Maddy, Chris, Natasha and Rachael for all the special moments and all the meaningful chats that sum up to the days that sum up to a degree. I know that that's a lot of people to thank, but you know what they say, it takes a village to raise a scientist.

ABTRACT

The presence of thousands of autoantibodies (aABs) in the human sera is typical, and therefore it is possible to identify an aAB profile for each individual. In the first part of this thesis, we will show the cerebrospinal fluid also exhibits an extraordinarily complex immunoglobulin G aAB profile that is composed of thousands of aABs. We show that the pattern of expression of individual aABs in CSF closely mimics that in the blood, indicative of a blood-based origin for CSF aABs. In addition, using longitudinal serum samples obtained over a span of nine years, we show remarkable stability in aAB profiles over time, establishing that in the absence of stressors, individual aAB profiles show fidelity over time. We next explore the effect of one specific physiological stressor, pregnancy, on an aAB profile, using longitudinal samples taken before, during and after pregnancy. We are able to show a global reduction in aAB titers, followed by almost a full recovery, indicating that aAB profiles have a set-point that they try to re-establish. Lastly, though the presence of glycosylated antibodies in serum has already been established, there are no studies that have looked at the prevalence and distribution of glycosylated aABs. Glycosylation of antibodies infers different consequences based on the location of the glycosylation on the antibody molecule. During pregnancy, there is shift in the distribution of aAB glycosylation, from the majority of aAB initially glycosylated at 10-39% in early pregnancy to 30-69% in late pregnancy. This number then shifts dramatically post-pregnancy with the majority of aABs glycosylated at 10-19%. The increase in glycosylation during pregnancy is speculated to play an immunomodulatory role to foster immune tolerance of the fetus.

CHAPTER I

INTRODUCTION TO AUTOANTIBODIES AND ANTIBODY GLYCOSYLATION

Fundamentals of Immunology

The immune system functions as a collection of cells and chemical process that work together to protect us from foreign agents such as bacteria, fungi, parasites, viruses, cancer cells and toxins. Two main principals have governed the field of immunology since its conception. Firstly, that immune defense is mediated by specific receptors against pathogenic agents, and secondly that the immune system does not react with self-antigens, the concept of self-tolerance [1]. The immune system is divided into two lines of immunity: innate immunity and adaptive immunity [2, 3].

The innate immune system is the antigen-independent arm of the immune system and therefore provides a non-specific defense mechanism. It depends on a limited group of receptors known as pattern recognition receptors (PRRs) to recognize microbial components that are highly conserved among a large groups of pathogens. These components are known as pathogen-associated molecular patterns (PAMPs). These PAMPs are usually components that are essential for survival or virulence of a particular microbe and therefore are less prone to evolve, mutate or be modified.

Examples of PAMPs include lipopolysaccharides (LPS) which is a component of the bacterial cell wall and double-stranded ribonucleic acid (RNA) which is produced during viral infections. The innate immune system is known for the speed by which it responds. It can mount an inflammatory response within minutes after exposure to a pathogen. Lastly, the innate immune response does not remember the antigenic components it has been exposed to, and therefore subsequent exposure to the same pathogen is met with a similar response as the first. By contrast, the adaptive immune system is antigen-dependent and therefore provides a specific or more directed defense mechanism. In contrast to the limited number of pathogen receptors of the innate immune response, the adaptive immune response is able to create a randomly generated diverse repertoire of receptors that can response to specific antigenic components. The cost of this specificity is the lapse in time between pathogen exposure and full immune response. Adaptive immunity provides a key advantage that is missing from innate immunity: memory. The adaptive immune response is able to "remember" the antigens it has been exposed to, and therefore, subsequent exposure by the same antigen is met with a more rapid and rampant immune response [2, 3].

Innate Immunity – the body's fast but non-specific immune response

Innate immunity is composed of four types of defensive barriers: anatomic barriers, physiologic barriers, endocytic and phagocytic barriers, and inflammatory barriers. The anatomic barrier includes the epithelial cells lining of the skin and the mucous membranes. The skin provides a mechanical barrier that prevents entry of microbes. The mucous membranes are covered with normal flora that compete with

pathogenic microbes for attachment sites and resources. Furthermore, the mucous secreted by the cells can trap microbes and the epithelia that are lined with cilia will propel microbes out of the body. Physiologic barriers refer to body temperatures, acidic pH and chemical mediators that prevent growth of pathogens. Chemical mediators include the bacteriolytic lysozymes present in tears, saliva and other secretions, interferon molecules and components of the complement system. The importance of these anatomic and chemical barriers is observed by taking note of the severity of infections that can happen in people with primary ciliary dyskinesia or burn patients [2, 3]. Many cells can internalize (endocytosis) and then break down foreign macromolecules, and specialized cells of the immune system are able to internalize (phagocytose) and kill whole organisms. These specialized cells include monocytes, neutrophils, and tissue macrophages. The inflammatory barrier refers to leakage of inflammatory components from the blood into the interstitial space in order to eliminate a pathogen or clear necrotic debris [2, 4].

Adaptive Immunity – some good things take time

The adaptive immune system evolved to contend with the incredible amount of antigenic variability, and the ability of pathogens to mutate in order to evade detection. The adaptive immune response relies on its diverse array of receptors recognizing specific antigens. The adaptive immune system receptors are made through a long process involving somatic recombination of a large number of gene segments in order to create many receptors with unique antigen specificity. During primary exposure to a pathogen, the cells that recognize the antigenic surfaces and respond, will then persist

and create an immunologic memory. This memory allows a more rapid and rampant response upon secondary exposure to the same pathogen [4, 5].

The adaptive immune system is composed of T lymphocytes and B lymphocytes. Lymphocytes develop in primary lymphoid organs; T lymphocytes develop in the thymus while B lymphocytes develop in the bone marrow. Following their development in the thymus and bone marrow, they migrate to the secondary lymphoid organs which include lymph nodes and the spleen and serve to capture antigens that are presented to them. Lymph nodes respond to antigens returning in the lymph, while the spleen responds to antigens circulating in the blood. Once activated, lymphocytes can then travel to different sites in the body to exert their effector functions. Signals from T-cells induce the development of plasma cells from B-cells. Plasma cells are the cells that produce circulating antibodies [5].

Antibodies, also known as immunoglobulins, are a class of proteins that defend our body against pathogens. When antibodies bind to pathogenic targets, they recruit a diverse array of downstream effector cells and molecules. Some examples of downstream antibody effector functions include phagocytosis, antibody-dependent cellular toxicity (ADCC), complement-mediated lysis or just neutralization of the antigen via binding [6, 7].

Generation of antibody diversity

Two main mechanisms are responsible for generating the diverse array of antibody receptors: V(D)J recombination and somatic hypermutation. Somatic hypermutation is a process that occurs after antigenic stimulation. When an antibody recognizes an antigen, at first it may have low affinity and show reactivity with more than just that one antigen. In somatic hypermutation, point mutations are induced in the binding region, generating antibodies that have higher or lower affinity, after which antibodies with higher affinity are preferentially selected. This process occurs in the germinal centers of lymphoid tissues [8, 9].

V(D)J rearrangement occurs long before this process. The light and heavy chains of the immunoglobulin molecule are encoded by random combinatorial joining of independent variable (V), diversity (D), and joining (J) gene elements. The random assembly of these three gene segments by a process known as V(D)J recombination is one of the key steps responsible for generating diversity in antigen receptors. In the development of lymphocytes, multiple V(D)J recombination steps occur. Each V(D)J recombination step introduces breaks in the double stranded DNA and is then repaired by the non-homologous end joining repair pathway. V(D)J recombination is initiated by recombination activating gene 1 (RAG-1) and recombinant activating gene 2 (RAG-2). RAG-1 and RAG-2 are almost exclusive to lymphocytes. These two genes encode for the RAG recombinase protein complex – the protein complex responsible for binding at specific recombination signal sequences that flank the V, D, and J gene segments and cleaves the DNA [8, 9].

V(D)J rearrangement occurs in a specific sequence that follows B-cell maturation. $D_H \rightarrow J_H$ joining takes place in the early stage pro-B cell, followed by $V_H \rightarrow DJ_H$ rearrangement in the late pro-B cell. This completes V(D)J rearrangement on the heavy chain and is followed by $V_L \rightarrow J_L$ joining in the pre-B cell. Successful VDJ rearrangement leads to production of a surrogate heavy chain that binds to a light chain and form IgM on the surface of the B-cell. The expression of IgM identifies an immature B cell. Alternative splicing of the constant region leads to co-production of an IgD on the cell surface, and the new IgM+IgD+ B cells are referred to as mature B cells. These mature B cells are released into the blood and migrate to the secondary lymphoid organs [5, 8, 9].

Immunological Tolerance

The elaborate gene rearrangement that allows for the creation of receptors that recognize a broad diverse array of antigenic components are bound to produce receptors that recognize self-components as well. Multiple mechanisms have evolved to achieve a state of self-tolerance [4, 10].

Newly generated B and T cells test their receptors for recognition of self-antigens in their immediate environments. The cells that recognize self-antigens undergo a process known as "negative selection" in which the cells are either destroyed or undergo receptor editing. The process of negative selection occurs in the thymus for T cells and in the bone marrow for B cells. The cells that survive negative selection

are released into the circulation. At this point, they may encounter new self-antigens in the secondary lymphoid organs such as the lymph nodes and the spleen [4, 10].

Immunoglobulin Structural Elements

Variable and constant domains are the building blocks of immunoglobulins

Immunoglobulins, also known as antibodies, are a class of proteins that defend our body against pathogens. Immunoglobulin structure consists of two heavy (H) and two light (L) chains bound together by disulfide bonds. The light chain can be composed of either a kappa (κ) or lambda (λ) chain. The heavy and light chains are composed of both variable (V) and constant (C) domains. The light chain is composed of one variable and one constant domain. The heavy chain is composed of one variable domain and three or four constant domains. Each variable and constant domain has a molecular weight of 12,000 – 13,000 Dalton on average, and is composed of roughly 110-130 amino acids. Therefore, each light chain is approximately 25 kDa and a heavy chain with one variable region and three constant regions is approximately 55 kDa. Enzymatic digestion of immunoglobulins can break them down into distinct fragments known as Fab (Fragment, antigen binding) and Fc (Fragment, crystalizable). The Fab fragment includes the complete light chain and the variable and first constant domain of the heavy chain. The Fc fragment is composed of the constant domains that represent a portion of the two heavy chains [8]. The Fab fragment, containing the variable region, is responsible for antigen binding, while the Fc tail is responsible for activating downstream effector functions [11, 12].

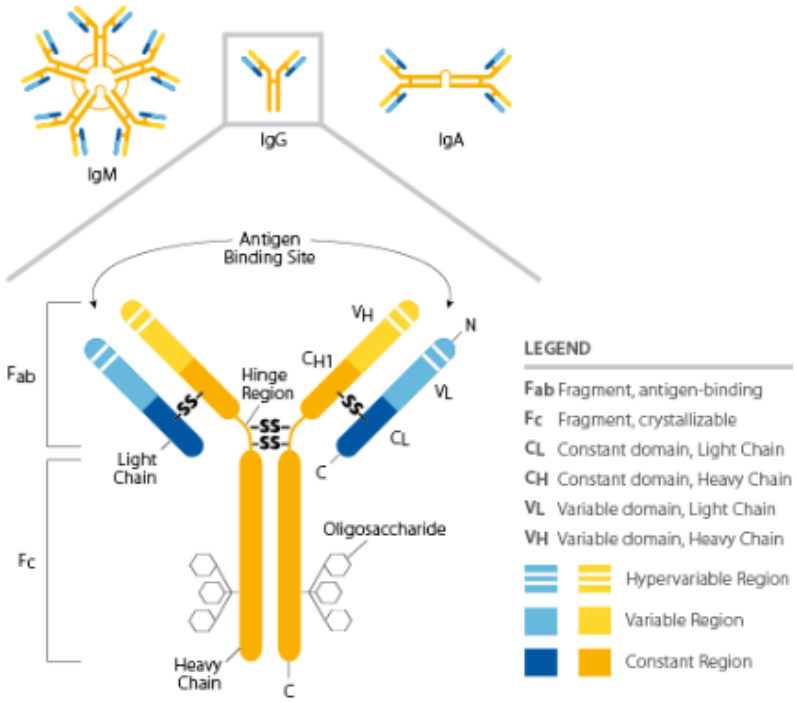

"Immunoglobulin Structure and Classes." Immunoglobulin Structure and Classes, ThermoFisher Scientific, https://www.thermofisher.com/us/en/home/life-science/antibodies/antibodies-learning-center/antibodies-resource-library/antibody-methods/immunoglobulin-structure-classes.html.

Immunoglobulin subclasses have different effector functions

The constant domain of immunoglobulins defines their effector functions. Antigenic stimulation and cytokine regulation allow variable domains to undergo class-switching and associate with different immunoglobulin isotypes. There are five major subclasses/isotypes of immunoglobulins: IgG (includes IgG1, IgG2, IgG3, and IgG4), IgM, IgD, IgA and IgE. The different isotypes are defined by the H chain constant domains as CH1-CH2-CH3 (IgG, IgA, IgD) and an additional CH4 domain for IgM and IgE [8].

IgM is the first isotype that is expressed on B cell surface. Upon antigenic stimulation, pentameric IgM is formed by individual IgMs linked together via disulfide bonds on their CH4 domain. IgM antibodies are associated with primary immune response. IgM antibodies have not undergone antigen-dependent somatic mutation. This allows them to be reactive to many different antigens (poly-reactive), allowing them to mount a low-affinity but quick response to a variety of antigens. They are also sometimes referred to as natural antibodies, and therefore in addition to participating in the primary immune response, they have an additional role in immune-regulation by recognizing self-antigens [8].

IgG is the predominant isotype of immunoglobulins. The four different subclasses of IgG differ in the structural and functional variation of their constant region in the heavy chain, particularly CH1 and CH3. These differences change the affinity and flexibility and response to different antigens. For example, IgG1 and IgG3 are induced in response to protein antigens and IgG2 and IgG4 are induced in response to polysaccharide antigens. However, all four IgG subclasses can cross the placenta and transfer to the fetus, and all of them participate in the secondary immune response [8].

IgA antibodies are secreted to protect mainly the mucosal surfaces from toxins, bacteria and viruses. Their levels are high in secretions, including saliva and colostrum. IgA is present as a monomer in serum and as a dimer when bound to mucosal surfaces. IgE is mainly associated with hypersensitivity and allergic reactions, as well as

responding to parasitic infections. IgE recruits mast cells, basophils, eosinophils and Langerhans cells by binding to the FcεRI receptor expressed on the cell surfaces. By recruiting these additional immune cells, IgE is able to mount a strong immune response. The role of the surface bound and circulating IgD isotype is poorly understood [8].

Presence of abundant natural IgG autoantibodies in human sera

Autoantibodies are present and have unique polyreactive profiles

Recent studies have shown the presence of antibodies in the serum that react with cell surface and intracellular antigens, along with antibodies that react with pathogenic and environmental antigens. These antibodies have been referred to as "natural antibodies" and can be of multiple immunoglobulin subtypes: IgM, IgG and IgA. These natural antibodies, from here on referred to as autoantibodies, have been identified in biological fluids other than serum, such as saliva, cerebrospinal fluid and colostrum [1, 13]. They are also known to bind to multiple proteins from different organs. Their reactivity has been tested to proteins derived from human liver, kidney, lung, and brain lysates [14].

Not all B-cells that produce self-reactive autoantibodies are deleted via negative selection in the bone marrow. These B-cells circulate in the blood and are selected for by the auto-antigens to which they bind to [15]. Evidence shows that these natural antibodies can be mono-reactive, however, the majority of them are polyreactive [1]. Polyreactive antibodies are capable of binding different antigens. This is explained by interactions of epitopes and paratopes. A paratope is part of the antibody that is capable of recognizing an antigen. An epitope is the part of the antigen that is recognized by the immune system. It is possible for an antibody to engage all of its potential binding sites when it is interacting with an antigen, and by engaging its full binding potential, it could theoretically be incredibly specific in recognizing precise antigens. However,

in most cases, the binding between epitopes and paratopes is more promiscuous, mainly due to a paratope's ability to recognize multiple antigens by simply binding at slightly different epitopes. This brings us to the conclusion that autoantibodies are able to bind to multiple antigenic epitopes; thus each of them has a unique "polyreactivity profile" [1].

Functions of autoantibodies as a separate component of the immune system

The network of autoantibodies is maintained by weak internal and external stimuli. Once a pathogenic insult in initiated, a higher than normal external stimulus pushes the production of more specific antibodies that act to clear the pathogen, and thus we see a burst in production of pathogen-specific antibodies. These antibodies bind to the pathogenic antigens, and recruit other components of the immune system in order to clear the foreign insult. Strong internal stimuli such as inflammation and apoptosis can stimulate a similar response, this time with antibodies that are recognizing self-antigens [1]. Some examples of internal stimulation of autoantibodies is removal of apoptotic cells, tumor cells and senescent cells, regulation of B and T cells, regulation of cytokines, inflammation, [16-19]. Other studies have shown that mature autoantibodies can even penetrate into cells, play a physiological role in regulation of the immune system, have catalytic activity on certain naturally occurring peptides, or promote re-myelination [20-22].

The development of human protein microarray technology has opened a big window into appreciating the complex nature and prevalence of autoantibodies

Human protein microarray technology has allowed us to look at the complexity of autoantibody profiles in human serum. For example, the human protein microarrays manufactured by ThermoFisher (Protoarrays) contain 9,486 full-length human protein antigens. Probing these arrays with human serum means that the any of the antibodies present in the serum that can react with a self-antigen (i.e., autoantibodies) will bind to the protein targets on the array. This study was performed for the first time in 2011 using a total of 166 human serum samples collected from individuals of different ages, genders and pathological states. The data from this study was analyzed using extremely stringent criteria, namely: (1) Z factor > 0.4; (2) Relative Fluorescence Unit > 5000. None of the individuals that had been tested had less than 301 distinct serum autoantibodies, but more importantly, most of the 166 samples had thousands of autoantibodies [14].

To look at the effect of age on the average number of serum autoantibodies, the samples were stratified into three age groups: (1) <45 years, 45-65 years, and >65 years. It was found that increasing age is accompanied by an increase in the number of detectable autoantibodies. "The >65 year old group had the highest number of detectable autoantibodies (2647.8 + 1139.2, n = 15); the 45-65 years group had the next highest number of serum autoantibodies (2335.6 + 1009.5, n = 32); and the youngest age group, <45 years, had the fewest autoantibodies (1498.2 + 545.7, n = 10)." Comparing the average number of autoantibodies between the youngest age group to

the 45-65 age group and the 65>years age group was found to be statistically significantly ($p = 0.0021$, $p = 0.0028$ respectively). This indicates a linear progression in the average number of detectable serum autoantibodies with increasing age [14]. In addition to establishing the abundant and ubiquitous presence of aABs in different age groups, other studies have shown that the presence of aABs remains stable with aging in otherwise healthy individuals [1].

Examining the average number of autoantibodies based on gender also showed statistically significant ($p = 0.004$) results, with females having a greater number of autoantibodies ($2772.5 + 714.8$, $n = 18$) than males ($2039.3 + 1092.7$, $n = 39$) detected on Protoarrays. When the study compared the average number of detectable autoantibodies in each disease to the age- and gender-matched controls, it was shown that in Alzheimer's, Parkinson's and Multiple sclerosis patients all showed significant reduction in the number of detectable autoantibodies compared to the controls ($p = 6.0 \times 10\text{-}5$, $p = 0.023$, and $p = 0.044$, respectively). Breast cancer patients also showed a decrease in their detectable autoantibodies but the difference was not significant [14].

Immunoglobulin Glycosylation

Immunoglobulins can be glycosylated at both their Fab and Fc regions, however, for the purposes of this study the focus of this background will be specifically Fab glycosylation of Immunoglobulin G. In IgG, Fab glycosylation is restricted to the variable domain, and can appear in both the heavy and light chains [11, 23]. N-linked glycosylation of Fab is contingent on presence of a consensus amino acid motif. This motif is Asn-X-Ser/Thr, where X can be any amino acid except Proline, Aspartic acid or Glutamic acid [24]. The presence of this glycosylation site alone is not sufficient for addition of a glycan however. In fact, IgG glycosylation is only present on approximately 10 – 25% of IgG in healthy individuals [11, 25-27].

Glycosylation at the Fab region is usually restricted to only one of the two Fab moieties, primarily affects antibody affinity for its target(s) [11, 28]. The presence of the glycan on one of the two Fabs creates steric hindrance that interferes with the binding of the glycosylated arm to antigens, rendering glycosylated antibodies to act as univalent antibodies [23]. The steric hindrance reduces the affinity of the glycosylated arm by almost 100 fold compared to the affinity of a non-glycosylated Fab site [27, 29]. A key feature of univalent glycosylated antibodies, also known as asymmetric antibodies, is that they fail to trigger an immune response such as activating the complement system or recruiting components of higher level immune effector functions [11, 25, 30]. This is one reason why it is suspected that Fab glycosylation

plays a role in regulating immunity, depending on if the antibodies that are glycosylated are those that recognize self or non-self antigens [11].

Glycosylated and non-glycosylated antibodies are produced from the same cellular clone [25]. Many factors can affect both the degree and the structure of Fab glycosylation. The position of the glycosylation site can influence the structural composition of the glycan. For example, introduction of glycosylation sites in the same region of identical antibodies resulted in the presence of complex-type biantennary glycans at asparagine 54 and asparagine 58, but a high-mannose glycan at asparagine-60 [31]. Furthermore, hormones and cytokines also play a role in regulating glycosylation, for example, progesterone and IL-6 can increase the production of glycosylated antibodies [32-34].

Pregnancy and Fab Glycosylation

During pregnancy, the mother's immune system must undergo changes in order to foster immune tolerance of the semi-allogenic fetus. Even though the fetus itself is never in contact with the maternal circulation, the placenta is derived from fetal trophoblasts and will contain both maternal and paternal antigens. One strategy for immune tolerance is mediated through the Progesterone-Induced Blocking Factor (PIBF) protein [25, 26]. PIBF is produced by Progesterone Receptor-positive pregnancy lymphocytes and mediates the immunological effects of progesterone [[23, 25, 35]. PIBF directly blocks degranulation of Natural Killer (NK) cells, thus inhibiting NK-mediated cytotoxicity. It also alters the Th1- Th2 lymphocyte balance by

promoting production of Th2 lymphocyte-favoring cytokines. Lastly, it acts as a transcription factor to induce production of asymmetrically glycosylated antibodies [23, 36-38]. Some reports state that the percentage of Fab glycosylated, asymmetric antibodies, can go as high as 50% during pregnancy [39]. Other studies have shown that, of the IgG molecules that had bound to the placenta, 60% of them were glycosylated and 80% had anti-paternal activity. To further support the hypothesis that PIBF plays an important role in maintaining a healthy pregnancy, it has been shown that the concentration of PIBF and the percentage of asymmetric, glycosylated antibodies are lower in women who show symptoms of threatened preterm pregnancy termination, such as spontaneous abortion, preterm labor and preeclampsia than in healthy pregnant women [26, 35, 38, 40].

REFERENCES

1. Avrameas, S., et al., Naturally occurring B-cell autoreactivity: a critical overview. J Autoimmun, 2007. 29(4): p. 213-8.

2. Marshall, J.S., et al., An introduction to immunology and immunopathology. Allergy Asthma Clin Immunol, 2018. 14(Suppl 2): p. 49.

3. Turvey, S.E. and D.H. Broide, Innate immunity. J Allergy Clin Immunol, 2010. 125(2 Suppl 2): p. S24-32.

4. Chaplin, D.D., Overview of the immune response. J Allergy Clin Immunol, 2010. 125(2 Suppl 2): p. S3-23.

5. Bonilla, F.A. and H.C. Oettgen, Adaptive immunity. J Allergy Clin Immunol, 2010. 125(2 Suppl 2): p. S33-40.

6. Forthal, D.N., Functions of Antibodies. Microbiol Spectr, 2014. 2(4): p. 1-17.

7. Vidarsson, G., G. Dekkers, and T. Rispens, IgG subclasses and allotypes: from structure to effector functions. Front Immunol, 2014. 5: p. 520.

8. Schroeder, H.W., Jr. and L. Cavacini, Structure and function of immunoglobulins. J Allergy Clin Immunol, 2010. 125(2 Suppl 2): p. S41-52.

9. Schatz, D.G. and Y. Ji, Recombination centres and the orchestration of V(D)J recombination. Nat Rev Immunol, 2011. 11(4): p. 251-63.

10. Schwartz, R.H., Historical overview of immunological tolerance. Cold Spring Harb Perspect Biol, 2012. 4(4): p. a006908.

11. van de Bovenkamp, F.S., et al., The Emerging Importance of IgG Fab Glycosylation in Immunity. J Immunol, 2016. 196(4): p. 1435-41.

12. Stanfield, R.L. and I.A. Wilson, Antibody Structure. Microbiol Spectr, 2014. 2(2).

13. Kheirkhah, R., et al., The origin and nature of the complex autoantibody profile in cerebrospinal fluid. Brain, Behavior, & Immunity - Health, 2019. 2.

14. Nagele, E.P., et al., Natural IgG autoantibodies are abundant and ubiquitous in human sera, and their number is influenced by age, gender, and disease. PLoS One, 2013. 8(4): p. e60726.

15. Julien, S., et al., B cell positive selection by soluble self-antigen. J Immunol, 2002. 169(8): p. 4198-204.

16. Peng, Y., et al., The role of IgM antibodies in the recognition and clearance of apoptotic cells. Mol Immunol, 2005. 42(7): p. 781-7.

17. Hornig, R. and H.U. Lutz, Band 3 protein clustering on human erythrocytes promotes binding of naturally occurring anti-band 3 and anti-spectrin antibodies. Exp Gerontol, 2000. 35(8): p. 1025-44.

18. Baker, N. and M.R. Ehrenstein, Cutting edge: selection of B lymphocyte subsets is regulated by natural IgM. J Immunol, 2002. 169(12): p. 6686-90.

19. Grossman, Z. and W.E. Paul, Autoreactivity, dynamic tuning and selectivity. Curr Opin Immunol, 2001. 13(6): p. 687-98.

20. Ruiz-Arguelles, A., L. Rivadeneyra-Espinoza, and D. Alarcon-Segovia, Antibody penetration into living cells: pathogenic, preventive and immuno-therapeutic implications. Curr Pharm Des, 2003. 9(23): p. 1881-7.

21. Paul, S., Natural catalytic antibodies. Mol Biotechnol, 1996. 5(3): p. 197-207.

22. Hunter, S.F., D.J. Miller, and M. Rodriguez, Monoclonal remyelination-promoting natural autoantibody SCH 94.03: pharmacokinetics and in vivo targets within demyelinated spinal cord in a mouse model of multiple sclerosis. J Neurol Sci, 1997. 150(2): p. 103-13.

23. Prados, M.B., et al., Progesterone induces a switch in oligosaccharyltransferase isoform expression: consequences on IgG N-glycosylation. Immunol Lett, 2011. 137(1-2): p. 28-37.

24. Zhu, D., et al., Acquisition of potential N-glycosylation sites in the immunoglobulin variable region by somatic mutation is a distinctive feature of follicular lymphoma. Blood, 2002. 99(7): p. 2562-8.

25. Kelemen, K., et al., A progesterone-induced protein increases the synthesis of asymmetric antibodies. Cell Immunol, 1996. 167(1): p. 129-34.

26. Barrientos, G., et al., Low levels of serum asymmetric antibodies as a marker of threatened pregnancy. J Reprod Immunol, 2009. 79(2): p. 201-10.

27. Malan Borel, I., et al., Asymmetric Fab glycosylation in guinea-pig IgG1 and IgG2. Immunology, 1990. 70(3): p. 281-3.

28. Kronimus, Y., et al., IgG Fc N-glycosylation: Alterations in neurologic diseases and potential therapeutic target? J Autoimmun, 2019. 96: p. 14-23.

29. Malan Borel, I., et al., Modulation of the humoral immune response by placental secretory factors. Am J Reprod Immunol, 1996. 35(6): p. 529-33.

30. Labeta, M.O., et al., Structure of asymmetric non-precipitating antibody: presence of a carbohydrate residue in only one Fab region of the molecule. Immunology, 1986. 57(2): p. 311-7.

31. Endo, T., et al., Glycosylation of the variable region of immunoglobulin G--site specific maturation of the sugar chains. Mol Immunol, 1995. 32(13): p. 931-40.

32. Gutierrez, G., I. Malan Borel, and R.A. Margni, The placental regulatory factor involved in the asymmetric IgG antibody synthesis responds to IL-6 features. J Reprod Immunol, 2001. 49(1): p. 21-32.

33. Margni, R.A., et al., The proportion of symmetric and asymmetric IgG antibody molecules synthesized by a cellular clone (hybridoma) can be regulated by placental culture supernatants. Cell Immunol, 1992. 142(2): p. 287-95.

34. Canellada, A., et al., In vitro modulation of protective antibody responses by estrogen, progesterone and interleukin-6. Am J Reprod Immunol, 2002. 48(5): p. 334-43.

35. Szekeres-Bartho, J., The Role of Progesterone in Feto-Maternal Immunological Cross Talk. Med Princ Pract, 2018. 27(4): p. 301-307.

36. Szekeres-Bartho, J. and A.E. Schindler, Progestogens and immunology. Best Pract Res Clin Obstet Gynaecol, 2019. 60: p. 17-23.

37. Faust, Z., et al., Progesterone-induced blocking factor inhibits degranulation of natural killer cells. Am J Reprod Immunol, 1999. 42(2): p. 71-5.

38. Polgar, B., et al., Molecular cloning and immunologic characterization of a novel cDNA coding for progesterone-induced blocking factor. J Immunol, 2003. 171(11): p. 5956-63.

39. Zenclussen, A.C., et al., Asymmetric antibodies and pregnancy. Am J Reprod Immunol, 2001. 45(5): p. 289-94.

40. Polgar, B., et al., Urinary progesterone-induced blocking factor concentration is related to pregnancy outcome. Biol Reprod, 2004. 71(5): p. 1699-705.

CHAPTER II

RATIONALE

More recent research has made the presence of aABs not a question of if but rather a question of why. Having already established that thousands of aABs are present in serum, the main focus of this thesis was to expand on and establish some of the fundamental concepts regarding aABs. We first look at the presence of aABs in a different biological fluid: cerebrospinal fluid, and provide evidence for why we believe that the source of CSF aABs is blood-based.

In previous work, we proposed that every cell derived debris generation creates thousands of antigenic products that need to be cleared from our system, and that these thousands of aABs serve that role. With this in mind, we propose that people have baseline aAB profiles and that, in the absence of pathology, these baseline profiles will remain stable over time. We hypothesized that the baseline profile would be composed of two components: (1) aABs that are common to most people and (2) aABs that are specific to each individual.

Stressors can include pathological events or physiological events such as major weight loss, pregnancy, minor inflammation or external influence such as major surgery. Previous work in our lab has exploited pathology-based changes in aAB

expression to look for blood-based biomarkers to utilize in early disease detection. In this thesis, we will look at how a physiological stressor (pregnancy) can impact baseline aAB profiles, and if after the removal of the stressor, aAB profiles return to their original state.

Lastly, the presence of glycosylated antibodies has long been established, however, no studies have looked at glycosylation in autoantibodies specifically. By utilizing human protein microarrays, we will try to answer two main questions regarding aAB glycosylation: (1) do autoantibodies also get glycosylated, and (2) if they are glycosylated, are they all glycosylated to the same extent.

The field of immunology has only recently started to make room for the presence of autoantibodies as a normal state. The hope of this thesis is to establish some fundamental concepts that will lay the groundwork for further work in the field of autoantibodies.

CHAPTER III

THE ORIGIN AND NATURE OF THE COMPLEX AUTOANTIBODY PROFILE IN CEREBROSPINAL FLUID

INTRODUCTION

The immune system is the body's primary defense system against pathological invasion. More recent research has expanded this role to include maintenance of a microenvironment within the body [1-3]. Over a century ago, Ehrlich introduced the dogma of "horror autotoxicus," stating that the immune system is designed to be unable to recognize self-antigens. Burnet built upon this observation and introduced the clonal selection theory, stating that B lymphocytes that recognize self-antigens are selectively deleted during their development, implying that if such lymphocytes are present in the peripheral immune system, it would indicate the presence of pathology or other abnormal situations [4, 5].

Autoantibodies are antibodies with specificity to self-antigens. In the past, the general consensus was that the appearance of autoantibodies in the blood was a relatively rare event linked to some type of pathology, as was most clearly shown in various autoimmune diseases [6-9]. More current research, however, now challenges

the idea of central tolerance, with evidence supporting the ubiquitous presence of thousands of self-reacting autoantibodies in the blood, even in the absence of pathology [10, 11]. The idea of production of self-recognizing autoantibodies in the absence of pathology supports a homeostatic role for this part of the immune system, including the response to sterile injury, immunosurveillance of cancer, facilitating wound resolution and tissue regrowth, and cell and tissue debris clearance. The specific nature of the response to pathology has led to exploration into the potential utility of autoantibodies as biomarkers for a number of diseases [1, 12-16]. In addition, the ubiquitous presence of such complex autoantibody profiles in the blood is likely to trigger a whole new field of endeavor, with the goal of elucidating details of its role in the maintenance of body-wide homeostasis as well as in the body response to the presence of disease.

Immune privilege is an active mechanism that allows immune tolerance of certain tissues such as the brain, via the presence of a physical barrier that restricts leukocyte and often antibody access [17]. It is generally believed that the purpose of immune privilege in the central nervous system is to minimize neural damage and cell death that might otherwise be caused by such access. This is likely to be particularly true in light of the fact that the blood-borne autoantibody profile includes a large number of brain-reactive autoantibodies, some of which appear to be reactive to the surfaces of certain types of neurons [18]. There are three main barriers that separate the brain from the products of the peripheral immune system: the Blood-Brain Barrier (BBB), the Blood-CSF Barrier (BCSFB) and the arachnoid epithelium forming the middle layer of the meninges covering the brain [17, 19]. The BBB is an endothelial

barrier of microvessels located in the deep brain parenchyma, whereas the BCSFB is the epithelium lining the choroid plexus – the CSF-producing cells located within brain ventricles [17, 20]. At all three barrier sites, tight junctions limit the para-cellular permeability of constituents of plasma, such as albumin and immunoglobulin [19]. Under conditions of pathology, any and all of these barriers can be disrupted. In the case of BBB disruption, such as that which occurs in stroke, traumatic brain injury, Alzheimer's disease, among others, the binding of brain-reactive autoantibodies may contribute to escalation of local pathology, with the nature and extent of the pathology dependent on the site and extent of the BBB breach. In line with this concept, increased BBB permeability in mouse models and in diabetic and hypercholesterolemic pigs has been shown to increase the rate and extent of internalization of Abeta1-42 peptide in neurons, a key and early feature of Alzheimer's disease [21-26].

The CSF has long been known to also contain immunoglobulins, although little is known about the number and type of immunoglobulins, their origin, and whether or not autoantibodies are also present in CSF as in blood [20, 27]. In view of this, in the present study, we have used highly sensitive human protein microarrays to detect autoantibodies in CSF, to shed light on their prevalence within the population and to get a better understanding of the complexity of individual CSF autoantibody profiles and their relationship to blood autoantibody profiles within the same individual.

MATERIALS AND METHODS

Blood collection and processing:

Plasma samples studied were collected from a total of 46 STRIDE participants and one serum sample was obtained from the New Jersey Institute for Successful Aging at Rowan University as described below. All samples were collected using standard procedures and stored at −80°C until use.

CSF collection and processing:

CSF samples were collected simultaneously with blood from the 46 STRIDE participants at the procedure for routine spinal anesthesia, before the injection of the anesthetics, aliquoted and stored at −80°C.

STRIDE participants (n=46) (Table 1):

Hip fracture patients enrolled in the randomized clinical trial "A Strategy to Reduce the Incidence of Postoperative Delirium in Elderly Patients" (STRIDE) [28] were analyzed. A detailed description of the STRIDE study has been published previously [28, 29]. Briefly, inclusion criteria were age ≥65, preoperative MMSE score ≥15, and eligible for spinal anesthesia. Main exclusion criteria were preoperative delirium, stage IV congestive heart failure, or severe chronic obstructive pulmonary disease. Informed consent was obtained from patients or appropriate legal representatives for patients unable to give informed consent due to cognitive impairment. STRIDE HFR subjects were cognitively assessed [28] prior to surgery

using both a mini-mental status exam (MMSE) [30] and a modified CDR as described previously [31]. Blood was taken pre-surgically and CSF was obtained during administration of spinal anesthesia.

Longitudinal control sample (n=5) (Table 1):

Serum was obtained from a healthy individual from the New Jersey Institute for Successful Aging at Rowan University. Serum samples were taken from the same individual over the course of 9 years: 2006, 2007, 2010, 2013, and 2015.

Table 1. Patient demographics information

	STRIDE Subjects			Healthy Control
	Total (n=46)	**Non-Delirium Control (n=24)**	**Delirium Patients (n=22)**	**Longitudinal Samples (n=5)**
Age, years				
Mean(SD)	81.6(8.1)	77.1(7.5)	86.6(5.5)	n/a
Range	65 – 96	65 – 91	76 – 96	53 – 62
Sex, n(%)				
Male, n(%)	12(26)	6(25)	6(27)	1(100)
Female, n(%)	34(74)	18(75)	16(73)	n/a

Table 1: The number of individuals (n), age and gender are listed for each group, as well as the 5 longitudinal samples from a single healthy control individual.

Human protein microarrays for detection of autoantibodies (aABs)*:*

Invitrogen's ProtoArray v5.1 Human Protein Microarrays (Cat. No. PAH0525020, Invitrogen, Carlsbad, CA, USA), each containing 9,486 unique human protein antigens (www.invitrogen.com/protoarray), were used for aAB detection. All proteins were expressed as glutathione s-transferase (GST) fusion proteins in insect cells, purified under native conditions, and spotted in duplicate onto nitrocellulose-coated glass slides. Arrays were probed with serum/plasma/CSF, processed and scanned according to the manufacturer's instructions. Briefly, microarrays were blocked using Blocking Buffer (Cat. No. PA055, Invitrogen) and each was incubated with either serum/plasma diluted to 1:500 in washing buffer, or CSF diluted 1:10 in washing buffer. After washing, arrays were probed with anti-human IgG (H + L) conjugated to AlexaFluor 647 (Cat. No. A-21445, Invitrogen) diluted 1:2000 in washing buffer. Arrays were then washed, dried, and immediately scanned with a GenePix 4000B Fluorescence Scanner (Molecular Devices, Sunnyvale, CA, USA).

Fluorescence data were acquired by aligning the Genepix Array List onto the microarray using the Genepix Pro analysis software. The resulting Genepix results files were imported into Invitrogen's *Prospector* 5.2.3 microarray analysis software for analysis. The “group characterization” and “two-group comparison” features in the Immune Response Biomarker Profiling (IRBP) toolbox within *Prospector* enabled M-statistical analysis of aAB expression among plasma and CSF in the 46 STRIDE subjects. The “group characterization” feature was used to examine serum samples from the same subject. *Prospector* was used to compare blood and CSF autoantibody

profiles in all subjects. Out of 9,486 potential protein target antigens, 676 antigens with negative and/or zero aAB RFU values were excluded from analysis, resulting in a total of 8,810 usable protein targets for analysis. All data are MIAME compliant and raw data from the microarrays have been deposited in a MIAME compliant database (GEO) under accession number GSE.

CSF/plasma autoantibody index to detect increased blood-brain barrier permeability

STRIDE participants were organized into two groups: 22 subjects that experienced post-operative delirium following surgery, and 24 subjects who did not experience delirium following surgery. CSF/plasma ratios were calculated for each individual by dividing each CSF RFU value for a specific autoantibody biomarker by the plasma RFU value for the same biomarker to obtain a CSF/plasma ratio for each autoantibody biomarker on the array. All biomarker CSF/plasma ratios was averaged in order to calculate a CSF/plasma ratio for each individual. The non-delirium control group and delirium patient group CSF/plasma ratios were calculated by averaging the individual CSF/plasma ratios in that group. A two-tailed, unequal variance t-test was used to determine if the difference between the two CSF/plasma ratio means was significant.

RESULTS

Human blood and cerebrospinal fluid have complex aAB profiles that include thousands of natural IgG autoantibodies

Pre-surgical plasma and cerebrospinal fluid (CSF) were obtained simultaneously from individual elderly hip fracture repair (HFR) patients and used to probe human protein microarrays. These microarray contains 9,486 native human proteins representing roughly one-third of the total human proteome. Each protein on the array serves as a potential protein target for aABs present in plasma or CSF. Plasma was diluted 500X with buffer, whereas CSF was diluted only 10X with the same buffer to compensate for the much lower levels of IgG in CSF and to bring aAB concentrations in CSF to levels that fall within the dynamic range of sensitivity of the microarrays. This facilitated direct comparison of plasma and CSF aAB profiles obtained from the same, as well as different subjects.

The relative abundance of aABs directed against each protein target was measured using Relative Fluorescence Units (RFUs). For this calculation, aAB hits were defined by a Z-Factor $\geq$ 0.4 and a minimum signal intensity of 1500 RFU. Using this approach, autoantibodies in plasma and CSF were found to be immunoreactive to thousands of protein targets. *An Outlier* test was performed on the percent overlap data, leading to exclusion of two samples from the total. On average, there are more aABs detected in plasma (3149) than in cerebrospinal fluid (1025). Thus, aABs are

immunoreactive with a substantial fraction (33.2% for plasma and 10.8% for CSF) of the total number (9,486) of potential protein targets represented on the array (Table 2).

Essentially all aABs detected in CSF are also present in the blood

We next sought to determine if the expression patterns of aABs in CSF correlate with that in plasma in the same individual. To test this, we compared the identity of the immunoreactive protein targets in CSF and plasma to determine the degree of overlap (Table 2). On average, an exceptionally high percentage (94.5 $\pm$ 2.8%, n=44) of aABs detected in CSF were also detected in plasma This high percentage of overlap between highly expressed autoantibodies provides further evidence that the source of the vast majority of autoantibodies in CSF is likely to be plasma.

Table 2. Average number and overlap of aABs in plasma and CSF

	Number of aABs in CSF	Number of aABs in plasma	CSF to plasma overlap	CSF to plasma overlap percentage
HFR Patients (n=44)	1025 $\pm$ 346	3149 $\pm$ 1251	971 $\pm$ 347	94.52 $\pm$ 2.80

Table 2: The average number of aABs detected in the specified dilutions of CSF and plasma obtained from STRIDE hip fracture repair patients (n = 44) using human protein microarrays was determined using a Z-factor $\geq$ 0.4 and a minimum signal intensity of 1500 RFU. An outlier test was performed that resulted in the exclusion of 2 patient samples. Many more aABs were detected in plasma than in CSF and a very high percentage of aABs detected in CSF were also found in plasma.

aAB profiles in CSF mirror that in the blood within the same individual

We next used human protein microarrays to compare autoantibody profiles in plasma and CSF obtained simultaneously from individual subjects. To accomplish this, blocks of 75 potential protein targets were randomly selected, and RFU values reflecting the extent of aAB binding at each protein spot are shown in Figure 1. The left and right panels compare aAB profiles of plasma and CSF obtained from an 84 year-old female non-delirium control subject and an 84 year-old male non-delirium control subject, respectively. RFU values are considered to be proportional to the relative number of aABs from plasma or CSF that are bound to each protein spot on the array, with higher RFUs in most cases linked to higher levels of expression (or titer) of that particular aAB in the blood or CSF. Since the dilution of the plasma working solution is 50-fold higher than CSF, it is clear that the expression of aABs in blood far exceeds that in CSF. When histograms representing the RFUs from each of the 75 protein targets in plasma and CSF are aligned, the observed pattern of RFUs is closely matched. This data also suggests that neither advanced age nor gender has an influence on this relationship, since the closely similar pattern of aAB expression between plasma and CSF is demonstrated in 8 randomly selected blocks of 75 proteins (4 from a female subject, and 4 from a male subject).

Figure 1. Comparison of aAB reactivity in plasma and CSF obtained from female and male non-delirium control subjects

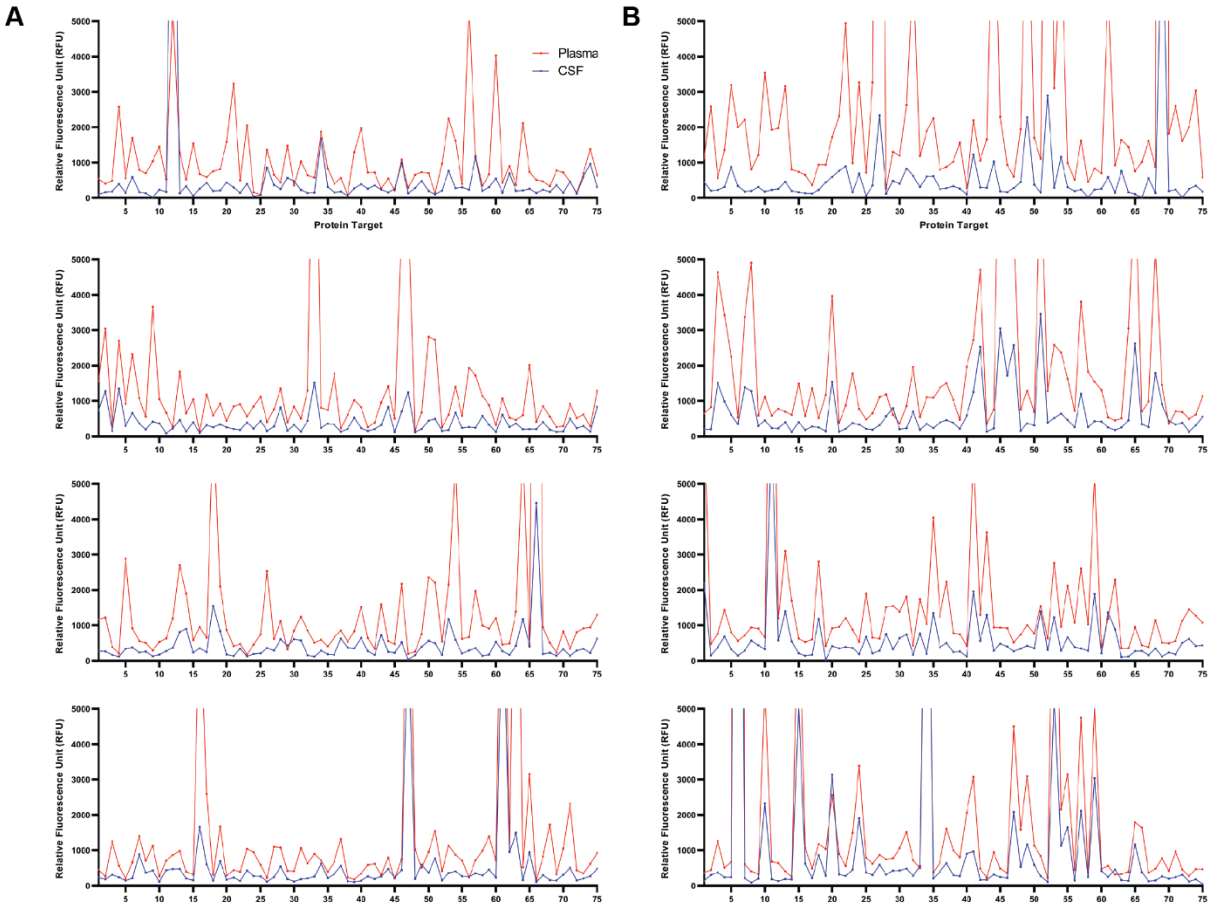

Figure 1: Blocks of 75 proteins on human protein microarrays that were probed with diluted plasma and CSF were randomly selected to generate plasma (red line) and CSF (blue line) aAB profiles derived from an 84 y/o female non-delirium control subject (A) and an 84 y/o male non-delirium control subject (B). When the histograms representing the RFUs from each of the 75 protein targets in plasma and CSF are aligned, the observed pattern of RFUs in plasma and CSF is closely matched, and neither advanced age nor gender was found to influence this relationship.

Autoantibody profiles of plasma and CSF are unique to each individual

Closer examination of aAB profiles described above suggests that each individual possesses a unique autoantibody profile. To further examine this possibility, RFUs from the same randomly selected block of 75 protein targets were plotted for each of the four subjects. In Figure 2, each of the four plots demonstrates the same closely matched autoantibody expression pattern between CSF and plasma in a single individual. However, the pattern clearly differs from person to person, with no two people sharing an identical pattern. Although individuals may share common peaks corresponding to specific protein targets, the amplitude of the RFU peaks display a wide range of variability, presumably reflecting variations in autoantibody titers between different individuals (e.g., see protein target 25).

Figure 2. Comparison of aAB reactivity in plasma and CSF among four different individuals

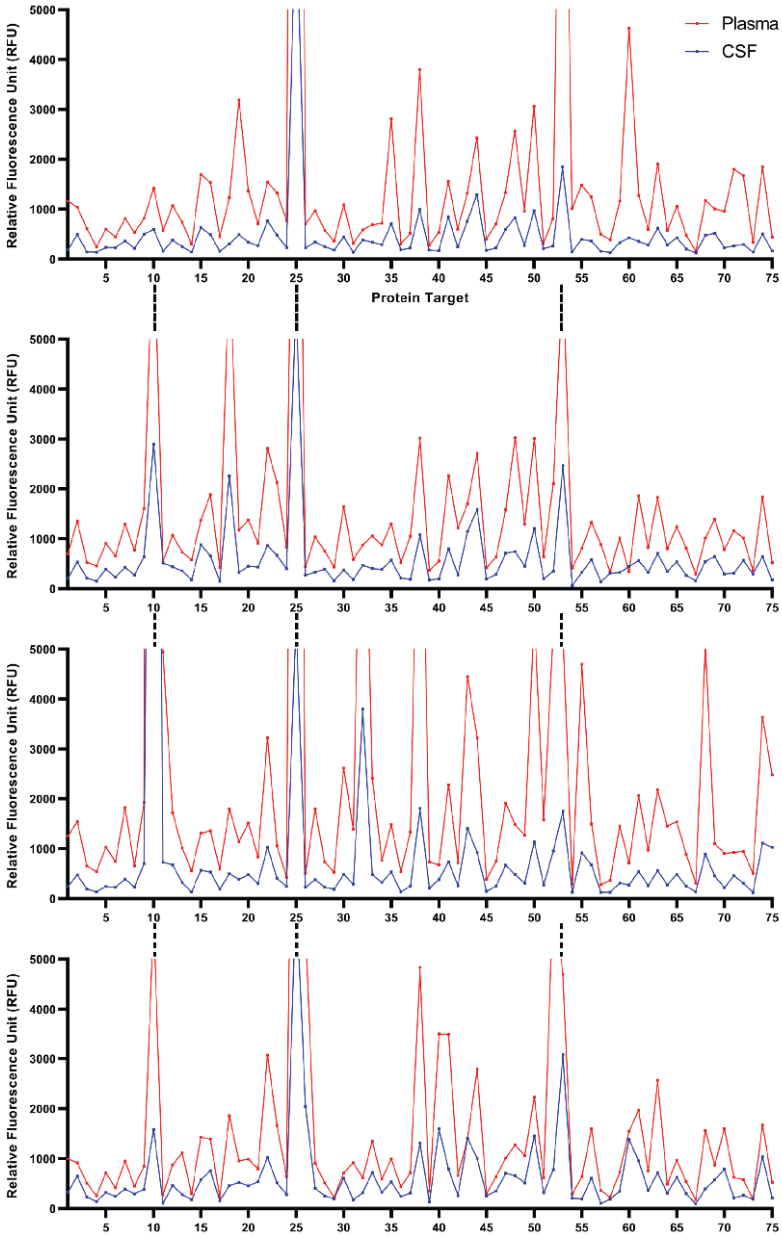

Figure 2: RFUs from an identical block of 75 randomly selected proteins were plotted for four individual subjects to demonstrate the close matching of plasma (red line) and

CSF (blue line) aAB profiles. Dashed lines indicate peaks representing aABs that are common among the four individuals.

Blood autoantibody profiles show a remarkable degree of fidelity over time

To examine how and to what extent aAB profiles vary over time, five longitudinal blood samples were obtained from a single healthy individual spanning a period of 9 years, and used to probe human protein microarrays. The autoantibody profiles for four randomly selected groups of 50 protein targets are shown in Figure 3. Remarkably, the aAB profiles essentially remained unchanged over the 9 year period, suggesting that the relative titers as reflected by the measured RFUs can remain constant in a healthy individual over time. This provides evidence that, in the absence of pathology, each individual has a unique and stable baseline autoantibody profile in the blood that demonstrates fidelity over time.

Figure 3. Fidelity of aAB profiles in a single individual over a period of 9 years

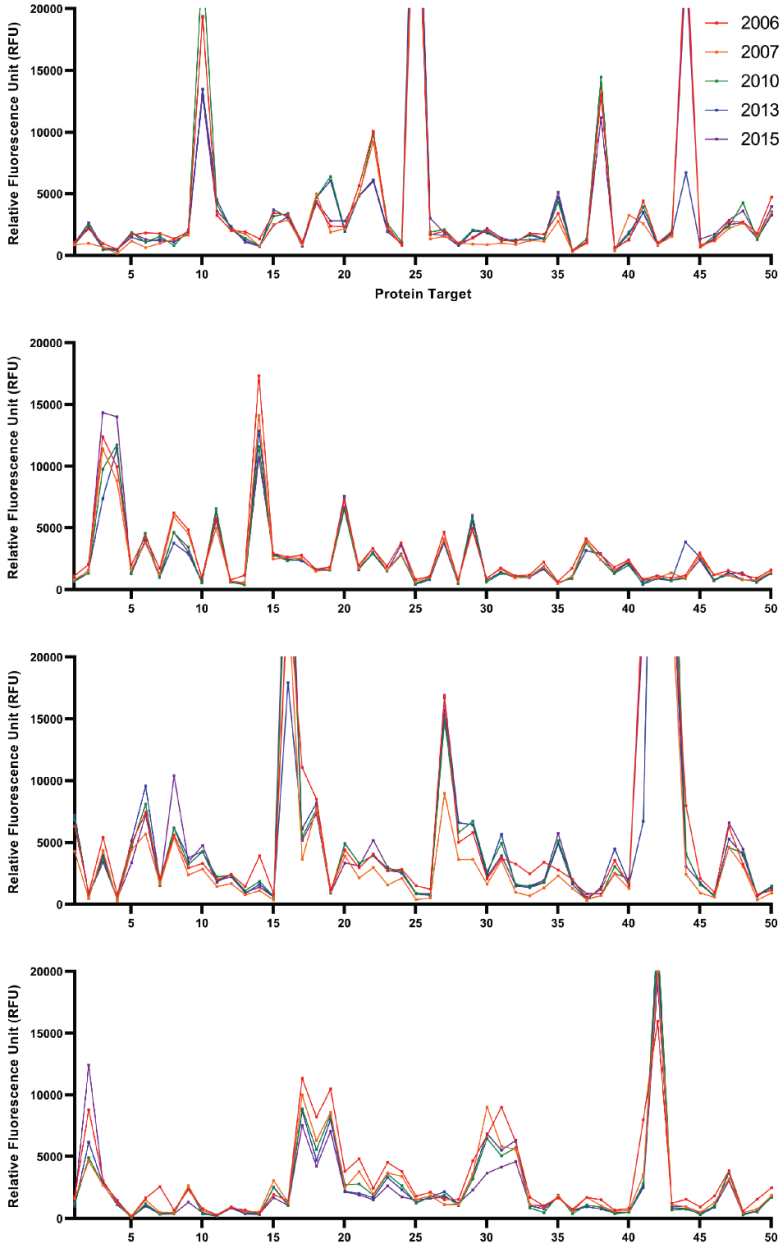

Figure 3: Four different blocks of 50 randomly selected proteins on human protein microarrays that were probed with serum from a single healthy individual spanning a period of 9 years. aAB profiles remained essentially unchanged over the 9 year period,

providing strong evidence that, in the absence of pathology, each individual has a unique and stable baseline aAB profile in the blood that demonstrates a high degree of fidelity over time.

A CSF/plasma aAB ratio suggests increased blood-brain barrier (BBB) permeability in elderly hip fracture repair patients experiencing post-operative delirium (POD)

A number of studies in humans and animal models have suggested that increased BBB permeability may be linked to an increased risk of POD in the elderly [32]. Here, we tested this possibility using pre-surgical, simultaneously drawn plasma/CSF paired samples from the same individuals. With the RFUs for aABs binding to each protein target corresponding to the relative abundance of the aABs binding to it, we calculated the CSF/Plasma (CP) aAB Ratio for each protein on the array. As the relative titer of CSF autoantibodies increases as indicated by elevated CSF RFU values, the CP aAB ratio also increases, presumably reflecting the severity of a BBB breach. An Outlier test was performed on the CP aAB Ratio data, excluding 3 non-delirium control samples and 1 delirium patient sample from the total. As shown in Table 3, the mean CP aAB ratio for the non-delirium controls was 0.57 + 0.2, whereas that for the delirium patients was 0.96 + 0.63. Using a two-tailed, unequal variance t-test, the difference between the mean CP aAB ratio of delirium vs non-delirium subjects was shown to be significant ($p < 0.013$), thus supporting a link between increased BBB permeability, higher CSF aAB titers and risk for POD.

$$Ratio = \frac{Protein\ A\ CSF\ RFU}{Protein\ A\ Plasma\ RFU}$$

Table 3. Comparison of CSF/Plasma (CP) aAB ratios in hip fracture repair patients with and without post-operative delirium

	Non-Delirium Control Patients	Delirium Patients
N	21	21
Mean (SD)	0.57 (0.2)*	0.96 (0.63)*

Table 3: The CP ratio was calculated for delirium vs. non-delirium patient groups, with delirium patients showing higher CP ratios than non-delirium subjects (unpaired t-test, $p = 0.013$). *Significant at $p < 0.05$.

Figure 4. Comparison of CSF/Plasma (CP) aAB ratios in hip fracture repair patients with and without post-operative delirium

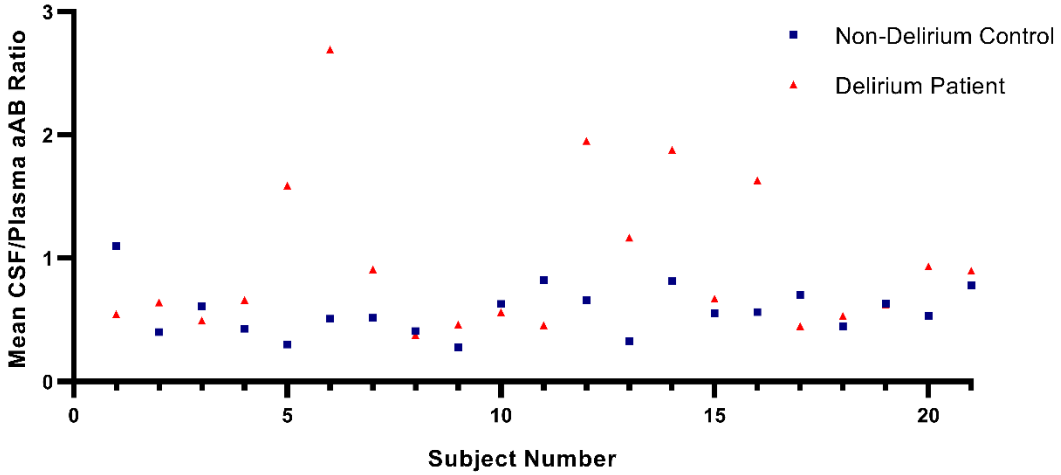

Figure 4: Comparison of individual CP aAB ratios of delirium patients (n=21, red triangle) and non-delirium controls (n=21, blue square). An outlier test was performed excluding a total of 4 patient samples. Note that the highest CP aAB ratios are among hip fracture patients who experienced post-operative delirium

DISCUSSION

In the present study, we have used human protein microarrays to determine if CSF, like blood, exhibits a similarly complex IgG aAB profile and, if so, examine its characteristics and investigate the possible origin of these aABs. The subjects for this study were elderly hip fracture repair patients, and the blood and CSF used were obtained pre-surgically and simultaneously. This study has six major findings. First, we show that CSF, like blood, has an extremely complex aAB profile composed of thousands of different aABs, although the levels of their expression in CSF are far lower than that in blood. Second, essentially all aABs detected in CSF are also present in the blood, suggesting the likely possibility that aABs in the CSF originate from blood, presumably through the blood-brain and blood-CSF barriers. Third, in strong support for a blood-based origin for CSF aABs, we found that levels of expression of individual aABs in the CSF mimic expression levels of the same aABs in the blood, regardless of age, gender or the presence or absence of disease. Fourth, aAB profiles in both blood and CSF have some features that are unique to each individual, collectively contributing to an individual's "aAB fingerprint". Fifth, we show that individual blood aAB profiles are remarkably consistent over long periods of time in overall healthy individuals, raising the possibility that each aAB has its own "set point" of constitutive expression in the absence of disease and other body stressors. Lastly, in elderly individuals undergoing hip fracture repair surgery, an elevated CSF/plasma aAB ratio, suggestive of increased blood-brain and/or blood-CSF barrier permeability,

is more common in patients that experience post-operative delirium (POD), suggesting that barrier compromise is an important risk factor for POD.

Relationship between expression of autoantibodies, autoimmune disorders and cancer

Historically, the appearance and detection of aABs in the blood has been attributed to immune dysregulation that facilitated their production [33]. The most well-known instances of this are the autoimmune diseases, hallmarked by the presence and often overexpression of specific aABs that are somehow linked to the pathology driving the phenotype. For example, Rheumatoid Arthritis (RA) is associated with Rheumatoid Factor and anti-citrullinated peptide antibodies (ACPA), Systemic Lupus Erythematosis (SLE) with abundant antinuclear aABs (ANA), and Systemic Sclerosis with antitopoisomerase 1 (anti-topo 1) and anticentromere antibody (ACA) [9, 34, 35]. The expression of these aABs is not exclusive to one disorder, and each disorder usually has more than just one aAB associated with it. The expression of such aABs has been used as biochemical confirmation of the presence of these diseases, in essence making them biomarkers for their associated disorders [33]. These aABs have not only been used to screen for pathology, but fluctuations in their titers often correlate with the course and severity of disease. An increasing number of aABs are showing promise for use as biomarkers for various cancers, including lung, colon, breast, prostate, ovarian and head and neck [36-41]. aABs are also hypothesized to be involved in

cancer immunosurveillance, responding to insults such as mutation, degradation, overexpression of proteins and misfolded proteins [33].

Blood and CSF typically contain thousands of aABs – proposed role in cell/tissue debris removal from body fluids and utility for disease diagnostics

Our previous studies using highly sensitive human protein microarrays have shown that, contrary to the well-established principle of self-tolerance, a central tenet of immunology, thousands of different aABs typically populate the blood. These aABs comprise an extremely complex profile in the blood, the nature of which is strongly influenced by age, gender and presence of disease [10, 14, 33]. Self-reactive immunoglobulins have been detected in a variety of biological fluids, including blood, colostrum, saliva and CSF [33]. In the present study, we have shown that like blood, CSF typically contains thousands of aABs. With only roughly one-third of the human proteome represented on the protein microarrays used in the present study, it is necessary to multiply the number of aABs detected on these microarrays by a factor of three to estimate the actual number of aABs present in blood and CSF. In the population of elderly hip fracture repair patients who were the subjects of this study, the mean number of aABs detected in CSF and blood using approach was 1025 and 3149, respectively, which translates to a total number of 3075 for CSF and 9447 for blood. It is also important to note that this study has focused only on the IgG subtype of immunoglobulins, and that we recognize that other immunoglobulin subtypes may also be involved, which will likely increase the total number of aABs in both CSF and

blood. Further studies will be needed to investigate potential aAB profiles involving other Ig subtypes.

We have proposed that one function of this extraordinarily complex aAB system is the maintenance of body-wide homeostasis via cell/tissue debris clearance [10, 33]. As a result of normal "wear and tear" in otherwise healthy individuals, it is expected that the body generates a certain amount of soluble debris every day that eventually makes its way into the various body fluids, especially the blood. Since this cell-derived debris would include the potential release of many thousands of different proteins, there would be a constant need for an extremely complex aAB profile to facilitate their daily removal. In the case of disease, the increased amount of debris released from the site of pathology would be expected to be at least somewhat disease-specific, since its composition would depend on the tissues/organs affected. If aAB profiles are truly involved in debris clearance and adaptive, one would expect a shift in aAB profiles reflecting the increased production of those aAB working to clear this debris. This concept has been the basis for our biomarker discovery strategy. We have already demonstrated the utility of using human protein microarrays to identify panels of aAB that are differentially expressed during disease that can be used as diagnostic indicators or biomarkers of several neurodegenerative disorders, such as Alzheimer's disease, Parkinson's disease and multiple sclerosis [12-16].

aAB profiles in CSF closely match that in blood in the same individual

We demonstrate here that essentially all aABs detected in CSF are also present in the blood (94.5 + 2.8% overlap). Furthermore, the aAB profiles of CSF, which include the expression levels of individual aABs as relative RFUs, mirror that in the blood. Together, this provides strong evidence that the source of the vast majority of aABs in CSF is the blood. There are several potential avenues of entry for aABs into CSF from the blood, the most important being through the blood-brain and blood-CSF barriers. Although we recognize blood as the main source of CSF aABs, there are also a very few aABs that appear in CSF that are not detected in blood using the cutoff of RFUs mentioned above, e.g., antibodies directed against ROBO3 and KCNAB3 proteins. The identity of these few aABs present exclusively in CSF seem to vary from one individual to the next, although it is possible that their low expression in CSF in combination with our RFU>1500 cutoff contributes to this variability. Nevertheless, their presence supports the possibility that this small subset of CSF-specific aABs may originate from an intrathecal immune system present in the brain of these individuals, which has been reported in previous studies [42-44].

Individual blood aAB profiles show both common and unique features and a remarkable degree of fidelity over time

Comparison of aAB profiles among different individuals has revealed that many aABs show common patterns of expression in blood and CSF across the

population. This was determined by comparing the aAB RFU profiles of randomly selected blocks of protein targets on the microarrays. We also found that, in addition to many aABs with common levels of expression, many aABs also show individual-specific alterations in aAB expression profiles, providing what amounts to an "aAB fingerprint" that is unique to each individual. Importantly, we also show here that, in otherwise healthy individuals, aAB profiles remain remarkably stable over long periods of time, as demonstrated in figure 3, with samples spanning nearly a decade. We hypothesize that, in the absence of pathology, significant body growth and renovation or physical decline associated with advanced age, aAB profiles of healthy individuals remain stable. We refer to this stable profile as the "baseline aAB profile" which, in the absence of stressors to the body, is maintained in each individual. This baseline aAB profile in each subject is composed of two conceptual subsets of aABs: a larger subset with levels that are comparable among multiple individuals and a much smaller subset with levels significantly higher or lower than the norm, thus making these aAB "stand out" as peculiar to this individual (i.e., contributing to an individual "autoantibody fingerprint"). Taken together, this suggests the presence of an "aAB setpoint" for each individual that is linked to the current status of the body. Deviation from this baseline or set point could be triggered by a number of events and body stressors, such as surgery, infections, menstruation, pregnancy, sudden weight loss and other short- and long-term pathologies.

Detection of increased blood-brain and blood-CSF barrier permeability in elderly hip fracture repair patients by calculating a CSF/plasma (CP) aAB ratio

We also investigated whether or not elevated risk for post-surgical delirium is associated with increased barrier permeability in elderly hip fracture repair patients from the STRIDE study. In an effort to test this, we calculated the pre-surgical CSF-Plasma (CP) Ratio for each aAB detected and then the average CP ratio representing all aABs detected for each individual, where a higher CP aAB ratio would imply an increased barrier permeability. Using this approach, the mean CP aAB ratio for patients experiencing delirium was significantly higher than that for non-delirium controls, suggesting that increased barrier permeability increases risk for POD. In previous in vitro and in vivo studies in mice, we provided evidence that, under conditions of blood-brain barrier compromise, aABs gain access to the brain interstitium and can bind to exposed cognate targets on the surfaces of neurons and glia [18, 21, 45]. Indeed, in the brains of patients with Alzheimer's disease, the same neurons showing particular vulnerability to AD pathological changes, including intraneuronal beta-amyloid deposition, are also the cells that are the most IgG-positive [21]. This raises the possibility that the chronic binding of IgG to neuronal surfaces under conditions of blood-brain barrier breach may play a key role in POD following surgery in the short-term, as well as the pathogenesis of neurodegenerative diseases, such as AD, PD, and MS, among others, in the long-term.

Strengths and weakness of the study

This study has several strengths. The first is the availability of simultaneous pre-surgical blood and CSF samples from a cohort of elderly hip fracture repair patients. This enabled us to determine that each individual possesses their own unique CSF and blood autoantibody profiles. Another is the availability of multiple longitudinal serum samples from the same healthy individual over a 9 year period, which allowed us to demonstrate the remarkable stability of aAB profiles over time. Finally, a significant strength of this study was the use of Invitrogen's Protoarray human protein microarray as a platform. Encompassing roughly one-third of the human proteome, these microarrays allowed us to survey nearly 10,000 full-length native-folded protein targets using both a high-throughput, sensitive, and unbiased protocol. This study also has several weaknesses, the most significant being the small sample size. Another limitation is the demographic homogeneity of the patient group, which limits the data to this small cohort of elderly individuals receiving hip fracture repair surgery. Although intended as a "proof of concept" study, we acknowledge the need for additional studies in larger community-based populations to further expand the scope of this work. An additional limitation of this study is the absence of matching CSF samples to accompany the longitudinal serum samples from the single healthy individual over the span of 9 years. Due to the invasive nature and risk of infection, obtaining serial lumbar punctures from this individual was not possible. As a result, although we expect to see maintenance of the same closely matching pattern of CSF

and blood aAB profiles, we have not confirmed the fidelity of CSF aABs longitudinally over this time period.

Conclusions and perspectives

We demonstrate, for the first time, evidence for the ubiquitous presence of thousands of individual aABs in human CSF, and also show that their profile closely mirrors that in the blood. Furthermore, we have found that while individuals may share common features, each person possesses their own unique CSF/blood aAB profile, akin to an "aAB fingerprint". Due to the striking similarity in pattern between the CSF and blood of every individual studied, we speculate the origin of these aABs in the CSF to be a result of blood-CSF and blood-brain barrier penetration, the latter allowing the infiltration of aABs into the brain parenchyma as a possible driver of subsequent neuropathology. However, the contribution of an intrathecal immune system in the brain cannot be ruled out, although it only accounts for a small fraction of total CSF aABs. We also demonstrated that in otherwise healthy individuals, aAB profiles remain remarkably stable over long periods of time, suggesting a production "set point" for each aAB that is linked to the "current status" of the body. Lastly, data in this study suggests that an increased CSF/plasma aAB ratio is indicative of increased blood-brain barrier (BBB) permeability in elderly hip fracture repair patients experiencing post-operative delirium (POD). Based on our previous studies, we have demonstrated that both age and the presence of disease cause specific alterations in aAB profiles that have utility in the diagnosis and staging of various neurodegenerative diseases, with the

potential for early or preclinical disease detection and disease monitoring during pharmacological treatment. Taken together, our data lead us to suggest that the observed extensive production of aABs for the purpose of soluble debris removal from the various body fluids involves a separate component of the adaptive immune system. Much additional work is needed to determine its origin, features and the detailed mechanisms associated with its function.

REFERENCES

1. Norris, G.T. and J. Kipnis, Immune cells and CNS physiology: Microglia and beyond. J Exp Med, 2019. 216(1): p. 60-70.

2. Cohen, I.R., Biomarkers, self-antigens and the immunological homunculus. J Autoimmun, 2007. 29(4): p. 246-9.

3. Avrameas, S., H. Alexopoulos, and H.M. Moutsopoulos, Natural Autoantibodies: An Undersugn Hero of the Immune System and Autoimmune Disorders-A Point of View. Front Immunol, 2018. 9: p. 1320.

4. Ehrlich, P., Croonian Lecture - On immunity with special reference to cell life. Proceedings of the Royal Society of London, 1900. 66(424-433).

5. Burnet, S.M., The clonal selection theory of acquired immunity. 1959, Cambridge, UK: University Press Cambridge.

6. Ippolito, A., et al., Autoantibodies in systemic lupus erythematosus: comparison of historical and current assessment of seropositivity. Lupus, 2011. 20(3): p. 250-5.

7. Wanleenuwat, P. and P. Iwanowski, Role of B cells and antibodies in multiple sclerosis. Mult Scler Relat Disord, 2019. 36: p. 101416.

8. Scott, D.L., F. Wolfe, and T.W. Huizinga, Rheumatoid arthritis. Lancet, 2010. 376(9746): p. 1094-108.

9. Wielosz, E., M. Dryglewska, and M. Majdan, Serological profile of patients with systemic sclerosis. Postepy Hig Med Dosw (Online), 2014. 68: p. 987-91.

10. Nagele, E.P., et al., Natural IgG autoantibodies are abundant and ubiquitous in human sera, and their number is influenced by age, gender, and disease. PLoS One, 2013. 8(4): p. e60726.

11. Avrameas, S. and T. Ternynck, Natural autoantibodies: the other side of the immune system. Res Immunol, 1995. 146(4-5): p. 235-48.

12. Nagele, E., et al., Diagnosis of Alzheimer's disease based on disease-specific autoantibody profiles in human sera. PLoS One, 2011. 6(8): p. e23112.

13. Han, M., et al., Diagnosis of Parkinson's disease based on disease-specific autoantibody profiles in human sera. PLoS One, 2012. 7(2): p. e32383.

14. DeMarshall, C.A., et al., Potential utility of autoantibodies as blood-based biomarkers for early detection and diagnosis of Parkinson's disease. Immunol Lett, 2015. 168(1): p. 80-8.

15. DeMarshall, C.A., et al., Detection of Alzheimer's disease at mild cognitive impairment and disease progression using autoantibodies as blood-based biomarkers. Alzheimers Dement (Amst), 2016. 3: p. 51-62.

16. DeMarshall, C., et al., Autoantibodies as diagnostic biomarkers for the detection and subtyping of multiple sclerosis. J Neuroimmunol, 2017. 309: p. 51-57.

17. Shechter, R., A. London, and M. Schwartz, Orchestrated leukocyte recruitment to immune-privileged sites: absolute barriers versus educational gates. Nat Rev Immunol, 2013. 13(3): p. 206-18.

18. Levin, E.C., et al., Brain-reactive autoantibodies are nearly ubiquitous in human sera and may be linked to pathology in the context of blood-brain barrier breakdown. Brain Res, 2010. 1345: p. 221-32.

19. Abbott, N.J., L.L. Mendonca, and D.E. Dolman, The blood-brain barrier in systemic lupus erythematosus. Lupus, 2003. 12(12): p. 908-15.

20. Regeniter, A., et al., A modern approach to CSF analysis: pathophysiology, clinical application, proof of concept and laboratory reporting. Clin Neurol Neurosurg, 2009. 111(4): p. 313-8.

21. Nagele, R.G., et al., Brain-reactive autoantibodies prevalent in human sera increase intraneuronal amyloid-beta(1-42) deposition. J Alzheimers Dis, 2011. 25(4): p. 605-22.

22. Gouras, G.K., et al., Intraneuronal beta-amyloid accumulation and synapse pathology in Alzheimer's disease. Acta Neuropathol, 2010. 119(5): p. 523-41.

23. LaFerla, F.M., K.N. Green, and S. Oddo, Intracellular amyloid-beta in Alzheimer's disease. Nat Rev Neurosci, 2007. 8(7): p. 499-509.

24. Bayer, T.A. and O. Wirths, Intracellular accumulation of amyloid-Beta - a predictor for synaptic dysfunction and neuron loss in Alzheimer's disease. Front Aging Neurosci, 2010. 2: p. 8.

25. Gouras, G.K., et al., Intraneuronal Abeta42 accumulation in human brain. Am J Pathol, 2000. 156(1): p. 15-20.

26. Clifford, P.M., et al., Abeta peptides can enter the brain through a defective blood-brain barrier and bind selectively to neurons. Brain Res, 2007. 1142: p. 223-36.

27. Riddoch, D. and R.A. Thompson, Immunoglobulin levels in the cerebrospinal fluid. Br Med J, 1970. 1(5693): p. 396-9.

28. Sieber, F.E., et al., Effect of Depth of Sedation in Older Patients Undergoing Hip Fracture Repair on Postoperative Delirium: The STRIDE Randomized Clinical Trial. JAMA Surg, 2018. 153(11): p. 987-995.

29. Li, T., et al., Design considerations of a randomized controlled trial of sedation level during hip fracture repair surgery: a strategy to reduce the incidence of postoperative delirium in elderly patients. Clin Trials, 2017. 14(3): p. 299-307.

30. Folstein, M.F., S.E. Folstein, and P.R. McHugh, "Mini-mental state". A practical method for grading the cognitive state of patients for the clinician. J Psychiatr Res, 1975. 12(3): p. 189-98.

31. Oh, E.S., et al., Abnormal CSF amyloid-beta42 and tau levels in hip fracture patients without dementia. PLoS One, 2018. 13(9): p. e0204695.

32. Yang, S., et al., Anesthesia and Surgery Impair Blood-Brain Barrier and Cognitive Function in Mice. Front Immunol, 2017. 8: p. 902.

33. DeMarshall, C., et al., Utility of autoantibodies as biomarkers for diagnosis and staging of neurodegenerative diseases. Int Rev Neurobiol, 2015. 122: p. 1-51.

34. Derksen, V., T.W.J. Huizinga, and D. van der Woude, The role of autoantibodies in the pathophysiology of rheumatoid arthritis. Semin Immunopathol, 2017. 39(4): p. 437-446.

35. Pisetsky, D.S., Antinuclear antibody testing - misunderstood or misbegotten? Nat Rev Rheumatol, 2017. 13(8): p. 495-502.

36. Broodman, I., et al., Serum Protein Markers for the Early Detection of Lung Cancer: A Focus on Autoantibodies. J Proteome Res, 2017. 16(1): p. 3-13.

37. Luna Coronell, J.A., et al., The Immunome of Colon Cancer: Functional In Silico Analysis of Antigenic Proteins Deduced from IgG Microarray Profiling. Genomics Proteomics Bioinformatics, 2018. 16(1): p. 73-84.

38. Qiu, J., et al., Autoantibodies as Potential Biomarkers in Breast Cancer. Biosensors (Basel), 2018. 8(3).

39. Ummanni, R., et al., Prostate cancer-associated autoantibodies in serum against tumor-associated antigens as potential new biomarkers. J Proteomics, 2015. 119: p. 218-29.

40. Chatterjee, M., et al., Diagnostic markers of ovarian cancer by high-throughput antigen cloning and detection on arrays. Cancer Res, 2006. 66(2): p. 1181-90.

41. Smith, E.M., et al., Does pretreatment seropositivity to human papillomavirus have prognostic significance for head and neck cancers? Cancer Epidemiol Biomarkers Prev, 2008. 17(8): p. 2087-96.

42. Anthony, I.C., D.H. Crawford, and J.E. Bell, B lymphocytes in the normal brain: contrasts with HIV-associated lymphoid infiltrates and lymphomas. Brain, 2003. 126(Pt 5): p. 1058-67.

43. Bouras, C., et al., Humoral immunity in brain aging and Alzheimer's disease. Brain Res Brain Res Rev, 2005. 48(3): p. 477-87.

44. Petzold, A., Intrathecal oligoclonal IgG synthesis in multiple sclerosis. J Neuroimmunol, 2013. 262(1-2): p. 1-10.

45. Acharya, N.K., et al., Diabetes and hypercholesterolemia increase blood-brain barrier permeability and brain amyloid deposition: beneficial effects of the LpPLA2 inhibitor darapladib. J Alzheimers Dis, 2013. 35(1): p. 179-98.

ATTRIBUTES

Figure 1. Human protein microarrays were processed by Cassandra DeMarshall, PhD. and Abhirup Sarkar, Ph.D. Data extraction and analysis was performed by Rahil Kheirkhah and Cassandra DeMarshall, Ph.D.

Figure 2. Human protein microarrays were processed by Cassandra DeMarshall, PhD. and Abhirup Sarkar, Ph.D. Data extraction and analysis was performed by Rahil Kheirkhah and Cassandra DeMarshall, Ph.D.

Figure 3. Human protein microarrays were processed by Cassandra DeMarshall, PhD. and Abhirup Sarkar, Ph.D. Data extraction and analysis was performed by Rahil Kheirkhah and Cassandra DeMarshall, Ph.D.

Figure 4. Human protein microarrays were processed by Cassandra DeMarshall, PhD. and Abhirup Sarkar, Ph.D. Data extraction and analysis was performed by Rahil Kheirkhah and Cassandra DeMarshall, Ph.D.

CHAPTER IV

THE EFFECT OF STRESSORS ON BASELINE AUTOANTIBODY PROFILES

INTRODUCTION

Two main principals have governed immunology since it emerged as a scientific discipline. The first is that the role of the immune system is to protect the organism from pathogenic antigens through defense mediated through recognition of specific receptors. The second was the establishment of the principle of self-tolerance, which states that antibodies produced by the adaptive immune system are selected in such a way that eliminates those that recognize self-antigens [1]. A recent deluge of studies have challenged the latter principal, creating space for a new component of the immune system composed mainly of self-reactive antibodies (autoantibodies) [1-5]. Studies have shown that autoreactive B-cells and autoantibodies are abundant and must play a role in physiological immunity. This physiologic role is thought to encompass maintenance of homeostasis, resolution of infection, immune-surveillance of cancer, assisting in wound resolution and tissue regrowth, contributing to removal of apoptotic and senescent cells, regulation of B cells, T cells and cytokine action [1, 3-5].

Studies done in the previous years by our lab were the first to show that the number of autoantibodies is in the many thousands, and that it is influenced by age, gender and the presence of disease [3, 6, 7]. Our lab has also shown that disease-specific changes in autoantibody profiles can be used to identify blood-borne autoantibody biomarkers for early disease detection [8, 9]. This method has been used to develop biomarkers for Alzheimer's disease, Parkinson's disease, Mild Cognitive Impairment, and Multiple Sclerosis [8-11]. The presence of autoantibodies is not limited to the blood; they have also been detected in other biological fluids such as colostrum, saliva and cerebrospinal fluid (CSF). Recently, we have shown that the CSF exhibits a complex IgG autoantibody profile that closely mimics that in the blood, indicating a blood-based origin for the CSF autoantibodies [1, 12].

In healthy individuals, cell and tissue debris is generated through every day "wear and tear", and we have proposed that one potential function of the autoantibody system is maintenance of body-wide homeostasis through clearance of this debris from the blood and other body fluids [12, 13]. Not surprisingly, the generation of cell-derived debris releases thousands of antigenic products, thus creating a constant need for a complex autoantibody profile to facilitate their removal. We have shown that this profile, referred to by us as the "baseline aAB profile" is not only present, but also incredibly stable over long periods of time. We further show that individual autoantibody profiles possess features that are individual-specific as well as features that are common to among different individuals [12]. In this study, we aimed to investigate the effect of "stressors" to this baseline aAB profile. Stressors can include

pathologic incidents such as disease-associated changes that lead to disease-associated shifts in autoantibody profiles; but can also include other common events such as surgeries and major weight loss or, as in the case of this study, a normal healthy physiologic event such as a pregnancy.

MATERIALS AND METHODS

Blood collection and processing:

Longitudinal Pregnant Patient Sample (n=6):

Serum samples were obtained from a healthy individual from the New Jersey Institute for Successful Aging at Rowan University. Serum samples were taken from the same individual over the course of six years: one sample in 2013, four samples in 2018, and one sample in 2019. Samples were stored at room temperature for 45 minutes (to allow for clotting), and then centrifuged at 3000 rpm for 10 minutes to separate serum from the clotted portion of blood. Serum was collected, aliquotted, and stored at -80oC.

Human protein microarrays for detection of autoantibodies (aABs):

Invitrogen's ProtoArray v5.1 Human Protein Microarrays (Cat. No. PAH0525020, Invitrogen, Carlsbad, CA, USA), each containing 9,486 unique human protein antigens (www.invitrogen.com/protoarray), were used for aAB detection. All proteins were expressed as glutathione s-transferase (GST) fusion proteins in insect cells, purified under native conditions, and spotted in duplicate onto nitrocellulose-coated glass slides. Arrays were probed with serum/plasma/CSF, processed and scanned according to the manufacturer's instructions. Briefly, microarrays were blocked using Blocking Buffer (Cat. No. PA055, Invitrogen) and each was incubated with either serum diluted 1:500 in washing buffer. After washing, arrays were probed with anti-human IgG (H + L) conjugated to AlexaFluor 647 (Cat. No. A-21445,

Invitrogen) diluted 1:2000 in washing buffer. Arrays were then washed, dried, and immediately scanned with a GenePix 4000B Fluorescence Scanner (Molecular Devices, Sunnyvale, CA, USA).

Fluorescence data were acquired by aligning the Genepix Array List onto the microarray using the Genepix Pro analysis software. The resulting Genepix results files were imported into Invitrogen's Prospector 5.2.3 microarray analysis software for analysis.

RESULTS

The number of aABs detected in maternal serum using human protein microarrays globally drops during pregnancy, but is later restored to pre-pregnancy levels

Six longitudinal serum samples obtained from a healthy woman (gravida 1, para 1) who experienced an uncomplicated pregnancy were used to probe human protein microarrays. Serum was diluted 500X with wash buffer before being used to probe the arrays. Each microarray contained 9486 native human proteins printed in duplicate, representing roughly one-third of the total human proteome. These proteins provide potential targets to which aABs can bind. The relative abundance of aABs bound to each cognate protein target is detected using fluorescent-labeled anti-human IgG antibodies and measured as Relative Fluorescence Units (RFUs). Most aABs show some degree of reactivity with almost all available protein targets, providing evidence that autoantibodies are produced against all proteins. However, in the present study, we have elected to maintain stringent criteria in our analysis where only aABs with a Z-factor $\geq$ 0.4 and a minimum RFU signal intensity of 1500 were recognized as bona fide autoantibody-antigen reactions on the microarrays. aABs that met these criteria are referred to here as "aAB hits." Using this approach, we evaluated the longitudinal effects of pregnancy on the number of aABs detected on microarrays using these criteria.

Table 1 shows the number of aABs detected in the serum approximately 5 years before the first pregnancy, throughout pregnancy, and up to 7 months post-pregnancy. The number of aAB hits detected 5 years before the pregnancy (P1) (6749) closely resembles the number of aAB hits detected 7 months after pregnancy (P6) (6549). Since it is possible to have a similar number of hits but have different aAB targets represented, we next examined how similar the identities of these aAB hits were in the two samples. Of 6549 aAB hits detected in P6 (7 months post-pregnancy), 6167 of these same aABs were also seen in P1 (5 years pre-pregnancy), indicating a 94.23% overlap in aAB profiles in pre- vs. post-pregnancy serum samples spanning a period of nearly six years. This provides additional supportive evidence that aAB profiles show an exceptional level of fidelity after experiencing a stressor, in this case pregnancy.

Examination of longitudinal serum samples at different stages of pregnancy revealed an initial reduction in the number of aAB hits during the second trimester [4590 aAB hits at 15 weeks gestation (P2) and 3226 aAB hits at 20 weeks gestation (P3)] followed by a recovery in the number of hits after the second trimester [4240 aAB hits at 28 weeks gestation (P4) and 5594 aAB hits at 37 weeks gestation (P5)]. We next looked at the identity overlap in each of the samples mentioned above taken during pregnancy with those identified five years prior to pregnancy (P1). In all four samples, we saw remarkable overlap in the identity of the aABs (Table 1), having the lowest percent overlap being 96.25% at 37 weeks gestation (P5). Of the 5594 total aAB hits in the 37 weeks gestation sample (P5), 5384 of them overlapped with sample P1 taken more than five years earlier, leaving only 210 (3.75%) new aAB hits that were not

detected in the earlier non-pregnancy sample. Likewise, in the 7 month post-pregnancy sample (P6), there were 378 (5.77%) aAB hits that were not detected in P1. We next compared the 210 new aAB hits from P5 to the 378 new aAB hits from P6 and found that 206 of them were common to both sample. To state this differently, of the 210 new aAB hits that appeared at 37 weeks gestation, 206 of them were retained at least up to 7 months post-pregnancy and were present in the P6 but not the P1 serum sample.

Table 1. Number of aAB hits in longitudinal serum samples taken from a healthy pregnant female

Healthy Pregnant Control				
Sample ID	**Date**	**Timeline**	**Number of aAB hits**	**Number of aAB hits shared with P1 (%)**
P1	8/15/2013	5 years Pre-pregnancy	6749	-
P2	3/14/2018	16 weeks	4590	4562 (99.39%)
P3	4/12/2018	20 weeks	3226	3210 (99.50%)
P4	6/7/2018	28 weeks	4240	4214 (99.39%)
P5	8/9/2018	37 weeks	5594	5384 (96.25%)
P6	3/19/2019	7 months post-pregnancy	6549	6171 (94.23%)

Table 1: The number of aAB hits detected in serum samples taken longitudinally over a period of almost 6 years. The samples include one taken before pregnancy (P1), one taken 7 months post-pregnancy (P6) and four samples taken during the course of the pregnancy (P2-P5). aAB hits were detected using human protein microarrays using a Z-factor $\geq$ 0.4 and a minimum signal intensity of 1500 RFU. The identity of each group was compared to the identity of the aAB hits in P1 and the percent identity was calculated.

Pregnancy causes an initial global reduction in the titers of individual aABs in the blood, but the overall pattern of aAB expression is well-preserved and titer almost completely restored by the end of pregnancy

We next looked at the effect of pregnancy as a stressor on the aAB profile. The pre-pregnant profile in this case was taken 5 years before this person experienced their first pregnancy. Even though multiple pre-pregnant longitudinal samples were not available from this individual, we previously showed great fidelity in aAB profiles over a long period of time in the absence of pathology [12]. Therefore, the pre-pregnant (P1) profile was used as the baseline aAB profile for this individual. To look at the initial effect of pregnancy on the baseline profile, we plotted the baseline P1 profile against the earliest available pregnancy sample (P2 – 16 weeks gestation) for four different and randomly selected blocks of 50 proteins (Figure 1). Results revealed that there is a global reduction in the titers of almost all of the individual aABs, with the exception of a very small subset of aABs whose titers did not increase (black arrows, to be discussed in the next section). Despite this global reduction in titer, we also found that the shape the aAB profile closely mimics that of the baseline profile. This is in line with our previous findings showing that the identity of the aAB hits remained very similar while the number of hits was reduced in the second trimester of pregnancy.

Figure 2 shows sequential changes in the aAB profile directed against a single block of randomly selected protein targets on the microarray during progression through pregnancy. We see that the observed global reduction in titer continues to

progress from 15-20 weeks gestation. However, it is evident that titers have again started to increase by 28 weeks gestation, and continue to do so through 37 weeks gestation. By 7 months post-pregnancy, the relative titers of aABs appear to be restored to the original baseline aAB levels determined at five years prior to pregnancy.

The return of relative aAB titers (or profiles) to the original pre-pregnant baseline levels in post-pregnant sample further strengthens our hypothesis that each individual has their own unique pattern of aAB titers that represents a "set point" for that individual. We have previously shown that in the absence of a stressor, baseline aAB profiles show remarkable fidelity [12]. Here, we see that baseline aAB profiles return to their original baseline levels after the removal of a stressor. To show this phenomenon another way, Figure 3 shows the same plots as Figure 1, however plotting only the pre- and post-pregnant sera shows the remarkable fidelity between these two samples. In this study, we see the return of the aAB profile to the baseline profile by 7 months post-pregnancy. However, since we did not have access to samples taken at earlier time points after pregnancy, we cannot rule out the possibility that this re-stabilization could have been achieved at an earlier time point.

Since we have shown that post-stress (post-pregnancy) profiles return to the baseline (pre-pregnancy) profile, we next sought to determine if these profiles are unique to each individual. We did this by comparing the pre-pregnant (baseline) RFU values from the same block of 50 randomly selected proteins (Fig. 4) to that of 5 other non-pregnant women. We have previously discussed that aAB profiles are composed

of two conceptual subsets: a much larger subset with aAB levels comparable among multiple individuals and a much smaller subset with aAB levels that are significantly higher or lower than the baseline, thus making these few aABs and their divergent titers "stand out" as peculiar to this individual (i.e., contributing to the subtle differences that define an individual "autoantibody fingerprint"). Figure 4 provides further evidence for this hypothesis by showing the unique profiles of six different women of similar age.

In summary, so far we have shown that (1) in the absence of a stressor, aAB profiles remain remarkably stable over time, (2) aAB profiles undergo changes in response to a stressor (such as pregnancy), (3) following removal of the stressor, aAB profiles can recover and return to their baseline, and (4) aAB profiles are unique to each individual, making it possible to say that each individual has their own unique "autoantibody fingerprint". We will next dive into a fifth principle: stressors that can leave a permanent imprint on the baseline aAB profile.

Figure 1. The effect of pregnancy on the baseline aAB profile (pre-pregnancy)

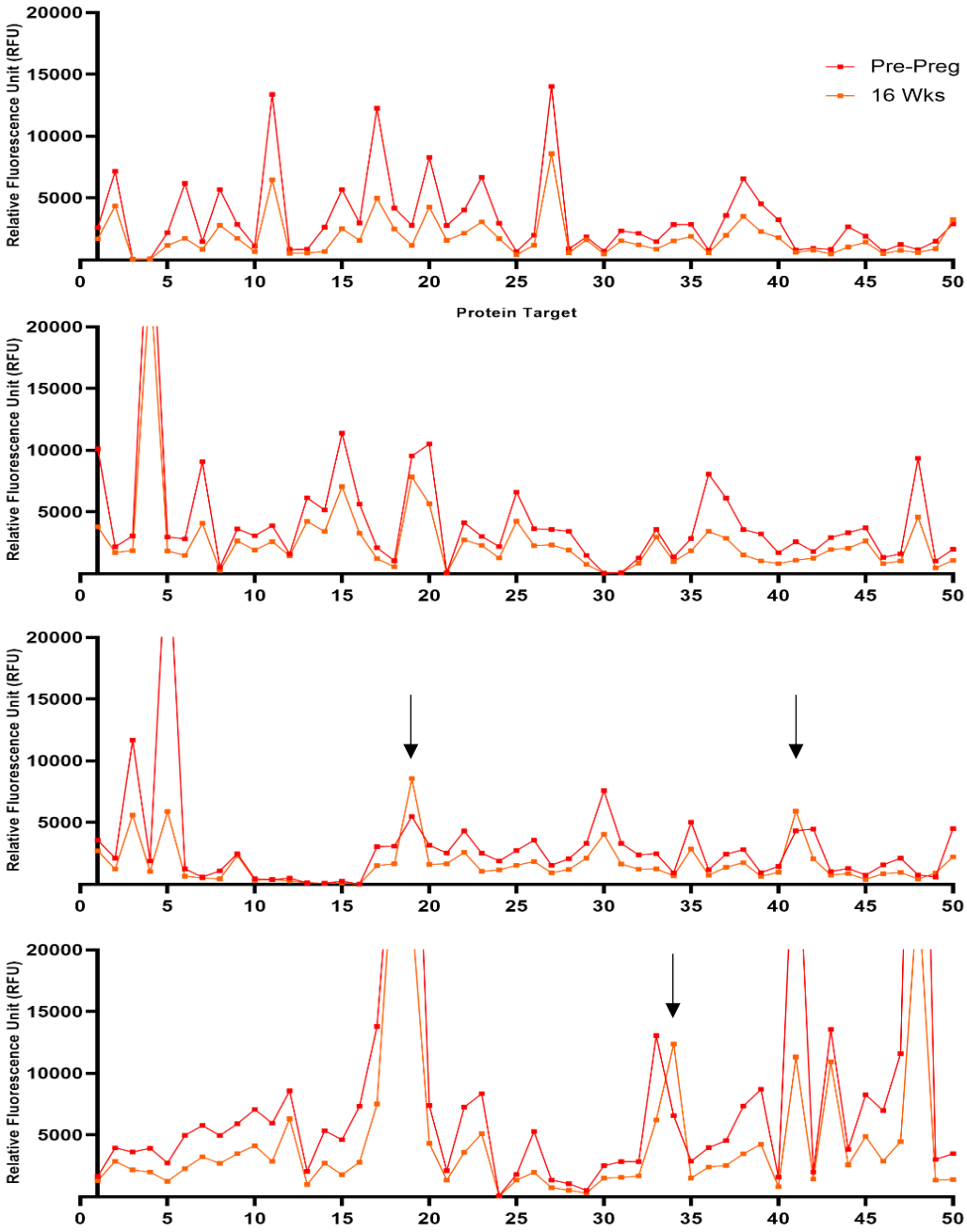

Figure 1: Four different blocks of 50 randomly selected protein targets on human protein microarrays that were probed with diluted serum (1:500) taken 5 years pre-pregnancy (red line) and at 15 weeks gestation (orange line). The plots show overall

fidelity in the shape of the profile despite a global reduction in the titers of the aABs (reflected by decreased RFUs), with the exception of a small subset of aABs (indicated by black arrows) whose titers increased during pregnancy.

Figure 2. Step-wise progression of the aAB profile throughout pregnancy and post-pregnancy as compared to the pre-pregnant baseline aAB profile

BLOCK 1

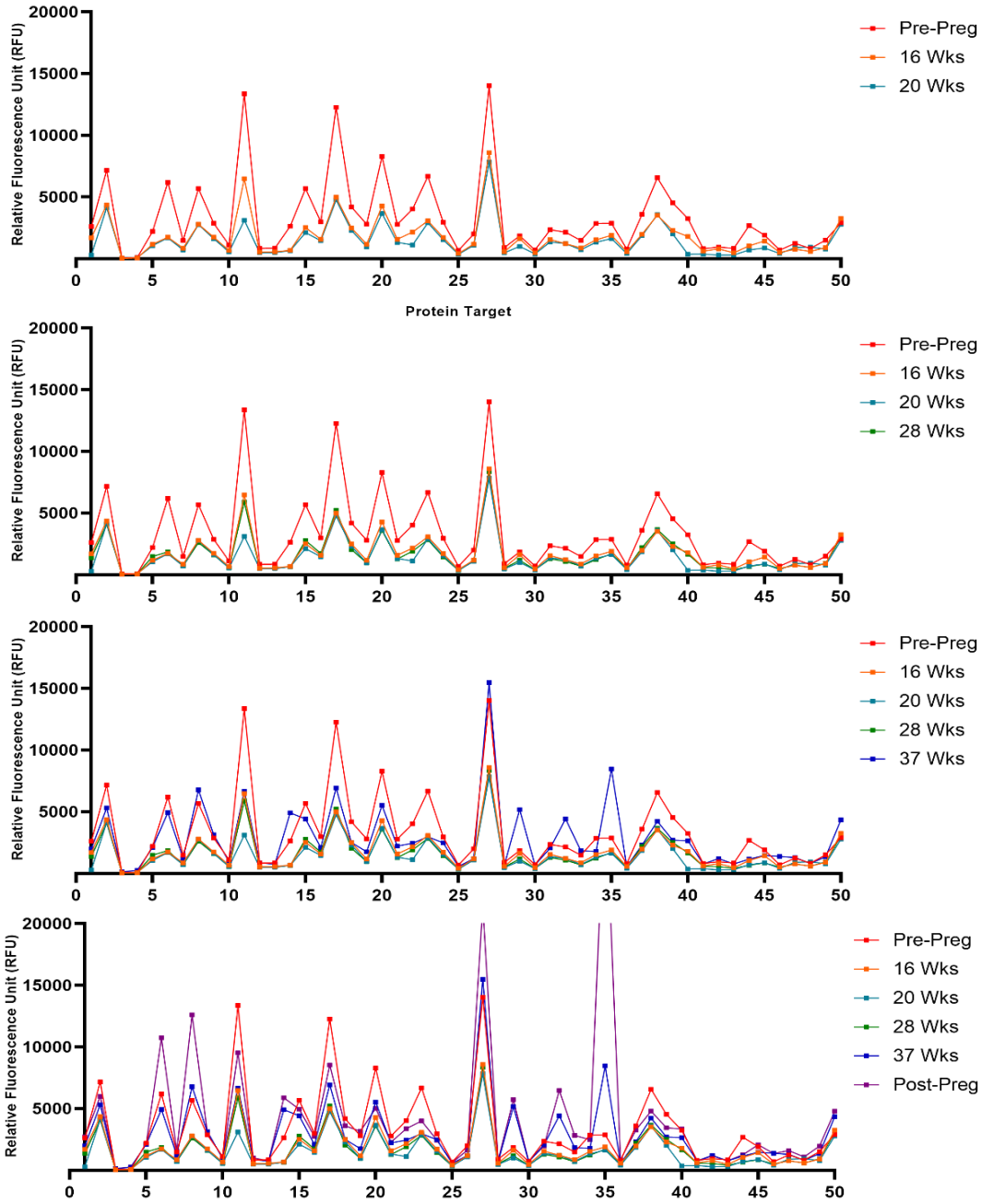

Figure 2 Continued:

BLOCK 2

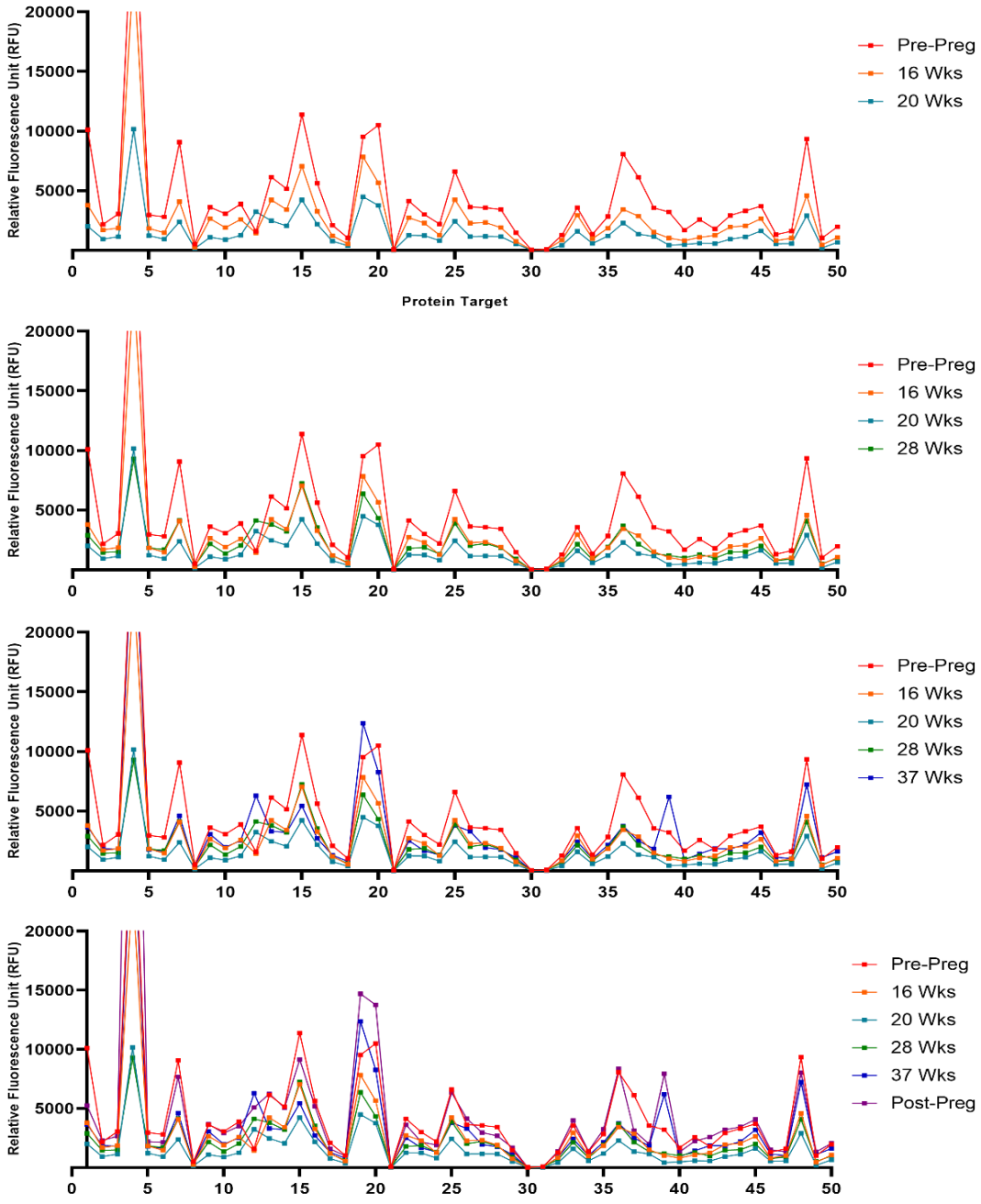

Figure 2 Continued:

BLOCK 3

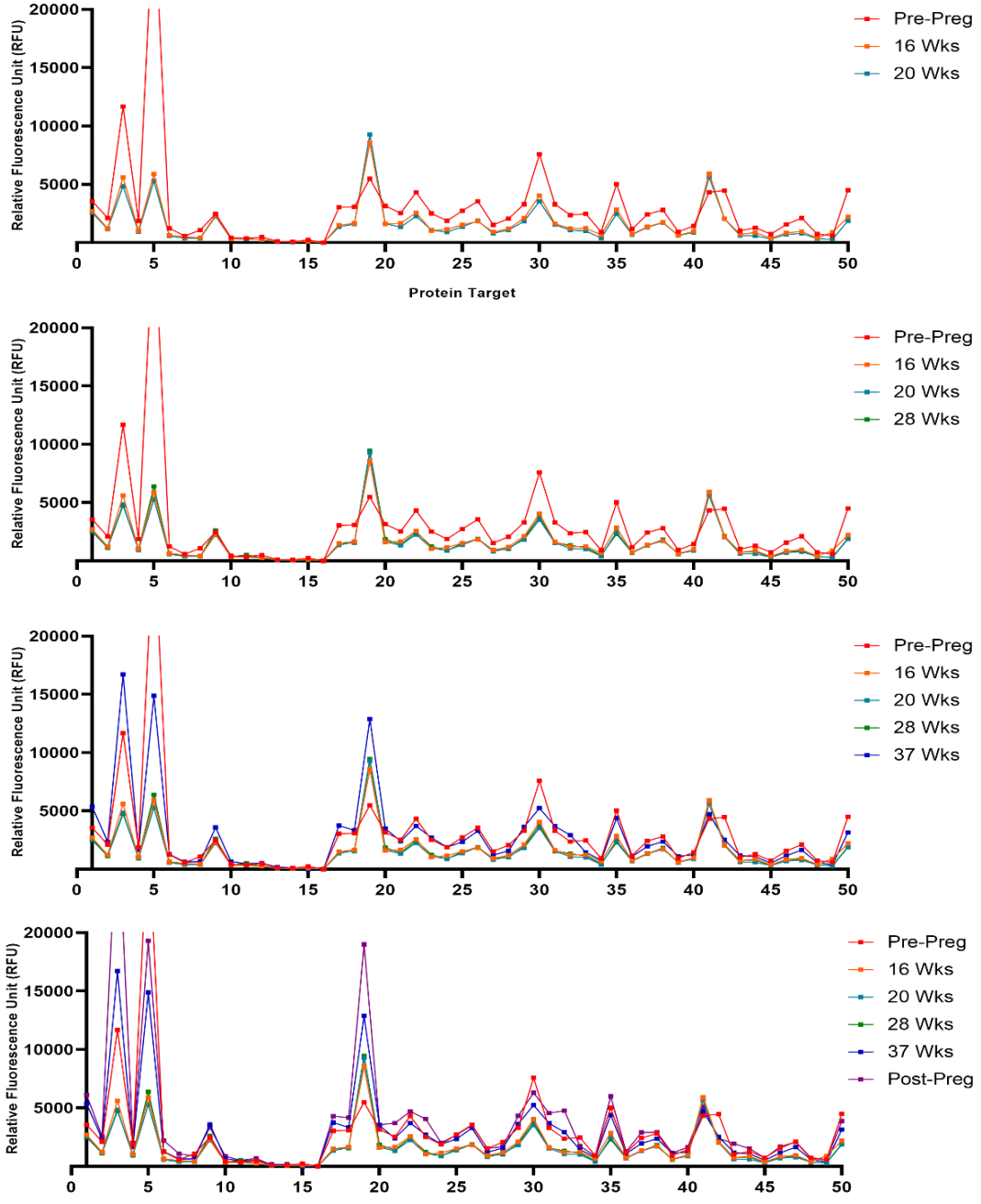

Figure 2 Continued:

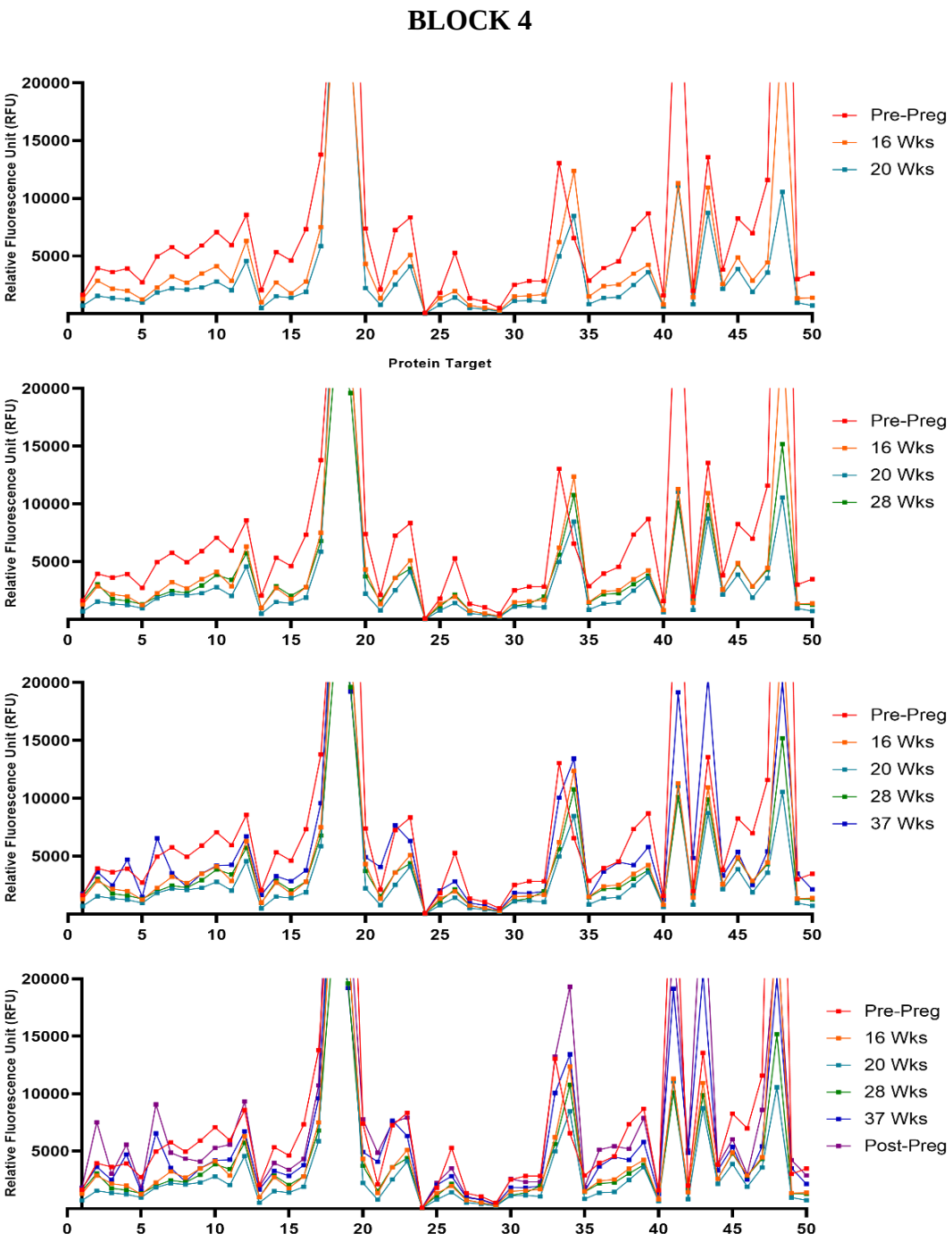

Figure 2: Longitudinal plots of four different blocks of 50 randomly selected proteins (same blocks as Fig. 1) on human protein microarrays that were probed with diluted

serum taken at 5 years pre-pregnancy (red line) as well as at the following gestational ages: 16 weeks (orange line), 20 weeks (light blue line), 28 weeks (green line), and 37 weeks (dark blue line). The graphs show the progression of changes in the aAB profile throughout pregnancy to post-pregnancy as compared to the original baseline (pre-pregnant) aAB profile established 5 years before.

Figure 3. Fidelity of aAB profiles of pre- and post-pregnancy samples – the return to the baseline profile after introduction and removal of a physiological stressor

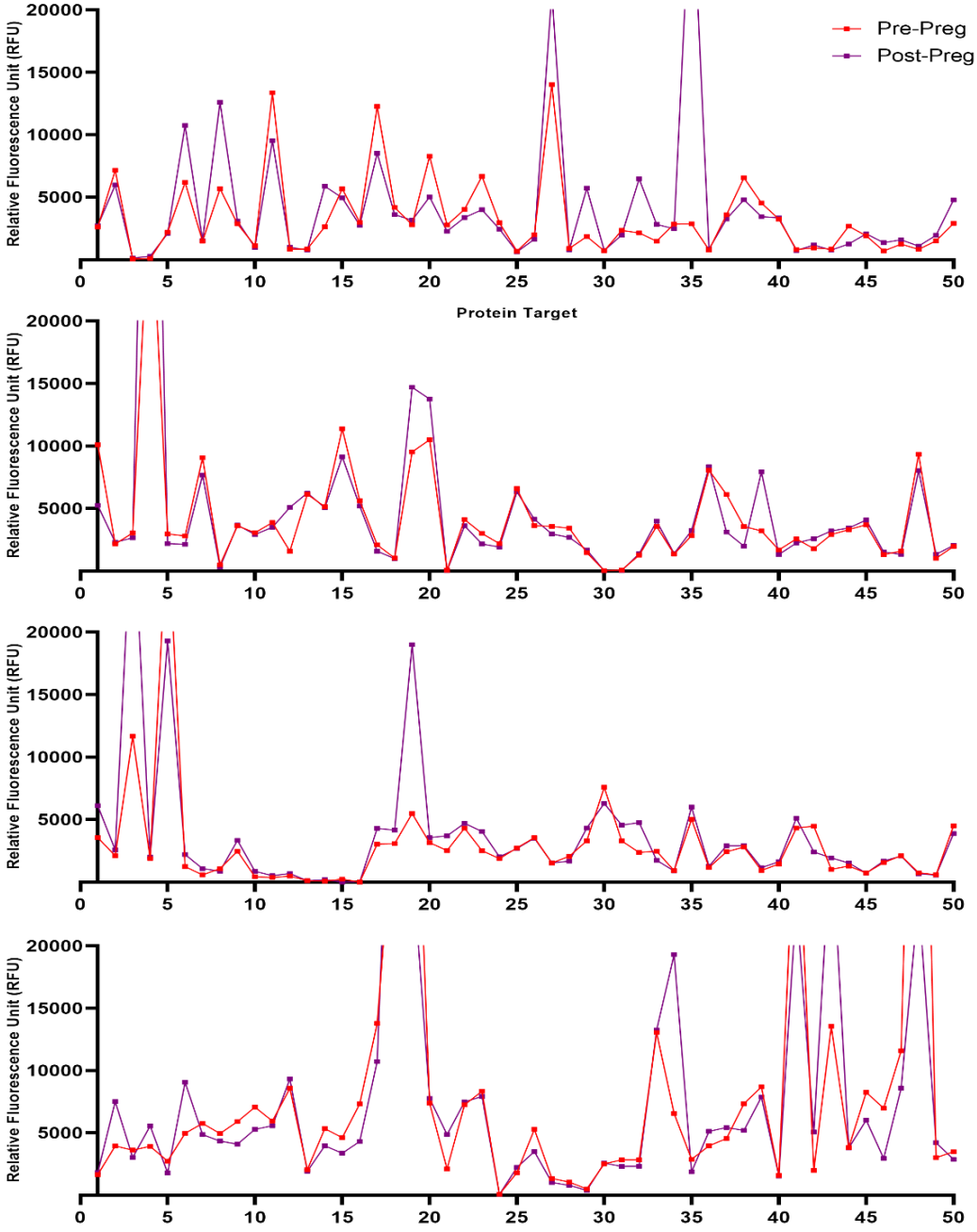

Figure 3: Comparison of the pre- and post-pregnancy profiles of four randomly selected blocks of 50 protein targets shows remarkable fidelity in aAB profiles in pre-

and post-pregnancy serum samples from the same individual. These data indicate that, when a stressor to the system is removed, the aAB profile returns to its original baseline levels, further indicating that each aAB in the profile has unique individual set-point.

Figure 4: aAB profiles are unique to each individual, as shown by comparing the same block of proteins in 6 different women

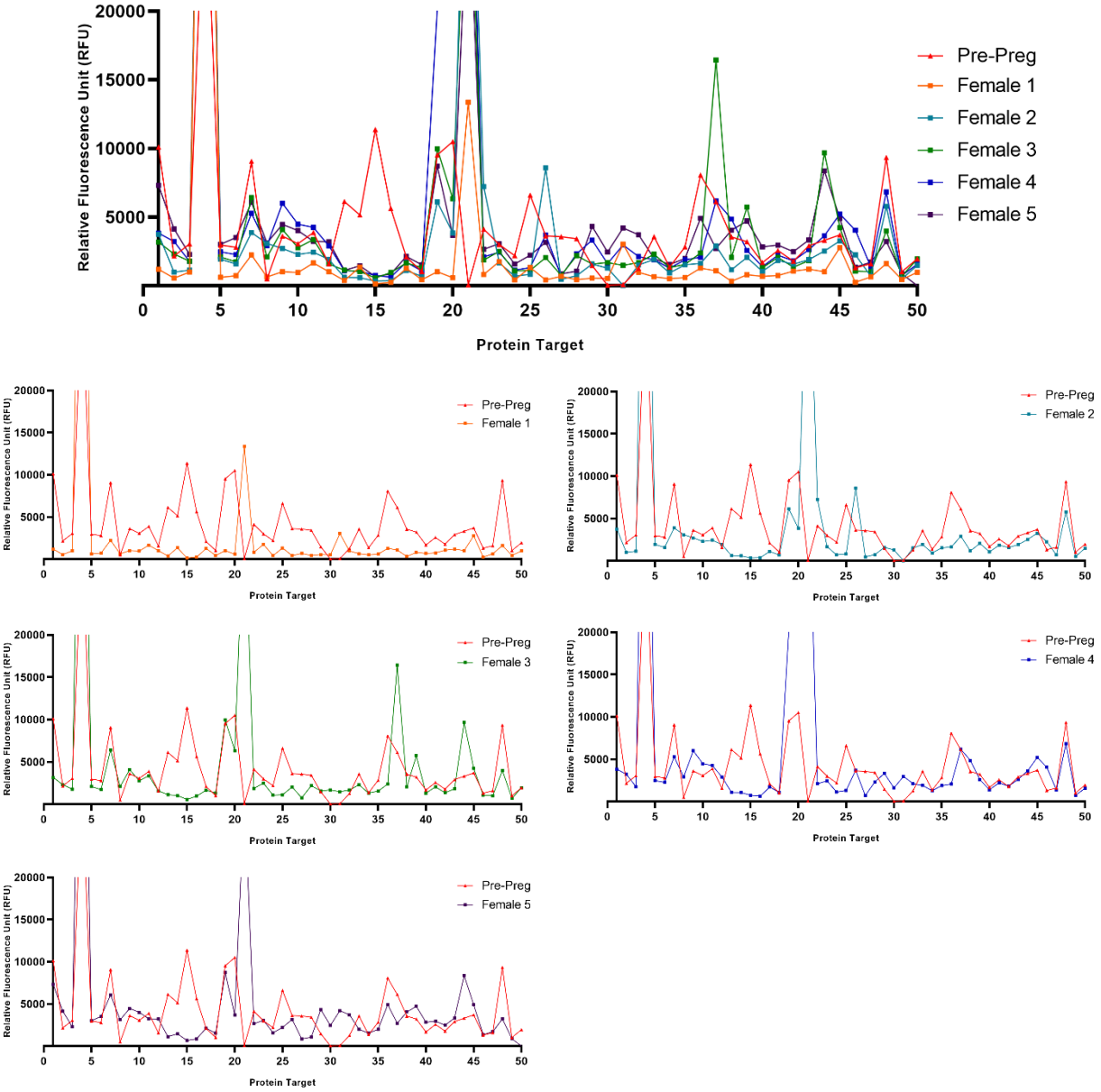

Figure 4: aAB profiles of six different women from the same randomly selected block of 50 proteins shows that aAB profiles are unique to each individual. Though there are certain commonalities between them, most individuals differ in their RFU expression

in a way that allows us to identify individual aAB fingerprints based on the unique features of individual profiles.

A small subset of aABs increased during pregnancy and remained high after removal of the stressor

We next more closely examined the aABs whose titers increased with pregnancy in the subject describe above. There were 369 aABs with titers that were increased from pre-pregnancy (P1) to 15 weeks pregnant (P2). The percent increase was calculated, and we saw that 61 of the 369 aABs had RFU values that increased by greater than 100%. 52 aAB were increased by 50-100%, and the remaining 250 aABs were increased by less than 50%. Focusing on the 61 aABs that had greater than 100% increase (Table 2), we divided them into two categories: (1) those with P1 RFU $\geq$ 1500 (hits) and (2) those with P1 RFU < 1500 (non-hits). This allowed us to divide the list into aABs that were (27 aABs) and were not (34 aABs) considered hits in the baseline profile. Next, we looked at the RFU values in P2 and further subdivided the aABs into hits and non-hits. All 27 aABs that were considered hits in P1 were also considered hits in P2. Of the 24 aABs that were not hits in P1, only 9 showed enough of an increase to meet the threshold for being considered a hit in P2.

Table 2. Flowchart following steps of categorization of aABs that showed an increase in titer between pre-pregnant sample (P1) and 15 weeks pregnant sample (P2).

<table>
<tr><td colspan="4">Increase in RFU from P1 → P2
369 aABs</td></tr>
<tr><td colspan="3">Greater than 100% Increase
61 aABs</td><td>Between 50-100% increase
52 aABs</td><td>Less than 50% Increase
250 aABs</td></tr>
<tr><td colspan="2">P1 RFU ≥ 1500
27 aABs</td><td colspan="2">P1 RFU < 1500
34 aABs</td><td rowspan="2" colspan="2"></td></tr>
<tr><td>P2 RFU ≥ 1500
27 aABs</td><td>P2 RFU < 1500
0 aABs</td><td>P2 RFU ≥ 1500
9 aABs</td><td>P2 RFU < 1500
25 aABs</td></tr>
</table>

Table 2: Despite the global reduction of aAB RFUs from pre-pregnancy to pregnancy, a small subset (369 aABs) showed an increase in aAB RFUs. This table summarizes how these aABs are categorized. Percent difference is calculated for each aAB. aABs with RFU ≥ 1500 and a Z-factor ≥ 0.4 are considered hits. P1 refers to the pre-pregnant sample and P2 refers to pregnant sample taken at 15 weeks.

We first focused on the longitudinal progression of the 27 aABs that showed an increase in titer between pre-pregnancy and first pregnant sample at 15 weeks gestation and were also considered "hits" in both P1 and P2. The first question that we wanted to answer was if the increase in RFU titers would be consistent throughout pregnancy and into post-pregnancy. Table 4 summarizes the percentage data while Figure 4 shows the stepwise progression of the increase in profile. The first key take away point when comparing the pre-pregnancy (P1, 5 years pre-pregnancy) to post-pregnancy sample (P6, 7 months post-pregnancy) is that all of the aABs show an increased titer. Secondly, we still see a global reduction in aAB titers between P2 (16 weeks gestation) and P3 (20 weeks gestation). This is in agreement with the known IgG transfer that occurs, starting the second trimester of pregnancy [14]. However, in this small subset of aABs, unlike the other aABs, there was an initial increase followed by a decrease.

In Figure 4A, we show the initial increase from the baseline profile to the profile established during pregnancy. It is important to note the change in scale of the y-axis in Figure 4 from 20,000 RFU to 75,000 RFU in order to include most of the data points. This new stressor-induced profile is established by 16 weeks gestation. However, since samples from earlier in the pregnancy period were not available, we cannot rule out that this stress-induced profile is established even earlier in pregnancy. In Figure 4C, we added the remaining pregnancy sample profiles in a sequential manner. This revealed that this stress-induced profile is maintained throughout the period when the stressor (i.e. pregnancy) is present. Furthermore, by comparing Figure 4A and 4B, we see that, unlike the vast majority of aABs, the post-pregnancy profile of this smaller

group of aABs resembles the stress-induced profile more closely than it resembles the original baseline profile, thus providing preliminary evidence that stressors to the system may leave a permanent imprint on the baseline profile.

Table 3. The longitudinal progression of a small subset of aABs showing both an initial pregnancy-associated and sustained post-pregnant increase in RFU

Protein Target	% change from P1 to P2	% change from P2 to P3	% change from P3 to P4	% change from P4 to P5	% change from P5 to P6		% change from P1 to P6
NP_003833.3	280%	0%	0%	0%	0%		280%
BC002769.1	420%	-35%	8%	64%	-6%		458%
NM_016485.3	294%	-27%	9%	70%	-15%		351%
NM_145021.1	284%	-45%	13%	-19%	17%		125%
BC059174.1	101%	-44%	-26%	232%	11%		206%
BC020885.1	240%	-40%	37%	43%	49%		493%
NM_003177.3	198%	-13%	-13%	27%	5%		203%
BC032347.1	252%	-49%	5%	133%	24%		445%
NM_003403.3	304%	-20%	-2%	33%	6%		346%
NM_181707.1	291%	-23%	22%	6%	22%		373%
NM_032345.1	289%	-71%	37%	337%	-17%		451%
BC098302.1	127%	-41%	-35%	135%	25%		157%
BC006104.1	105%	-26%	12%	36%	45%		235%
BC024746.1	145%	-25%	11%	35%	78%		393%
NM_001790.2	156%	-16%	-8%	31%	21%		213%
NM_015000.1	482%	-32%	6%	-16%	-10%		216%
BC039832.1	223%	-39%	1%	56%	84%		478%
BC039306.1	146%	-29%	18%	41%	11%		221%
BC059386.1	141%	-41%	2%	-17%	23%		51%
NM_032472.3	178%	-32%	17%	144%	27%		580%
NM_016487.1	126%	-24%	10%	45%	-17%		127%
NM_018393.2	101%	-55%	-11%	153%	0%		104%
BC039306.1	146%	-29%	18%	41%	11%		221%
NM_006370.1	258%	-46%	78%	45%	18%		493%
PV3857	107%	-49%	18%	14%	44%		104%
NM_006948.1	102%	-60%	155%	192%	20%		618%
NM_000327.2	110%	-47%	44%	-11%	580%		879%

Table 3: This table includes the 27 aABs whose RFUs increased with pregnancy and remained increased after pregnancy (i.e., failed to return to pre-pregnancy baseline levels. The green text annotates percent increase in RFU titer between the two time-points while the red text annotates a percent decrease between the two titers. We see

that even though there is a uniform drop between P2 (16 weeks gestation) and P3 (20 weeks gestation), there is an overall trend of increasing aAB titers in the indicated small subset of aABs, with a uniform increase sustained 7 months post-pregnancy (P1 → P6 column).

Figure 5. The progression of a selected group of 27 aABs showing persistently increased titers during and post-pregnancy

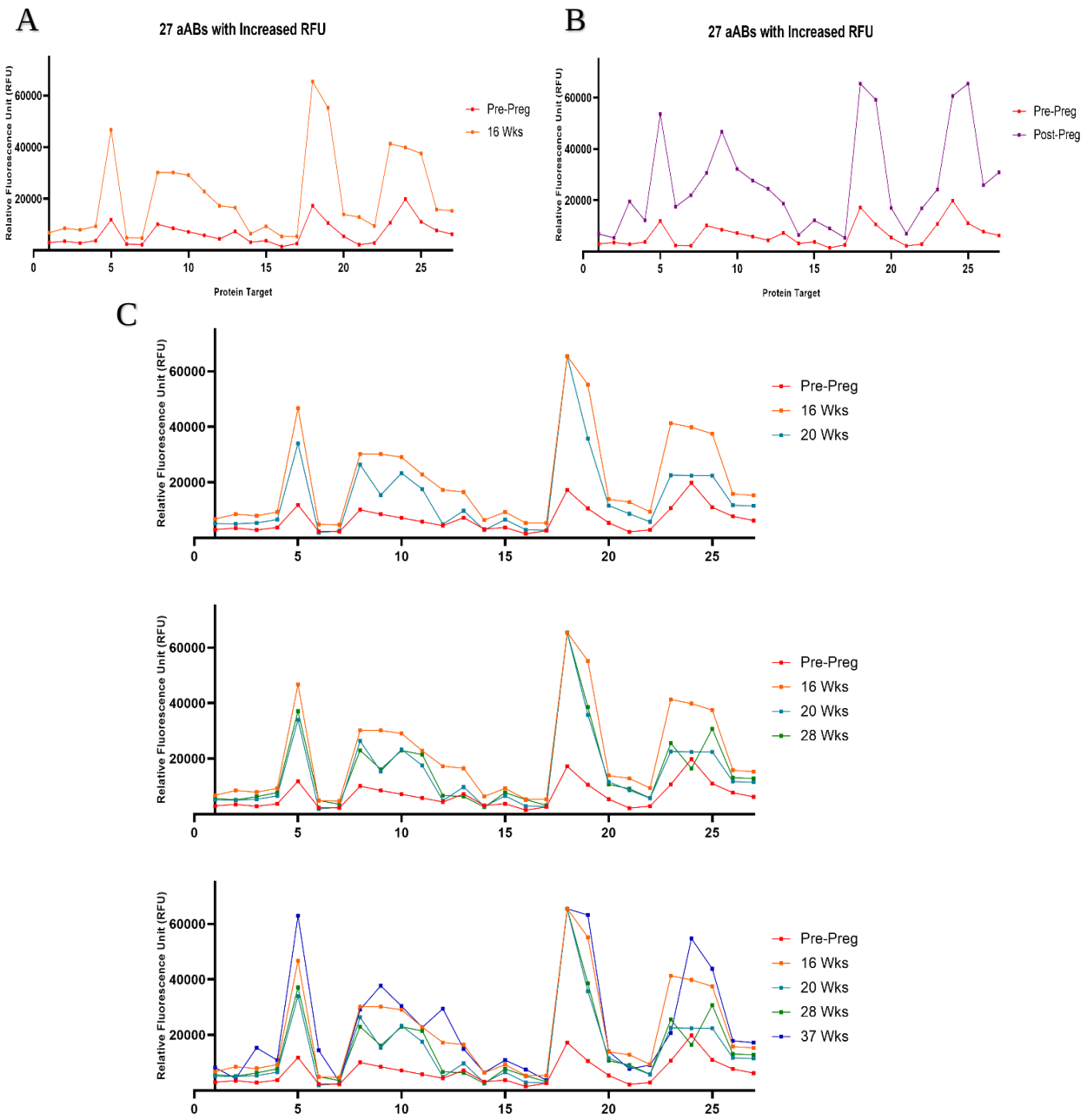

Figure 5: Of the 369 aABs that showed an increase in RFU between P1 and P2, 27 aABs had a percent increase greater than 100% and RFU $\geq$ 1500 in both P1 and P2. In

A, we see the establishment of the stress-induced profile by 16 weeks gestation. In B, the post-pregnant profile is significantly different from the baseline profile, and in fact by comparing it to A, we see that it more closely resembles the stress-induced profile. In C, we see the step-wise addition of the gestational samples taken at 20 weeks, 28 weeks and 37 weeks.

DISCUSSION

In this study, we have investigated the question of whether a "normal" or non-disease-related physiologic event (i.e., pregnancy) can trigger changes in individual aAB profiles and, if so, if these changes are transient. We sought to determine whether or not a specific set of pregnancy-associated aAB profile changes are maintained over the course of pregnancy as well as whether aAB profiles return to baseline (non-pregnancy) after the birth of the child. To address these and other questions, a longitudinal series of serum samples from a single individual was taken before, during and after pregnancy, and each sample was used to probe human protein microarrays in an effort to establish the aAB profile for each time-point. This approach facilitated comparison of the pregnancy and non-pregnancy profiles in the same individual and allowed us to potentially identify any changes in aAB profiles associated with a particular stage of pregnancy.

In previous studies, we introduced the concept of a baseline aAB profile. We have shown that in the absence of pathology or major stressors to the body, each individual has a baseline (or "set point") aAB profile that can remain stable over many years, and that the baseline profile for each individual has a unique features. Thus, each individual has a unique "aAB fingerprint". We have also previously shown that common, disease-specific changes from the baseline aAB profile can be identified and used as biomarkers. Exploring the effects of non-disease body associated stressors such as illness, major weight loss, surgeries has not yet been attempted before this

study. The question remaining to be answered is two-fold: does a physiological stressor affect the baseline aAB profile, and if so, does the aAB profile recover once this physiological stressor is removed.

To address these questions, we began by determining how the onset of pregnancy as a stressor changes the overall aAB profile. Our results revealed a global drop in the number of aAB hits as we progressed into the pregnancy up to week 20. Our pre-pregnant sample had 6749 aAB hits detected, and this number steadily declined until we reach 20 weeks, with the number of detectable aAB hits at slightly less than half the original level (i.e., 3226). This reduction in the number of detectable aAB hits is expected, since any global reduction in RFUs will drive a large number of aABs below our detection threshold (i.e., 1500 RFUs). The number of aAB hits then steadily increases up to the end of pregnancy, with 37 week sample and our post-pregnancy sample having almost the same number of aABs hits (6549) as our pre-pregnant sample taken nearly 6 years earlier. This restoration of the aAB profile toward the original baseline level is further supported by the fact that 94.23% of the 6549 aAB hits was identical to those in our pre-pregnant sample. This high percentage of overlap in identity of aAB hits is maintained throughout pregnancy, and comparing the identity of each sample to the pre-pregnant aABs, we saw 99.39% overlap at 16 weeks, 99.50% at 20 weeks, 99.39% at 28 weeks and lastly, 96.25% at 37 weeks. Thus, if one assumes that aABs have a debris-clearing function, these results may have a straightforward explanation. It is not so much that new aABs are required to clear "new" debris, but rather that there is an increased production of the same type of debris, leading to a

general reduction across-the-board in aAB titers due to the demand for increasing debris clearance. During the first half of pregnancy, organ morphogenesis and remodeling to a final form might be expected to produce a high level of cell and tissue debris, thus taxing the aAB debris-clearance system and resulting in chronically reduced aAB titers during this developmental period. By contrast, the later stages of pregnancy largely involve the rapid growth of the already formed organs, in which there is a lot of growth but less remodeling. This would be expected to produce comparatively less debris despite the increase in the size of the baby, giving an opportunity for aAB titers to be restored to default baseline levels.

This is also in line with previous research that tells us that the maternal IgG transfer to the fetus begins as early as the second trimester (week 14) and continues throughout to term [14]. With the transfer of the IgG from the mother to the fetus, we expect to see a global decline in the titers of aABs in the mother's blood and, as mentioned above, we would expect less antibodies to meet the threshold for being considered hits (RFU > 1500, Z-factor > 0.4). This further confirms that the IgG transfer of aABs to the fetus is also not selective, but rather a representative sample of all IgG in human serum are transferred to the serum. If it was possible to collect simultaneous samples from the fetus and the mother, we hypothesize that the aAB profiles would closely mimic one another in pattern. It is currently thought that the majority of the IgG is transferred from mother to fetus during the third trimester, however, we see an increase in our IgG titers that seems to be in direct contradiction with this. We hypothesize that the initiation of the IgG transfer serves as a signal for

the mother to increase her production of immunoglobulins in order to restore her aAB profile to original levels.

The percentage overlap in the identity of aAB hits evident in the longitudinal samples examined prompted us to examine the expression pattern of individual aABs within these profiles throughout pregnancy. This was accomplished by randomly selecting blocks of 50 protein targets and plotting their corresponding aAB RFU expression values. Results revealed that the reduction in hits was accompanied by a global reduction in RFU values, however, the shape of the baseline profile was maintained for most of the individual aABs, suggesting that the mother passes her own aAB baseline profile to the fetus non-selectively. Comparing the pre-pregnant to the post-pregnant profile, we saw remarkable fidelity in both the shape of the profiles and the pattern of individual RFU levels. This indicates that, once the stressor (pregnancy) was removed, the aAB profile was able to return to the original baseline levels that were show to be in place 5 years prior to the onset of pregnancy, further suggesting that baseline aAB profiles have a defined set-point that is maintained with great fidelity.

Even though the vast majority of the aABs behaved as described above, a small subset of aABs showed an increase in the RFUs with progression of pregnancy. We identified 27 aABs that met the threshold for being an aAB hit at P1 and P2, we followed their expression over the course of pregnancy and after. We saw that these aABs showed deviation from the original profile, with their expression having gone up significantly, and remaining high even at 7 months post-pregnancy. This is unique

since most of our aAB had lower expression and returned to similar levels as their pre-pregnant RFU after the pregnancy had ended. This suggests that the presence of a stressor may, in certain circumstances, leave a permanent imprint on the original aAB profile. Interestingly, this stress-induced profile seems to be established by 16 weeks pregnancy, indicating that the inciting event was well under way by 16 weeks, creating a unique aAB profile that was maintained throughout the course of the pregnancy and even after pregnancy had ended. Comparing the pre- and post-pregnant profiles in these 27 protein targets, we see marked differences, in sharp contrast to the other randomly selected blocks of 50 proteins that we've shown in this work. This implies that even though pregnancy may not alter the entire aAB profile expression pattern, it may cause substantial changes in a small subset of aABs. Moreover, these changes are maintained after the stressor (i.e., pregnancy) is removed, as evidenced by a post-pregnancy profile that is almost identical to the "stress-induced profile" and very different from the pre-pregnancy profile.

In previous unpublished studies carried out in our laboratory, we have produced evidence that the autoantibody profile of the child tends to closely resemble that of the mother, even many years after birth. This should not be surprising, given that the fetus, despite not yet having a functional immune system, is born with a full complement of the mother's IgG aAB profile that was transferred through the placenta. Based on this, we have proposed but not yet fully tested the possibility that the child's aAB profile is initially derived from a template aAB profile that is provided by the mother. From on the above discussion, our expectation is that, initially, the aAB profile generated by the

child's own immune system is identical to that of the mother. However, as shown above, subsequent encounters throughout life with various life stressors can cause persistent and additive deviations from this initial aAB profile that leads to various degrees of departure from the maternal profile and the evolution of a new aAB profile unique to each individual. If true, then the magnitude of the departure from the maternal baseline pattern would be dependent on the number, type and severity of the stressors encountered by each individual. Likewise, minimal encounters with stressors would be predicted to allow the profile of the child to more closely resemble that of the mother throughout life. Further work will be needed to test these possibilities.

Taken together, we have seen that stressors to the system can cause skewing of a subset of aABs from the baseline aAB profile. Even though some of the deviations from baseline (for example, a global reduction) can return to baseline afterwards (or a subset of aAB that did significantly change but returned to baseline levels), there is a subset of aAB that undergo stress-induced deviation and remain skewed even after the stressor is removed. This implies that stressors to the system are able to create an imprint on the baseline aAB profile. Further studies of baseline aAB profiles, and longitudinal studies of different stressors, can elucidate specific patterns of expression that are stressor specific. However, it is also possible that each individual's baseline aAB profile reacts differently to the presence of even the same stressor. We have already seen that baseline aAB profiles are unique to each individual. Regardless, it is important to consider that the imprints that stressors may leave on baseline aAB profiles can serve as an immunological history of what our bodies have endured and

remembered, similar to the immunologic memory exhibited by the antibodies that target pathological infections.

REFERENCES

1. Avrameas, S., et al., Naturally occurring B-cell autoreactivity: a critical overview. J Autoimmun, 2007. 29(4): p. 213-8.

2. Avrameas, S., H. Alexopoulos, and H.M. Moutsopoulos, Natural Autoantibodies: An Undersugn Hero of the Immune System and Autoimmune Disorders-A Point of View. Front Immunol, 2018. 9: p. 1320.

3. Nagele, E.P., et al., Natural IgG autoantibodies are abundant and ubiquitous in human sera, and their number is influenced by age, gender, and disease. PLoS One, 2013. 8(4): p. e60726.

4. Norris, G.T. and J. Kipnis, Immune cells and CNS physiology: Microglia and beyond. J Exp Med, 2019. 216(1): p. 60-70.

5. Avrameas, S. and C. Selmi, Natural autoantibodies in the physiology and pathophysiology of the immune system. J Autoimmun, 2013. 41: p. 46-9.

6. Levin, E.C., et al., Brain-reactive autoantibodies are nearly ubiquitous in human sera and may be linked to pathology in the context of blood-brain barrier breakdown. Brain Res, 2010. 1345: p. 221-32.

7. Nagele, R.G., et al., Brain-reactive autoantibodies prevalent in human sera increase intraneuronal amyloid-beta(1-42) deposition. J Alzheimers Dis, 2011. 25(4): p. 605-22.

8. Han, M., et al., Diagnosis of Parkinson's disease based on disease-specific autoantibody profiles in human sera. PLoS One, 2012. 7(2): p. e32383.

9. Nagele, E., et al., Diagnosis of Alzheimer's disease based on disease-specific autoantibody profiles in human sera. PLoS One, 2011. 6(8): p. e23112.

10. DeMarshall, C.A., et al., Detection of Alzheimer's disease at mild cognitive impairment and disease progression using autoantibodies as blood-based biomarkers. Alzheimers Dement (Amst), 2016. 3: p. 51-62.

11. DeMarshall, C., et al., Autoantibodies as diagnostic biomarkers for the detection and subtyping of multiple sclerosis. J Neuroimmunol, 2017. 309: p. 51-57.

12. Kheirkhah, R., et al., The origin and nature of the complex autoantibody profile in cerebrospinal fluid. Brain, Behavior, & Immunity - Health, 2019. 2.

13. DeMarshall, C., et al., Utility of autoantibodies as biomarkers for diagnosis and staging of neurodegenerative diseases. Int Rev Neurobiol, 2015. 122: p. 1-51.

14. Simister, N.E., Placental transport of immunoglobulin G. Vaccine, 2003. 21(24): p. 3365-9.

ATTRIBUTES

Figure 1. Human protein microarrays were processed by Rahil Kheirkhah and Cassandra DeMarshall, PhD. Data extraction and analysis was performed by Rahil Kheirkhah.

Figure 2. Human protein microarrays were processed by Rahil Kheirkhah and Cassandra DeMarshall, PhD. Data extraction and analysis was performed by Rahil Kheirkhah.

Figure 3. Human protein microarrays were processed by Rahil Kheirkhah and Cassandra DeMarshall, PhD. Data extraction and analysis was performed by Rahil Kheirkhah.

Figure 4. Human protein microarrays were processed by Rahil Kheirkhah and Cassandra DeMarshall, PhD. Data extraction and analysis was performed by Rahil Kheirkhah.

Figure 5. Human protein microarrays were processed by Rahil Kheirkhah and Cassandra DeMarshall, PhD. Data extraction and analysis was performed by Rahil Kheirkhah.

CHAPTER V

PREVALENCE AND DISTRIBUTION OF GLYCOSYLATED AUTOANTIBODIES

INTRODUCTION

Glycosylation of immunoglobulins can occur at either the Fab or Fc region. In healthy non-pregnant individuals, the fraction of total IgG that is Fab-glycosylated varies between 15 to 25% [1]. During pregnancy, the percentage of glycosylated IgGs increases to as high as 50% [2]. The presence of the glycan on one of the two Fabs creates steric hindrance that interferes with the binding of the glycosylated arm to antigens, rendering glycosylated antibodies to act as univalent antibodies [3]. Since glycosylated antibodies compete with non-glycosylated antibodies for the same target antigen, they can act as "blocking antibodies" that can reduce inflammatory sequellae with an effectiveness that is proportional to their titer relative to their non-glycosylated counterparts [4].

It has been postulated that the increase in glycosylation with pregnancy plays a regulatory role that prevents immune rejection of the fetus, which also carries paternal antigens that can be recognized as foreign to the maternal immune system. Apparently, one of the strategies used to foster immune tolerance of the semi-allogeneic fetus is to

univalently glycosylate antibodies that are directed towards paternal antigens so that they fail to induce an immune response that could lead to fetal rejection by the mother [4, 5].

The increase in glycosylation may be regulated by Progesterone-Induced Blocking Factor (PIBF), a protein secreted by human pregnancy lymphocytes [3, 4]. During pregnancy, through its immunomodulatory effects, PIBF creates a habitable environment for the fetus. PIBF directly blocks degranulation of Natural Killer (NK) cells thus inhibiting their cytotoxicity, alters the Th1 lymphocyte to Th2 lymphocyte balance by promoting the production of Th2 lymphocyte-favoring cytokines, as well as acting as a transcription factor to induce production of asymmetrically glycosylated antibodies [3, 6-8]. To further support the importance of glycosylation in maintaining a healthy pregnancy, it has been shown that the percentage of asymmetric antibodies is lower in women who show symptoms of threatened preterm pregnancy termination, such as spontaneous abortion or preterm labor and preeclampsia [5, 7, 9, 10]. Furthermore, there have been reported cases of pregnant women who experienced remission of symptoms of their autoimmune disorders such as Rheumatoid Arthritis, Multiple Sclerosis, Systemic Lupus Erythematosis and Inflammatory Bowel Disease during pregnancy [11-13]. Though this has not been directly linked to an increase in glycosylation during pregnancy, it is possible that the increase in glycosylation of antibodies involved in those pathologies is the reason why a remediation of symptoms is observed.

In this study, we took a closer look at the prevalence and distribution of glycosylation in autoantibodies (aABs) specifically using longitudinal samples obtained over a period of 6 years, spanning a period prior to, post, and during pregnancy. Using chromatography columns, we isolated immunoglobulin G and, furthermore, separated the glycosylated and non-glycosylated fractions. We used these to probe human protein microarrays, and investigate the breakdown and extent of glycosylation of autoantibodies.

MATERIALS AND METHODS

In normal serum, immunoglobulin G (IgG) makes up 80% of the total immunoglobulin content, followed by IgA (15%), IgM (5%), IgD (0.2%) and IgE (trace amounts) [14]. The total IgG is composed of antibodies that target non-self antigens, referred to in this study as p-IgG (pathogen directed IgG) and those that can bind to self-antigens, referred to as a-IgG (autoantibody IgG). Furthermore, these immunoglobulins can either be glycosylated (G-p-IgG, G-a-IgG) or non-glycosylated (NG-p-IgG) and (NG-a-IgG). Other subclasses of immunoglobulins can also be glycosylated or non-glycosylated, and previous research has indicated that the IgM subclass is also able to bind self-antigens [15]. For the purposes of this study, our goal was to first isolate the IgG subclass of immunoglobulins from serum or plasma. The next aim was to separate the glycosylated and non-glycosylated components, and obtain a relative concentration for each subset. Table 4 provides an overview of the protocol.

Collection of Human Serum

Blood is initially collected in red-top tubes (containing no anticoagulants or preservatives). The blood is stored at RT for about 45 to 60 minutes to allow for coagulation to occur. Serum is obtained from clotted blood that is not mixed with an anticoagulant. The clotted blood is then spun down at 3000 rpm for 10 min to allow for separation of the serum from the clotted portion of blood [14, 16]. The serum is then

collected, aliquoted, and stored at -80^{o}C. At this point in the process, the serum contains all subclasses of immunoglobulins.

Longitudinal Pregnant Patient Sample (n=6):

Longitudinal serum samples were obtained from a healthy individual from the New Jersey Institute for Successful Aging at Rowan University. Serum samples were taken from the same individual over the course of six years: one sample in 2013, four samples in 2018, and one sample in 2019. Table 1 highlights the dates and gestational period at which samples were taken.

Isolation of IgG subclass with Protein G vs. Protein A

Both Protein G and Protein A have high affinity for the Fc region of polyclonal and monoclonal IgG antibodies, allowing for purification of IgG from other immunoglobulin subclasses. Protein G is a bacterial protein derived from Group G Streptococci and Protein A is a bacterial protein derived from *Staphylococcus Aureus.* They can both be coupled to Sepharose to create chromatography media that can be readily used for antibody purification. The relative binding strengths of human immunoglobulin subclasses to Protein A and Protein G are shown in table 2. Even though both Protein A and Protein G bind IgG with high affinity, Protein G binds to all IgG subclasses, while Protein A is not able to bind to IgG_3. For this reason, we decided to use Protein G for purification of IgG in our study.

Protein G HP SpinTrap Columns (GE Healthcare, Cat. No. 45-001-485)

Protein G HP SpinTrap Columns are pre-packed with Protein G Sepharose High Performance Medium to be used for small-scale purification of monoclonal and polyclonal antibodies (IgG) from samples such as serum. The Ab Buffer Kit (GE Healthcare, Product No. 28903059) was used and Table 3 lists the components of each buffer.

All protocol steps in using the Protein G column were done at room temperature. Storage solution is removed by centrifugation (30s, 100 x g). The column is equilibrated using 600 uL of binding buffer, followed by centrifugation (30s, 100 x g). Serum sample, not to exceed the max volume of 600uL, is added to the column and incubated for 4 minutes with end-over-end mixing to allow for IgG to bind to the Protein G Sepharose. The column is then centrifuged (30s, 100 x g) to discard the initial flow-through, containing the remaining components of serum, followed by two washes with 600 uL of binding buffer (30s, 100 x g). Next, the IgG is eluted using 400 uL of elution buffer, mixed briefly by inversion and centrifuged (30s, 70 x g) into a collection tube containing 30 uL of neutralizing buffer. The elution step is repeated once more, for a total of two elution fractions, since most of the bound antibody is eluted after two elution steps.

Isolation of glycoproteins with Concanavalin A (ConA) vs. Wheat Germ Agglutinin (WGA)

Both ConA and WGA are lectins that can act as ligands for specific classes of glycoproteins. ConA recognizes alpha-linked mannose and terminal glucose residues. WGA selectively binds *N*-Acetyl glucosamine (GlcNac) groups and sialic acid. Since glycosylation is also present on both the Fab and Fc region of antibodies, we were concerned about non-specific Fc binding of IgG. However, a study done by Huang et. al. showed that ConA lectins only bind to the glycosylation on Fab region because they were exposed and accessible to the lectin, in contrast to the N-linked oligosaccharides attached to the Fc region, which are not accessible to the lectin since they are located inside the natural protein [17]. For this reason, we decided to use ConA columns for separation of Fab glycosylated-IgG from non-glycosylated IgG in our study.

Pierce Glycoprotein Isolation Kit, ConA (ThermoFisher Scientific, Catalog No. 89804)

The buffers for the ConA column must be equilibrated to room temperature before use. A sample containing up to 1.5 mg of total protein is diluted with the 5X binding/wash Stock solution.

The column is prepared by adding 200 uL of 50% resin slurry. The storage buffer is centrifuged (1 min, 250 x g) to be discarded. The column is equilibrated with 200 uL of the 1X binding/wash buffer (1 min, 250 x g), for a total of three times. The sample is then added and incubated for 10 min at room temperature with end-over-end

mixing, and then centrifuged (1 min, 250 x g) to discard the flow-through. The flow-through in this column contains non-glycosylated IgG. The column is then washed twice more with 400 uL of 1X binding/wash buffer (1 min, 250 x g) to give us flow-through fractions 2 and 3. Next, 400 uL of 1x binding/wash buffer is added and incubated for 5 min before centrifugation (1 min, 250 x g) (flow-through 4). This step is repeated once more, giving us flow-through 5. The bound portion is then eluted with 200 uL of elution buffer, incubated for 10 min with end-over-end mixing and then centrifuged out (1 min, 250 x g). This is repeated twice more for a total of 3 elution fractions.

SimplyBlue SafeStain (Invitrogen, Cat. No. LC6060)

Samples were run on 1.5mm gels (12% resolving, 4% stacking). The gels were run at 100V at room temperature. The gels were then placed in approximately 20mL of SimplyBlue Safestain and incubated for 1 hour at room temperature. The gel was then washed with 100 mL of water for 1 hour at room temperature. A second wash was done with 100 mL of water overnight at room temperature to increase band intensity and reduce background.

Western Blots

The gels were run as mentioned above for the SimplyBlue SafeStain procedure. They were then transferred for 45 min, at 100V in 4^{o}C. Once the transfer was complete, the nitrocellulose membrane was blocked in 5% non-fat dry milk in PBS-T for one hour at room temperature. It was then incubated with goat anti-Human IgG (H+L) HRP

conjugate (1:5000 in 5% dry-milk in PBS-T) for 1 hour at 4^{o}C. Once the incubation was over, five 10-min washes were performed with PBS-T at room temperature. The membrane was then developed using an ECL Kit.

***Human protein microarrays for detection of autoantibodies**:*

Invitrogen's ProtoArray v5.1 Human Protein Microarrays (Cat. No. PAH0525020, Invitrogen, Carlsbad, CA, USA), each containing 9,486 unique human protein antigens (www.invitrogen.com/protoarray), were used for aAB detection. All proteins were expressed as glutathione s-transferase (GST) fusion proteins in insect cells, purified under native conditions, and spotted in duplicate onto nitrocellulose-coated glass slides. Arrays were probed with serum, processed and scanned according to the manufacturer's instructions. Briefly, microarrays were blocked using Blocking Buffer (Cat. No. PA055, Invitrogen) and each was incubated with either the glycosylated or non-glycosylated fractions from the ConA column. The glycosylated fraction was diluted to 1:34 in washing buffer, and the non-glycosylated fraction was diluted 1:192 in washing buffer. These dilutions were chosen to ensure that sufficient quantities of autoantibodies would be present to fall within the dynamic range of detection of the arrays. After washing, arrays were probed with anti-human IgG (H + L) conjugated to AlexaFluor 647 (Cat. No. A-21445, Invitrogen) diluted 1:2000 in washing buffer. Arrays were then washed, dried, and immediately scanned with a GenePix 4000B Fluorescence Scanner (Molecular Devices, Sunnyvale, CA, USA). Fluorescence data were acquired by aligning the Genepix Array List onto the microarray using the

Genepix Pro analysis software. The resulting Genepix results files were imported into Invitrogen's *Prospector* 5.2.3 microarray analysis software for analysis.

Table 1. Timeline of samples taken from the pregnant patient

Healthy Pregnant Control		
Sample ID	**Date**	**Timeline**
P1	8/15/2013	5 years Pre-pregnancy
P2	3/14/2018	16 weeks
P3	4/12/2018	20 weeks
P4	6/7/2018	28 weeks
P5	8/9/2018	37 weeks
P6	3/19/2019	7 months post-pregnancy

Table 1: The dates and gestational times of the longitudinal samples taken from a single healthy pregnant patients, spanning a period of 6 years.

Table 2. Relative binding strength for protein A and protein G

Species	Subclass	Protein A binding	Protein G binding
Human	IgA	Variable	-
	IgD	-	-
	IgG_1	++++	++++
	IgG_2	++++	++++
	IgG_3	-	++++
	IgG_4	++++	++++
	IgM	Variable	-

https://cdn.gelifesciences.com/dmm3bwsv3/AssetStream.aspx?mediaformatid=10061&destinationid=10016&assetid=11660

Table 2: Relative binding strength of different antibody subclasses from humans to Protein A and Protein G, measured on a competitive ELISA test.

Table 3. Recommended buffers to use with Protein G HP SpinTrap Columns

Binding Buffer	20 mM sodium phosphate, pH 7.0
Elution Buffer	0.1 M glycine-HCl, pH 2.7
Neutralizing Buffer	1M Tris-HCl, pH 9.0

Table 3: Chemical components of the buffers used for the Protein G HP SpinTrap Columns.

Table 4. Protocol Overview

Human Serum	**Protein G Column**	**Protein G Elution Fraction**	**Con-A Column**	**Bound to ConA Column** G-p-IgG G-a-IgG	**Human Protein Microarray**
G-p-Ig NG-p-Ig G-a-Ig NG-a-Ig	*Purify IgG from other IgM, IgA, IgD and IgE*	G-p-IgG NG-p-IgG G-a-IgG NG-a-IgG	*Purify G-IgG from NG - IgG*	**ConA Column Flow Through** NG-p-IgG NG-a-IgG	*Only the a-IgG, recognizing human derived antigens, will bind*
G = Glycosylated *NG = Non-Glycosylated* *p = Antibodies targeting pathogenic or non-self-antigen* *a = Autoantibodies targeting self-antigens* *Ig = Immunoglobulin (composed of IgG, IgA, IgM and IgD, and IgE)* *IgG = Immunoglobulin G*					

Table 4: Protocol overview for purifying glycosylated and non-glycosylated IgG fractions from serum.

RESULTS

Separation of the glycosylated and non-glycosylated IgG from human serum using column chromatography and confirmation using western blots

We first isolated IgG, and further the glycosylated and non-glycosylated IgG from serum obtained from a healthy female control. Supplementary tables S1 to S3 have the detailed information regarding how many milligrams of IgG were present in each fraction of interest coming off of both the Protein G and ConA columns in each experiment, and supplementary figures S1 to S5 show the western blot and Coomassie stains for each respective trial. Using between 300-350 uL of serum produced elution fractions from the PG column that were concentrated enough for the ConA column, without overwhelming the binding capacity of the PG column. In the western blots that contain the flow-through fractions 1 through 3 of the PG column, we expect to see a lack of bands in these respective lanes, indicating that most of the IgG has bound to the column at this point and therefore would be absent in these flow-through fractions. In all three experiments, we confirmed that, in both the PG and ConA columns, the majority of the target protein (IgG, Glycosylated IgG and Non-glycosylated IgG) was eluted in the first two elution fractions, as demonstrated both by the reduced milligrams of IgG measured by the spectrophotometer, and the dimming of the IgG heavy and light chain bands on the western blots.

Calculation of percent glycosylated antibodies

The protein G column binds to almost all of the IgG in human serum. Therefore, the elution fractions of the Protein G column contain the purified IgG. This purified IgG is then loaded onto the ConA column. The initial flow-through fractions contain the non-bound IgG which, in this case, corresponds to the non-glycosylated IgG. The elution fractions contain the glycosylated IgG. However, determining which fractions contribute to the non-glycosylated IgG and which fractions contribute to the glycosylated IgG is not as straightforward as flow-through vs. elution fractions. In theory, all of the glycosylated antibodies would come out in the elution fractions. However, it is possible that some of the glycosylated IgG which had bound to the ConA lectin with lower affinity can come off in flow-through fractions 4 and 5.

In table 5, we have demonstrated how the percent glycosylation changes depending on where we assume the line for dividing glycosylated vs. non-glycosylated fractions is. We started with a simple assumption that all flow-through fractions contained the non-glycosylated IgG and all the elution fractions contained the glycosylated IgG. Using this assumption, 94.70% $\pm$ 1.52% of the recovered IgG was non-glycosylated, and 5.3% $\pm$ 1.52% was glycosylated. If we assume that the majority of the non-glycosylated and glycosylated antibodies comes out in the first two fraction (F1, F2, E1, E2), then 94.75% $\pm$ 1.36% of the recovered IgG was non-glycosylated and 5.25% $\pm$ 1.36% was glycosylated. Next we assumed that the weakly bound glycosylated IgG may come off starting at the fourth and fifth flow through fractions.

Using that assumption, 87.60% $\pm$ 5.16% of the recovered IgG is non-glycosylated while 12.40% $\pm$ 5.16% of the recovered IgG is glycosylated.

Based on previously published values, we were expecting to see ~10% of the recovered IgG to be glycosylated, so we suspected that we were perhaps not recovering sufficient protein in our elution fractions. To address this, we decided to increase the incubation time for each elution fraction from 5 minutes to 10 minutes. Supplementary table S4 shows the milligrams of IgG recovered in each fraction, when elution fractions were incubated for 10 minutes, and supplementary figures S6 and S7 have the western blot and SDS-PAGE visualization for IgG purification. The longer period of incubation for the elution fraction almost doubled our glycosylated IgG percentages (table 5), and placed it into a range that was more in line with previous research. Therefore, we decided to make this change in the protocol from this point forward. Since with the longer period of incubation, our assumption that the flow-through fractions hold the non-glycosylated components and the elution fractions hold the glycosylated components fell within percentages that was in line with previous research, we decided to stay with that method of calculating our percent glycosylated antibodies.

Table 5. Calculation of percent glycosylated vs non-glycosylated antibodies

Fractions from the Pierce Glycoprotein Isolation Kit, ConA					
Fraction	**Experiment 1 500 uL Serum**	**Experiment 2 100 uL Serum**	**Experiment 3 250 uL Serum**	**Avg* (SD)**	**Experiment 4 300 uL Serum 10 min Elution**
Flow-Through 1	1.303	0.532	0.790		0.551
Flow-Through 2	0.449	0.059	0.119		0.182
Flow-Through 3	0.204	0.015	0.056		0.111
Flow-Through 4	0.139	0.012	0.081		0.068
Flow-Through 5	0.096	0.007	0.040		0.062
Elution 1	0.057	0.015	0.041		0.070
Elution 2	0.047	0.008	0.021		0.047
Elution 3	0.037	0.000	0.011		0.029
Total IgG	2.332	0.648	1.159		1.120
F1 – F5	93.95%	96.45%	93.70%	**94.70% (1.52%)**	86.96%
E1 – E3	6.05%	3.55%	6.30%	**5.30% (1.52%)**	13.04%
F1 – F2	94.40%	96.25%	93.61%	**94.75% (1.36%)**	86.24%
E1 – E2	5.60%	3.75%	6.39%	**5.25% (1.36%)**	13.76%
F1 – F3	85.23%	93.52%	84.06%	**87.60% (5.16%)**	77.36%
F4 – E2	14.77%	6.48%	15.94%	**12.40% (5.16%)**	22.64%

Table 5: Determination of percent glycosylated antibodies based on which flow-through and elution fractions we assume contain glycosylated and non-glycosylated antibodies. Weakly bound non-glycosylated antibodies may come off in later flow-through fractions (flow-through 4 or 5), however, this has not been confirmed.

*****Average values do not include experiment 4 data

Separation of glycosylated and non-glycosylated IgG from longitudinal samples taken during and after pregnancy

We next utilized the protocol established above to separate the glycosylated and non-glycosylated IgG fractions from our pregnancy sera. Three samples were selected: from early pregnancy (P3, 20 weeks gestation), late pregnancy (P5, 37 weeks gestation) and 7 months post-pregnancy (P6). The amount of protein recovered was determined by using a Bradford Assay (tables 6-8). We further confirmed separation of the glycosylated and non-glycosylated fractions using western blots (figures 1, 3, and 5 respectively) and Coomassie stains with Simplyblue SafeStain (figures 2, 4, and 6 respectively).

Table 6. Spectrophotometer readings from purification of IgG, glycosylated IgG and non-glycosylated IgG from serum of a healthy pregnant woman obtained at 20 weeks gestation

Protein G HP SpinTrap Column					
Fraction	**Fraction Volume (uL)**	**Dilution Factor**	**OD @ 595nm**	**Protein Concentration (ug/uL)**	**mg of IgG**
Elution 1	405	1:10	0.100	3.333	1.350
Elution 2	410	1:1	0.154	1.027	0.421
Pierce Glycoprotein Isolation Kit, ConA					
Flow-Through 1	365	1:1	0.287	1.913	0.698
Flow-Through 2	390	-	0.127	0.423	0.165
Flow-Through 3	380	-	0.024	0.08	0.030
Flow-Through 4	375	-	0.041	0.137	0.051
Flow-Through 5	400	-	0.030	0.100	0.040
Elution 1	190	-	0.099	0.330	0.063
Elution 2	190	-	0.055	0.183	0.035
Elution 3	190	-	0.016	0.053	0.010

Table 6: IgG was purified from 350 uL of serum from a woman at 20 weeks gestation (P3) using a Protein G HP SpinTrap Column according to manufacturer's protocol. The protein concentration of each elution fraction was determined using a spectronic spectrophotometer. The first fraction from the Protein G column served as the starting sample for the ConA Column (Pierce Glycoprotein Isolation Kit, ConA). The sample was diluted 4:1 with 5X Binding/Wash Buffer provided in the kit. The protein concentration of each flow-through fraction (corresponding to the non-glycosylated IgG) and elution fraction (corresponding to the glycosylated IgG) was determined as mentioned above.

Figure 1. Purification of IgG, glycosylated IgG and non-glycosylated IgG from serum of a healthy pregnant woman obtained at 20 weeks gestation

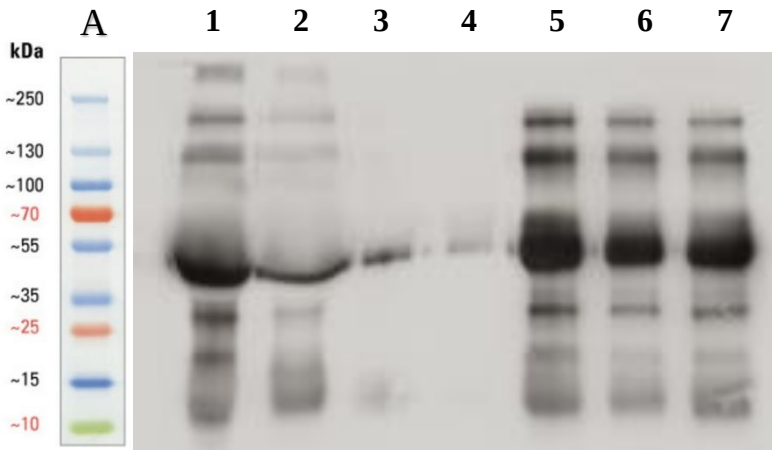

1. **Serum at 20wks gestation**
2. **PG Flow-Through 1**
3. **PG Flow-Through 2**
4. **PG Flow-Through 3**
5. **PG Elution Fraction 1**
6. **PG Elution Fraction 2**
7. **ConA Flow-Through 1**

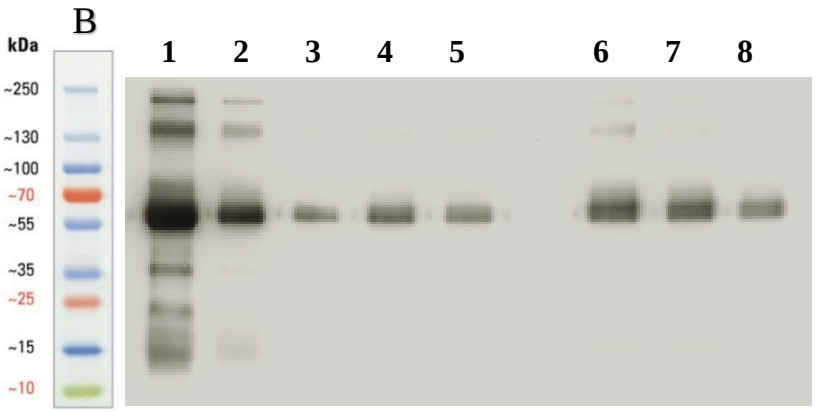

1. **ConA Flow-Through 1**
2. **ConA Flow-Through 2**
3. **ConA Flow-Through 3**
4. **ConA Flow-Through 4**
5. **ConA Flow-Through 5**
6. **ConA Elution Fraction 1**
7. **ConA Elution Fraction 2**
8. **ConA Elution Fraction 3**

Figure 1: IgG was purified from 350 uL serum obtained at 20 weeks gestation (A1), and the flow-through and elution fractions from the Protein G (A2-A6) and ConA Columns (A7, B1-B8) were collected and samples were prepared for a western blot using 6X Laemmli buffer. Goat anti-human IgG (H+L) HRP conjugate was used as the primary antibody (1:5000).

Figure 2. Purification of IgG, glycosylated IgG and non-glycosylated IgG from serum of a healthy pregnant woman obtained at 20 weeks gestation

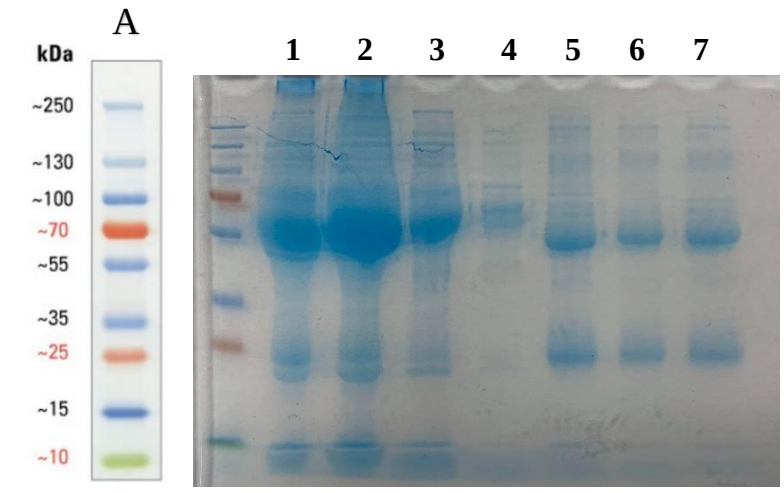

1. **Serum at 20wks gestation**
2. **PG Flow-Through 1**
3. **PG Flow-Through 2**
4. **PG Flow-Through 3**
5. **PG Elution Fraction 1**
6. **PG Elution Fraction 2**
7. **ConA Flow-Through 1**

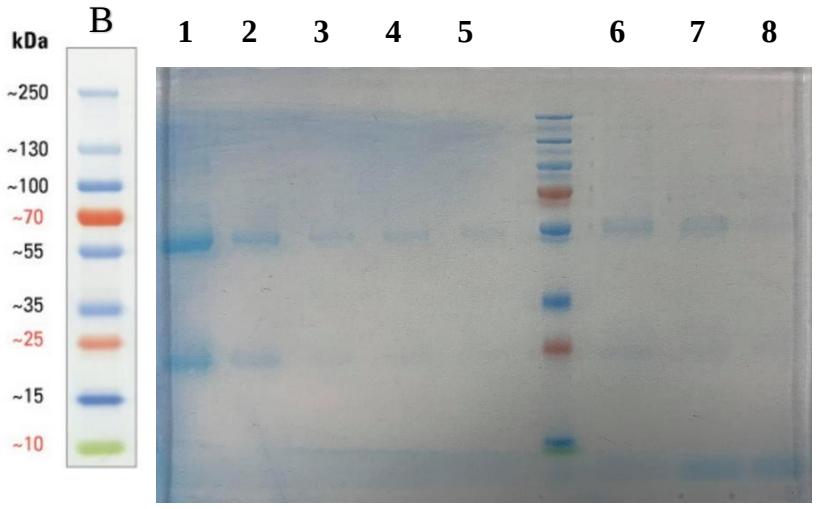

1. **ConA Flow-Through 1**
2. **ConA Flow-Through 2**
3. **ConA Flow-Through 3**
4. **ConA Flow-Through 4**
5. **ConA Flow-Through 5**
6. **ConA Elution Fraction 1**
7. **ConA Elution Fraction 2**
8. **ConA Elution Fraction 3**

Figure 2: IgG was purified from 350 uL serum obtained at 20 weeks gestation (A1), and the flow-through and elution fractions from the Protein G (A2-A6) and ConA Columns (A7, B1-B8) were collected and samples were run on an SDS-PAGE Gel to be stained using SimplyBlue SafeStain.

Table 7. Spectrophotometer readings from purification of IgG, glycosylated IgG and non-glycosylated IgG from serum of a healthy pregnant woman obtained at 37 weeks gestation

Protein G HP SpinTrap Column					
Fraction	**Fraction Volume (uL)**	**Dilution Factor**	**OD @ 595nm**	**Protein Concentration (ug/uL)**	**mg of IgG**
Elution 1	385	1:10	0.107	3.567	1.373
Elution 2	425	1:1	0.139	0.927	0.394
Pierce Glycoprotein Isolation Kit, ConA					
Flow-Through 1	340	1:1	0.216	1.440	0.490
Flow-Through 2	365	-	0.119	0.397	0.145
Flow-Through 3	425	-	0.050	0.167	0.071
Flow-Through 4	390	-	0.032	0.107	0.042
Flow-Through 5	400	-	0.039	0.130	0.052
Elution 1	190	-	0.089	0.297	0.056
Elution 2	190	-	0.061	0.203	0.039
Elution 3	190	-	0.039	0.130	0.025

Table 7: IgG was purified from 300 uL of serum from a woman at 37 weeks gestation (P3) using a Protein G HP SpinTrap Column according to manufacturer's protocol. The protein concentration of each elution fraction was determined using a spectronic spectrophotometer. The first fraction from the Protein G column served as the starting sample for the ConA Column (Pierce Glycoprotein Isolation Kit, ConA). The sample was diluted 4:1 with 5X Binding/Wash Buffer provided in the kit. The protein concentration of each flow-through fraction (corresponding to the non-glycosylated IgG) and elution fraction (corresponding to the glycosylated IgG) was determined as mentioned above.

Figure 3: Purification of IgG, glycosylated IgG and non-glycosylated IgG from serum of a healthy pregnant woman obtained at 37 weeks gestation

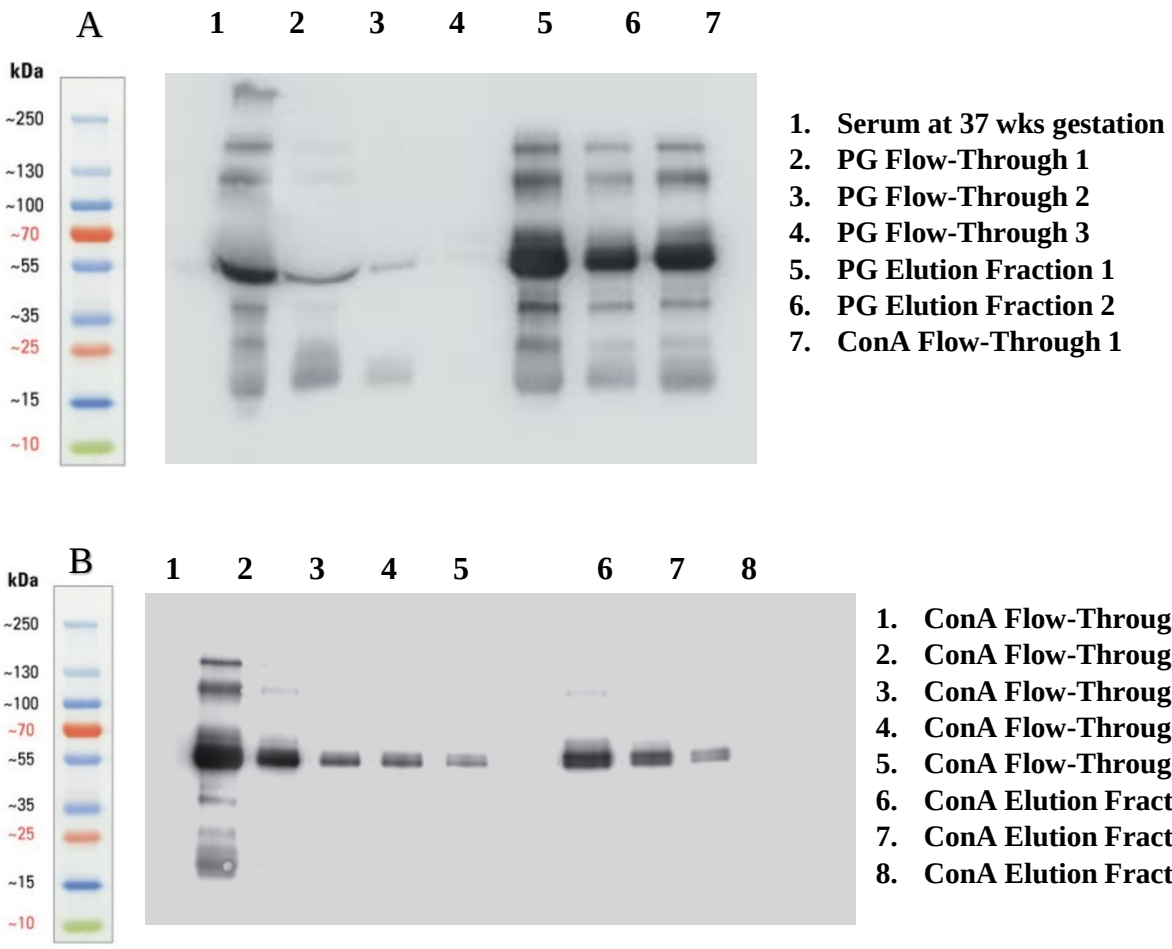

Figure 3: IgG was purified from 300 uL serum obtained at 37 weeks gestation (A1), and the flow-through and elution fractions from the Protein G (A2-A6) and ConA Columns (A7, B1-B8) were collected and samples were prepared for a western blot using 6X Laemmli buffer. Goat anti-human IgG (H+L) HRP conjugate was used as the primary antibody (1:5000).

Figure 4. Purification of IgG, glycosylated IgG and non-glycosylated IgG from serum of a healthy pregnant woman obtained at 37 weeks gestation

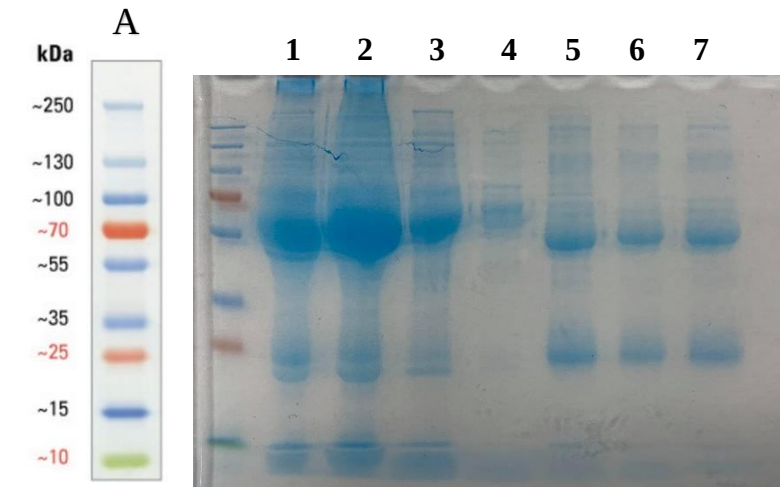

1. **Serum at 37 wks gestation**
2. **PG Flow-Through 1**
3. **PG Flow-Through 2**
4. **PG Flow-Through 3**
5. **PG Elution Fraction 1**
6. **PG Elution Fraction 2**
7. **ConA Flow-Through 1**

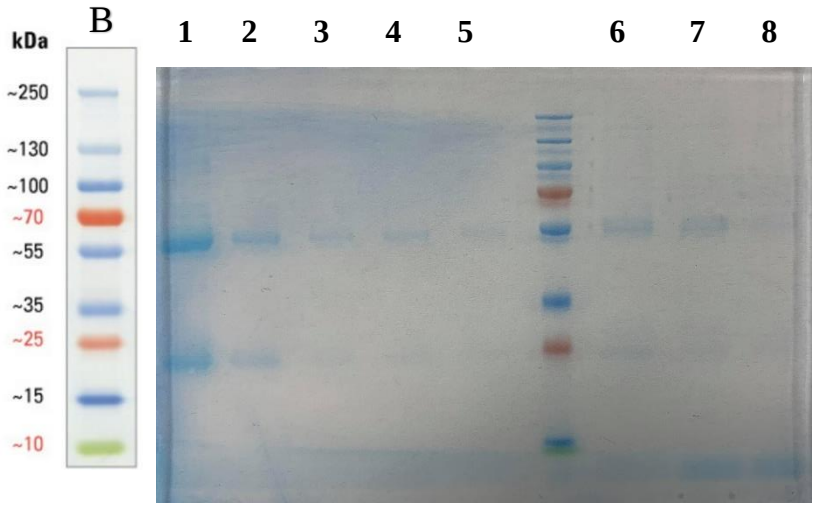

1. **ConA Flow-Through 1**
2. **ConA Flow-Through 2**
3. **ConA Flow-Through 3**
4. **ConA Flow-Through 4**
5. **ConA Flow-Through 5**
6. **ConA Elution Fraction 1**
7. **ConA Elution Fraction 2**
8. **ConA Elution Fraction 3**

Figure 4: IgG was purified from 300 uL serum obtained at 37 weeks gestation (A1), and the flow-through and elution fractions from the Protein G (A2-A6) and ConA Columns (A7, B1-B8) were collected and samples were run on an SDS-PAGE Gel to be stained using SimplyBlue SafeStain.

Table 8. Purification of glycosylated and non-glycosylated IgG from serum collected at 7 months post-pregnancy

Protein G HP SpinTrap Column					
Fraction	**Fraction Volume (uL)**	**Dilution Factor**	**OD @ 595nm**	**Protein Concentration (ug/uL)**	**mg of IgG**
Elution 1	405	1:10	0.151	5.033	2.039
Elution 2	420	1:1	0.232	1.547	0.650
Pierce Glycoprotein Isolation Kit, ConA					
Flow-Through 1	320	1:1	0.353	2.353	0.753
Flow-Through 2	400	-	0.190	0.633	0.253
Flow-Through 3	340	-	0.058	0.193	0.066
Flow-Through 4	320	-	0.041	0.137	0.044
Flow-Through 5	485	-	0.033	0.110	0.053
Elution 1	190	-	0.117	0.390	0.074
Elution 2	190	-	0.089	0.297	0.056
Elution 3	190	-	0.036	0.120	0.023

Table 8: IgG was purified from 350 uL of serum from a woman 7 months post-pregnancy (P6) using a Protein G HP SpinTrap Column according to manufacturer's protocol. The protein concentration of each elution fraction was determined using a spectronic spectrophotometer. The first elution fraction from the Protein G column served as the starting sample for the ConA Column (Pierce Glycoprotein Isolation Kit, ConA). The sample was diluted 4:1 with 5X Binding/Wash Buffer provided in the kit. The protein concentration of each flow-through fraction (corresponding to the non-glycosylated IgG) and elution fraction (corresponding to the glycosylated IgG) was determined as mentioned above.

Figure 5: Purification of IgG, glycosylated IgG and non-glycosylated IgG from serum of a healthy pregnant woman obtained 7 months post-pregnancy

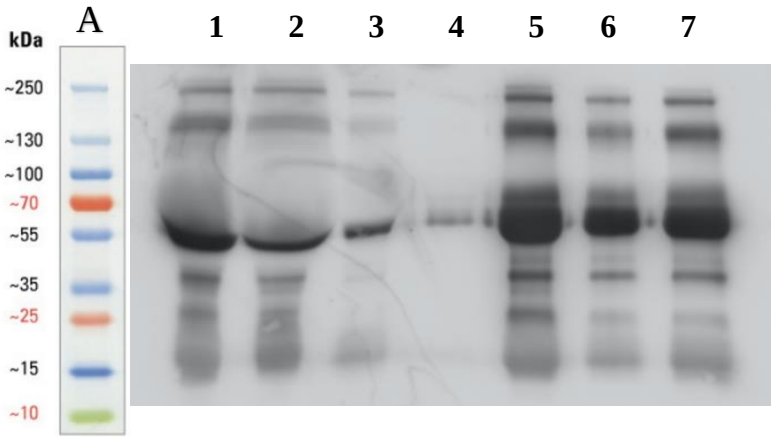

1. **Serum at 7 months post-pregnancy**
2. **PG Flow-Through 1**
3. **PG Flow-Through 2**
4. **PG Flow-Through 3**
5. **PG Elution Fraction 1**
6. **PG Elution Fraction 2**
7. **ConA Flow-Through 1**

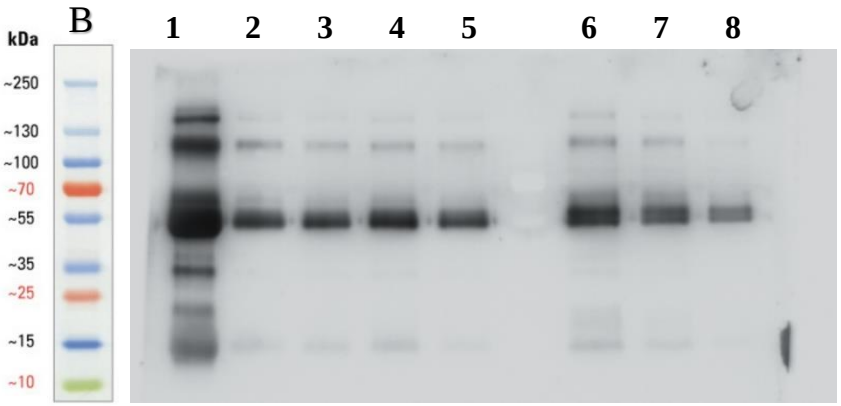

1. **ConA Flow-Through 1**
2. **ConA Flow-Through 2**
3. **ConA Flow-Through 3**
4. **ConA Flow-Through 4**
5. **ConA Flow-Through 5**
6. **ConA Elution Fraction 1**
7. **ConA Elution Fraction 2**
8. **ConA Elution Fraction 3**

Figure 5: IgG was purified from 350 uL serum obtained 7 months post-pregnancy (A1), and the flow-through and elution fractions from the Protein G (A2-A6) and ConA Columns (A7, B1-B8) were collected and samples were prepared for a western blot using 6X Laemmli buffer. Goat anti-human IgG (H+L) HRP conjugate was used as the primary antibody (1:5000).

Figure 6. Purification of IgG, glycosylated IgG and non-glycosylated IgG from serum of a healthy pregnant woman obtained at 7 months post-pregnancy

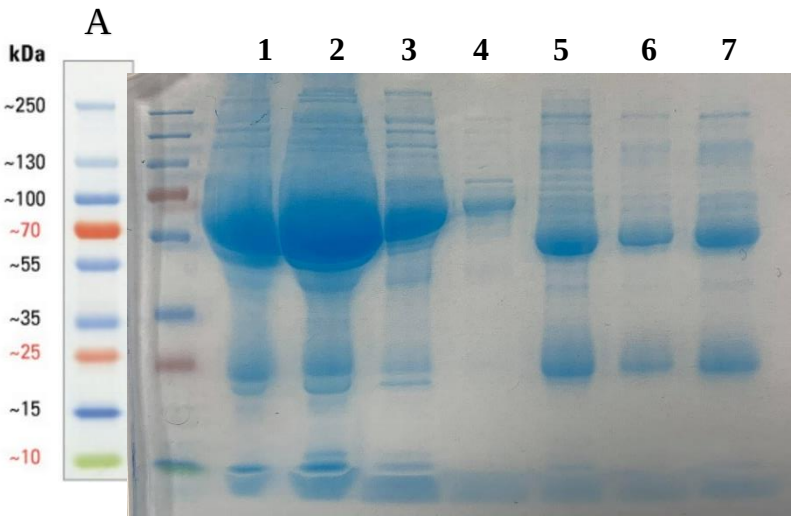

1. **Serum at 7 months post-pregnancy**
2. **PG Flow-Through 1**
3. **PG Flow-Through 2**
4. **PG Flow-Through 3**
5. **PG Elution Fraction 1**
6. **PG Elution Fraction 2**
7. **ConA Flow-Through 1**

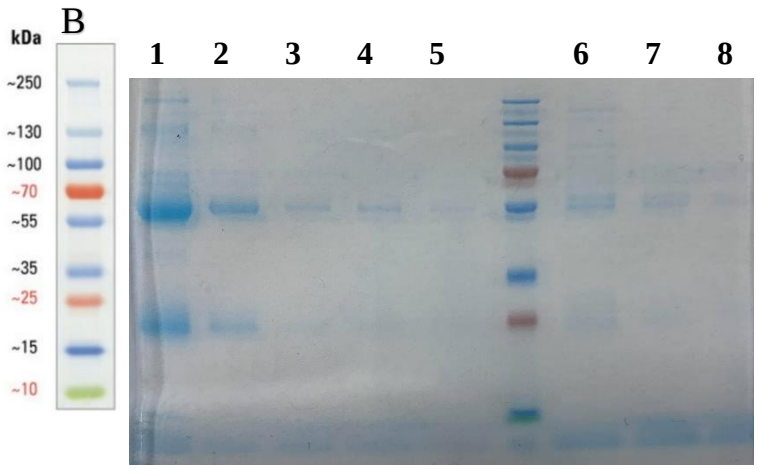

1. **ConA Flow-Through 1**
2. **ConA Flow-Through 2**
3. **ConA Flow-Through 3**
4. **ConA Flow-Through 4**
5. **ConA Flow-Through 5**
6. **ConA Elution Fraction 1**
7. **ConA Elution Fraction 2**
8. **ConA Elution Fraction 3**

Figure 6: IgG was purified from 350 uL serum obtained 7 months post-pregnancy (A1), and the flow-through and elution fractions from the Protein G (A2-A6) and ConA Columns (A7, B1-B8) were collected and samples were run on an SDS-PAGE Gel to be stained using SimplyBlue SafeStain.

Table 9: Calculation of percent glycosylated vs non-glycosylated antibodies throughout pregnancy

Mg of IgG in each fraction from the Pierce Glycoprotein Isolation Kit, ConA			
Fraction	**20 Weeks Gestation**	**37 Weeks Gestation**	**7 Months Post-Pregnancy**
Flow-Through 1	0.698	0.490	0.753
Flow-Through 2	0.165	0.145	0.253
Flow-Through 3	0.030	0.071	0.066
Flow-Through 4	0.051	0.042	0.044
Flow-Through 5	0.040	0.052	0.053
Elution 1	0.063	0.056	0.074
Elution 2	0.035	0.039	0.056
Elution 3	0.010	0.025	0.023
Total IgG	1.092	0.920	1.322
F1 – F5	90.11%	86.96%	88.43%
E1 – E3	9.89%	13.04%	11.57%
F1 – F2	89.80%	86.99%	88.56%
E1 – E2	10.20%	13.01%	11.44%
F1 – F3	81.78%	76.74%	81.09%
F4 – E3	18.22%	23.26%	18.91%

Table 9: Determination of percent glycosylated antibodies based on which flow-through and elution fractions we assume contain glycosylated and non-glycosylated antibodies. Weakly bound non-glycosylated antibodies may come off in later flow-through fractions, however, this has not been confirmed.

Determining dilution factors that will allow us to analyze the data within the dynamic range of the microarrays

Starting with 350 uL of sample P3 (20 weeks gestation), we first purified IgG from the serum, and then further separated the non-glycosylated and glycosylated fractions. The protein content (mg IgG) in each fraction is shown in table 10. Below is the logic we followed to determine our dilution for each sample. A few key assumptions had to be made, and will be highlighted as they come up.

350 uL serum = 35 arrays

If 10 uL of serum contains enough antibody content to probe one array, then 350 uL serum will contain enough antibodies to probe 35 arrays.

When using unmodified and undiluted serum to probe arrays, the serum is typically diluted 1:500 with wash buffer (10 uL serum into 4990 uL wash buffer). Therefore, since we started with 350 uL serum, in theory, we have enough antibody to probe 35 arrays.

350 uL serum = **35 arrays**

Elution 1	**Elution 2**
405 uL	410 uL
1.35 mg IgG	0.421 mg IgG
26.6 arrays	**8.4 arrays**

The 350 uL of loaded onto the protein G column, and two elution fractions were collected. Elution fraction 1 (405 uL) had 1.35 mg of IgG, while elution fraction 2 (410 uL) had 0.421 mg of IgG, for a total of 1.771 mg of IgG.

Key Assumption 1: Almost all of the IgG from the serum is retained by the PG column, and eluted out in the two elution fractions.

With that assumption in place, we determined that elution fraction 1 contains 76.2% of the total IgG, and elution fraction 2 contains 23.8% of the total IgG, and divide the theoretical number of arrays that each fraction would be able to probe accordingly.

Elution Fraction 1 – 405 uL

$$\frac{1.35\ mg\ IgG}{405\ uL} = \frac{X\ mg\ IgG}{330\ uL}$$

X = 1.1 mg of IgG
21.7 arrays

To prepare the sample for the ConA column, 330 uL of PG elution fraction 1 was diluted with 82.5 uL of the 5X wash/binding buffer. 330 uL of elution fraction 1 contains 1.1 mg of IgG (enough to probe 21.7 arrays).

1.1 mg of IgG = **21.6 arrays**

FT 1	**EF 1**
365 uL	190 uL
0.698 mg IgG	0.063 mg Ig
14 arrays	**1.3 arrays**

ConA flow-through 1 (FT1) contains the majority of the non-glycosylated portion IgG, while the ConA elution fraction 1 (EF1) contains the majority of the glycosylated portion of IgG. Flow-through 1 contained 0.698 mg of IgG (64% of the amount of IgG loaded into the column), while elution fraction 1 contained 0.063 mg of IgG (5.8% of the IgG loaded on).

Key Assumption 2: The IgG content of each flow through and elution fraction is representation of the total IgG content of the serum, therefore, allowing us to use a single fraction to probe on the array.

Prevalence of glycosylated vs non-glycosylated aABs – nearly all individual aABs seem to be glycosylated and show profile similarity to the original profile derived from unaltered serum

Human protein microarrays were probed with flow-through fraction 1 and elution fraction 1 from samples P3 (20 weeks gestation), P5 (37 weeks gestation) and P6 (7 months post-pregnancy), using dilutions that were determined using the methodology explained above (table 10). Figures 7 – 9 show a comparison of the aAB profiles of serum, compared to the glycosylated and non-glycosylated fractions obtained from serum. Even though the dilutions for the three samples are different, we see that there is a great degree of profile similarity by comparing the glycosylated and non-glycosylated profiles to the serum profile. Some of the portions of the profile that deviate from the serum profile are highlighted in yellow as examples.

Table 10: Respective dilutions used to probe human protein microarrays

Sample	Fraction	Dilution
P3 (20 weeks gestation)	Flow-Through (NG)	1:192
	Elution Fraction (G)	1:34
P5 (37 weeks gestation)	Flow-Through (NG)	1:122
	Elution Fraction (G)	1:42
P6 (7 months post-pregnancy)	Flow-Through (NG)	1:152
	Elution Fraction (G)	1:37

Table 10: Dilutions were determined based on total protein recovered, and what fraction of the total protein each flow-through or elution fraction corresponded to. Samples were diluted with wash buffer for a total volume of 5mL to be used as the primary antibody used to probe human protein microarrays. NG = Non-Glycosylated, G = Glycosylated.

Figure 7. Autoantibody profiles of serum, glycosylated and non-glycosylated fractions from a pregnant patient at 20 weeks gestation

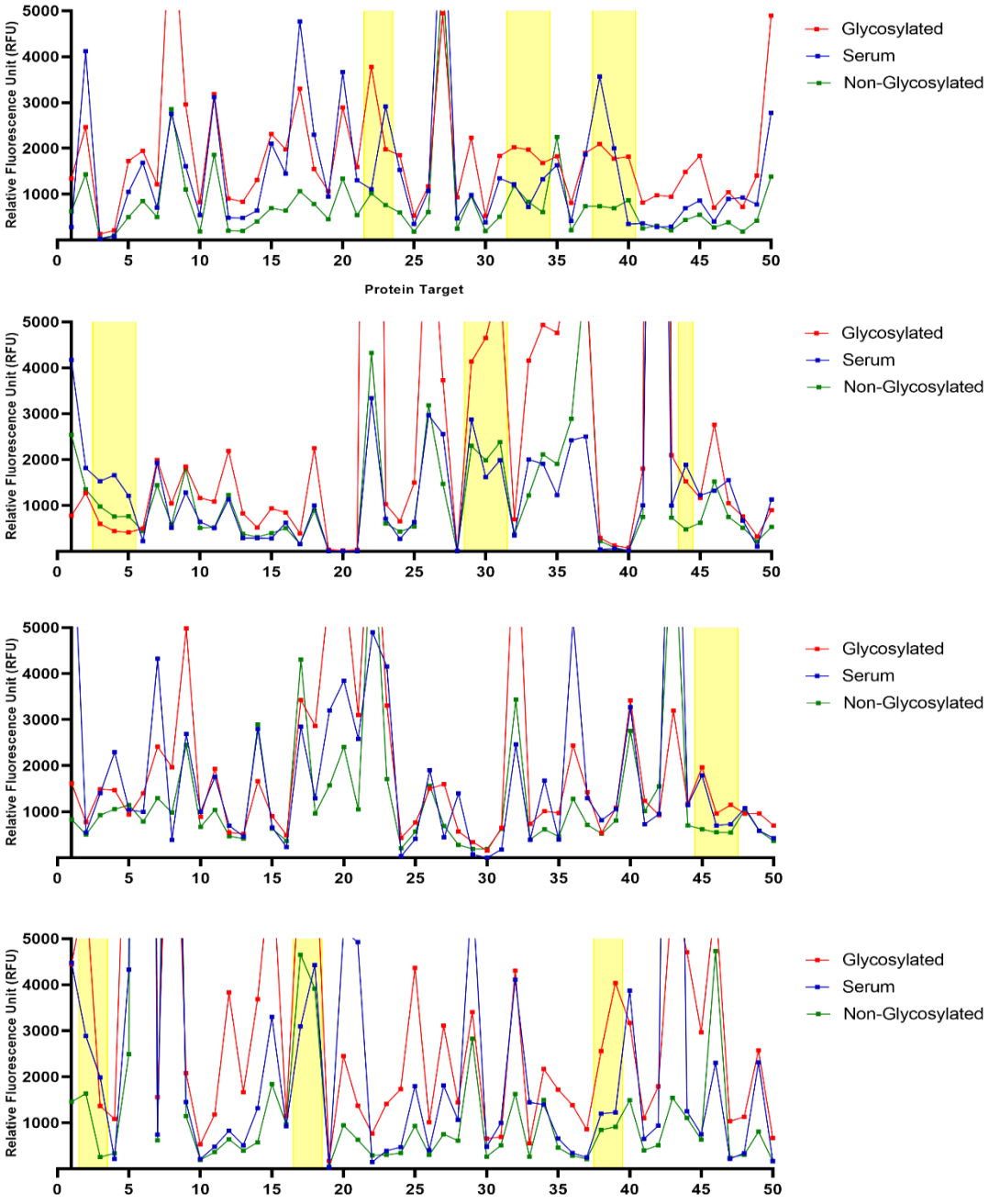

Figure 7: Four different blocks of 50 randomly selected proteins on human protein microarrays that were probed with serum, purified glycosylated IgG, and purified non-

glycosylated IgG obtained from a pregnant women at 20 weeks gestation. aAB profiles remain closely similar in all three profiles, indicating that almost all aAB are glycosylated and able to react with protein antigens despite being functionally univalent. Serum was diluted 1:500, glycosylated fraction 1:34 and the non-glycosylated fraction 1:192 with wash buffer.

Figure 8. Autoantibody profiles of serum, glycosylated and non-glycosylated fractions from a pregnant patient at 37 weeks gestation

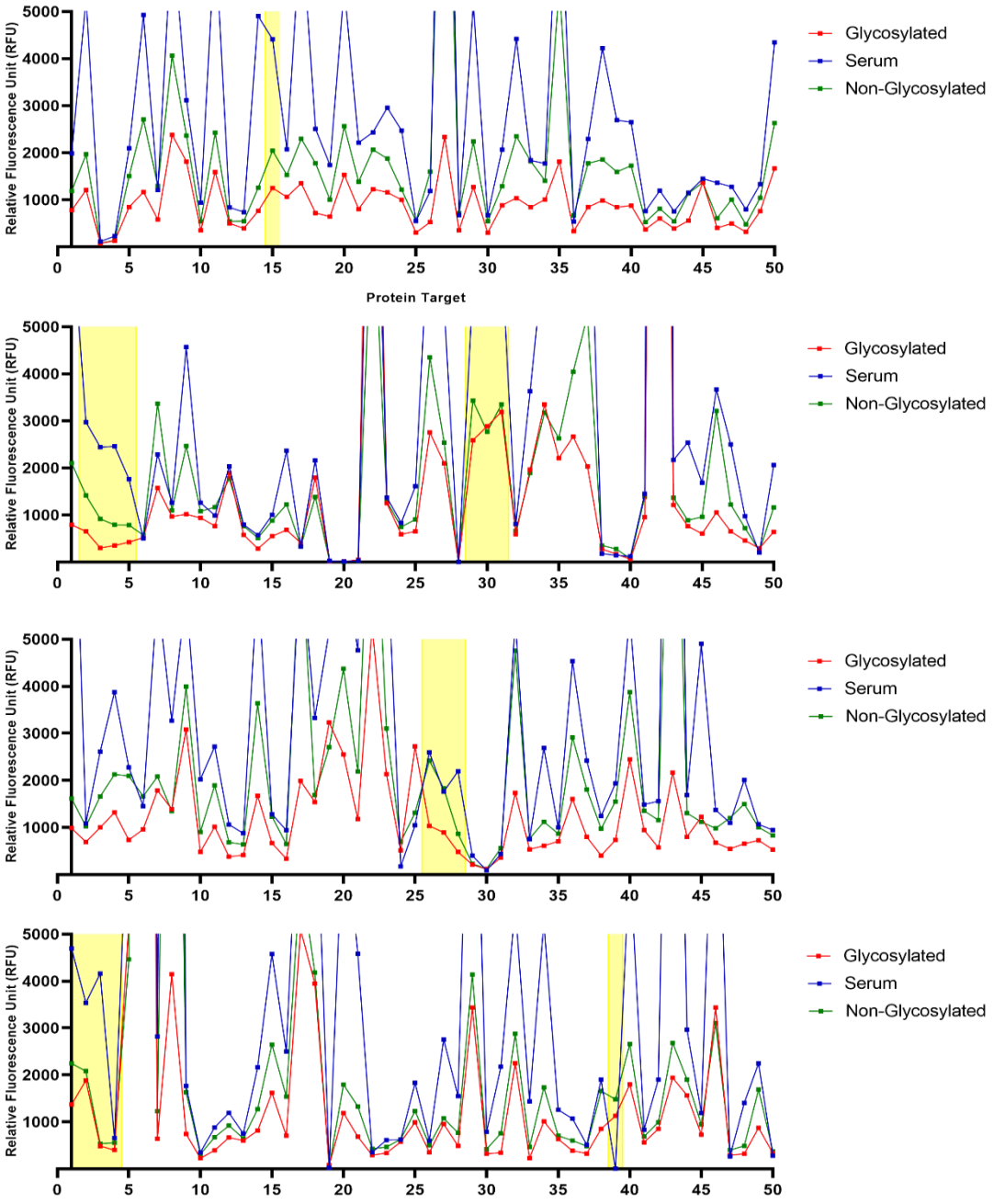

Figure 8: Four different blocks of 50 randomly selected proteins on human protein microarrays that were probed with serum, purified glycosylated IgG, and purified non-

glycosylated IgG obtained from a pregnant women at 37 weeks gestation. aAB profiles remain closely similar in all three profiles, indicating that almost all aAB are glycosylated and able to react with protein antigens despite being functionally univalent. Serum was diluted 1:500, glycosylated fraction 1:42 and the non-glycosylated fraction 1:122 with wash buffer.

Figure 9. Autoantibody profiles of serum, glycosylated and non-glycosylated fractions from a pregnant patient 7 months post-pregnancy

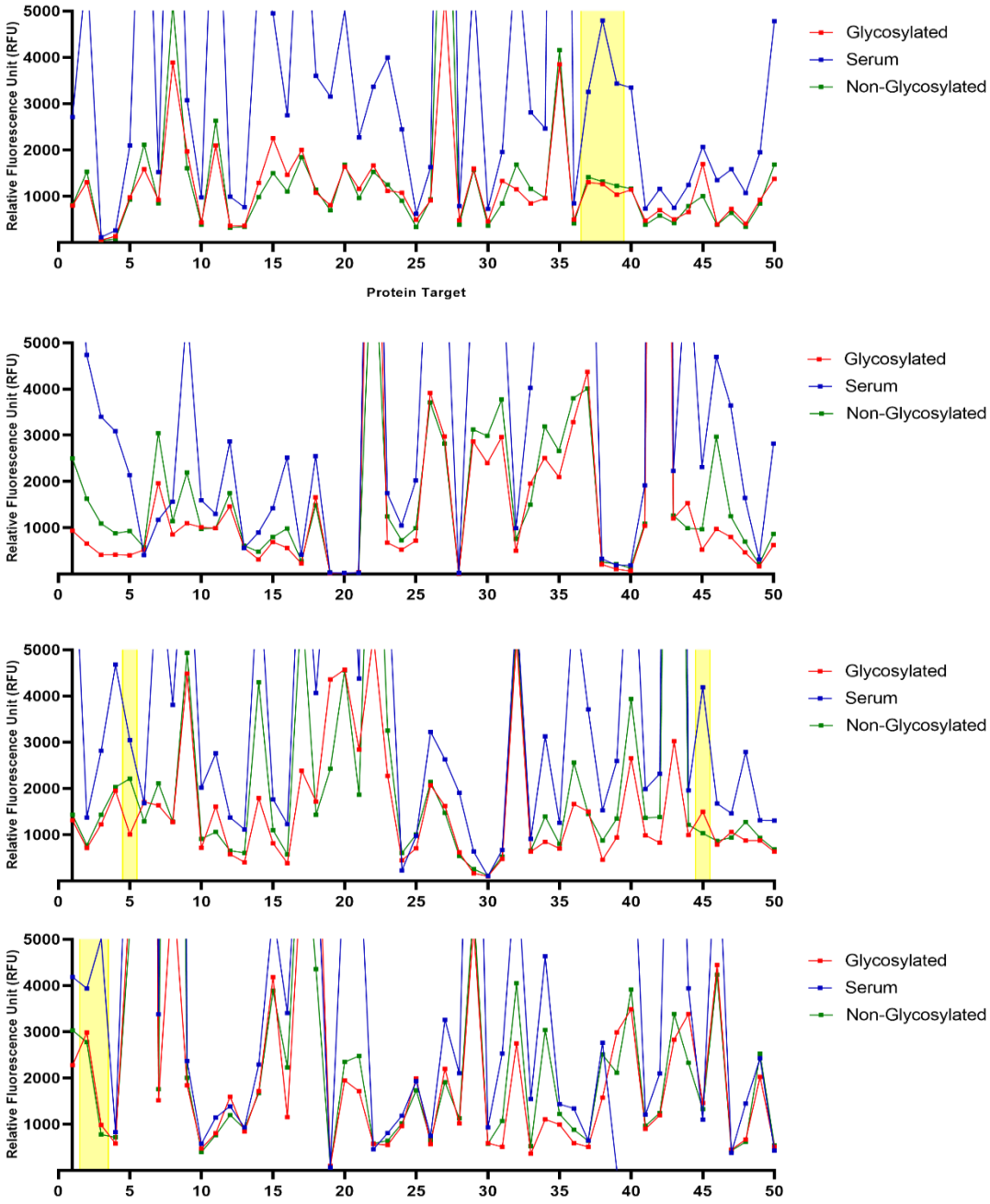

Figure 9: Four different blocks of 50 randomly selected proteins on human protein microarrays that were probed with serum, purified glycosylated IgG, and purified non-

glycosylated IgG obtained from a pregnant women at 7 months post-pregnancy. aAB profiles remain closely similar in all three profiles, indicating that almost all aAB are glycosylated and able to react with protein antigens despite being functionally univalent. Serum was diluted 1:500, glycosylated fraction 1:37 and the non-glycosylated fraction 1:152 with wash buffer.

Not all aABs are glycosylated to the same extent, and the extent of aAB glycosylation differs throughout pregnancy

Having already determined that almost all individual aABs were glycosylated, we next wanted to determine if all aABs were glycosylated to the same extent. Since each flow-through and elution fraction was probed onto the array using a different dilution, we first normalized the data by dividing the raw values by a factor that would normalize the raw data. We next calculated what percent of each aAB target was glycosylated and non-glycosylated. The number of aABs was divided into 10% subcategories and is represented in table 11 and figure 9.

Table 11. The total number of aABs categorized based on the extent of glycosylation and non-glycosylation

	% of total that is non-glycosylated									
	0-10%	**11-20%**	**21-30%**	**31-40%**	**41-50%**	**51-60%**	**61-70%**	**71-80%**	**81-90%**	**91-100%**
P3 20wks	10	4	12	42	145	648	2850	4067	1322	233
P5 37wks	40	60	334	914	1863	2708	2273	928	171	32
P6 7m post	1	2	2	6	10	24	159	1987	6518	625

Table 11: Distribution of the aABs based on what fraction of total is non-glycosylated. The samples include P3 (20 weeks gestation), P5 (37 weeks gestation), and P6 (7 months post-pregnancy).

Figure 10. Distribution of the extend of glycosylation in each aAB throughout pregnancy

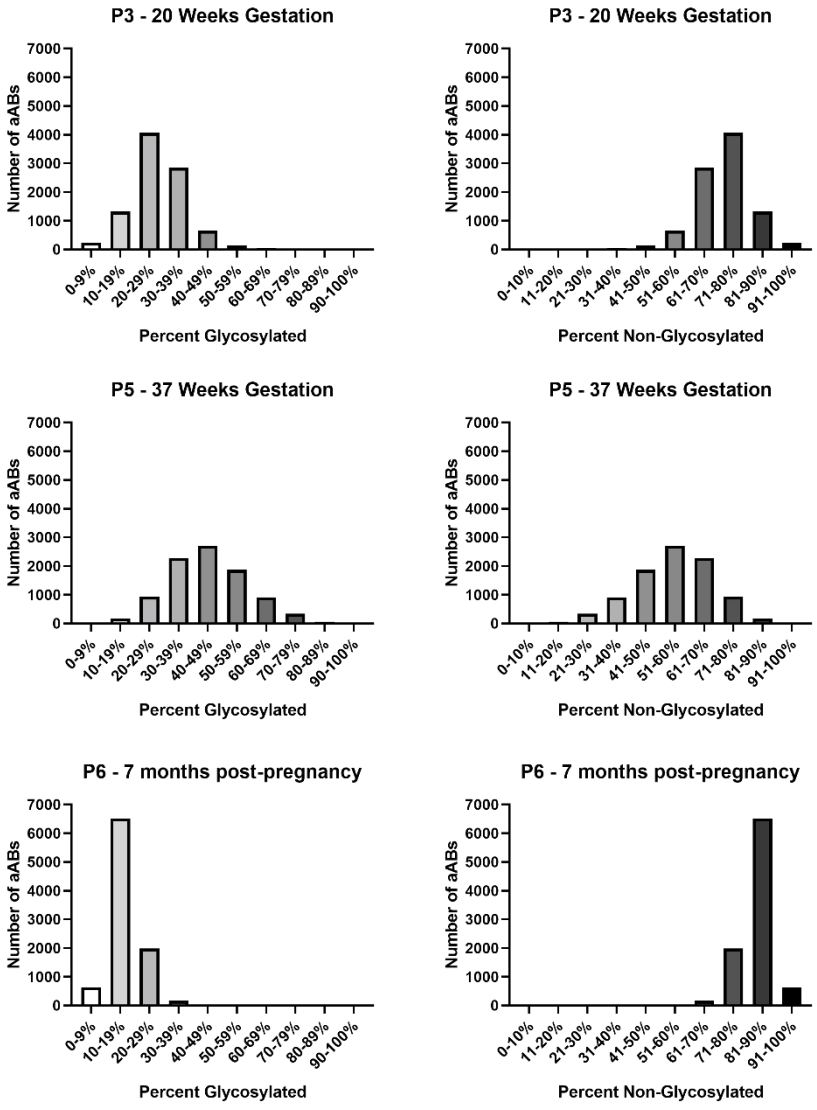

Figure 10: The percent glycosylation and non-glycosylation was calculated for each autoantibody. The aABs were categorized based on the extent of their glycosylation. There is a shift towards most aAB species being 70 – 100% non-glycosylated after pregnancy.

DISCUSSION

In this study, we used chromatography and human protein microarrays to determine the prevalence and distribution of glycosylated aABs on longitudinal samples taken from a pregnant patient. We separated the glycosylated and non-glycosylated IgG from serum in order to answer two key questions: (1) do autoantibodies also get glycosylated, and (2) if they are glycosylated, are they all glycosylated to the same extent.

Previous research had documented an increase in the percentage of total glycosylated antibodies during pregnancy, to levels as high as 50% [2], while only 15 to 25% of antibodies are glycosylated in healthy non-pregnant individuals [1]. We used Protein G affinity chromatography columns in order to separate the IgG subclass of immunoglobulins. This was followed by the use of Concanavalin A (ConA) chromatography columns to further separate the glycosylated IgG from the non-glycosylated IgG. For the purposes of this study, we were focused on specifically separating Fab glycosylated antibodies. Previous research had shown that ConA lectins bind specifically to the Fab glycosylated regions because they are more exposed and easily accessible. Glycosylation on the Fc region is located inside the naturally folded protein and is therefore not accessible to ConA lectins [17].

In our experiments, we determined that in healthy non-pregnant individuals, 13.04% of the recovered antibodies were glycosylated. However, this number did not

change with our longitudinal pregnant samples. The percent glycosylation remained relatively constant throughout and even post-pregnancy, with 9.89% glycosylation at 20 weeks gestation, 13.04% glycosylation at 37 weeks gestation and 11.57% glycosylation at 7 months post-pregnancy. This did not match what has been reported previously in the literature. In our future directions, we would like to repeat these experiments in order to be able to determine an average value and standard deviation for each sample, and to also perform the experiment on our other three longitudinal samples (pre-pregnancy, 16 weeks gestation, and 24 weeks gestation). However, since determining the percent glycosylation was not in the direct scope of our study, we decided to continue forward with our separated glycosylated and non-glycosylated antibody fractions to answer our first question: are autoantibodies also glycosylated? Does the 10 – 13% glycosylated fraction contain autoantibodies as well?

To answer this question, we probed human protein microarrays using ConA flow-through fraction 1 (representing our non-glycosylated fraction) and ConA elution fraction 1 (representing our glycosylated fraction). When serum samples are used to probe microarrays, they are diluted 1:500 with wash buffer. Ideally, after separating the glycosylated and non-glycosylated portions of serum IgG, we would be able to probe the arrays having diluted them 1:500 as well, in order to be able to directly compare our results. However, suspecting that separation of fractions might reduce the titers of aABs so low that it might fall under detection thresholds, we decided to probe the arrays with more concentrated dilutions to be within the dynamic range of detection. Therefore, since each sample and its corresponding fractions are diluted differently, it

makes direct comparison between our serum data and data from the glycosylated and non-glycosylated fractions difficult from a quantitative perspective, but still allows us to use this approach to answer a few key questions and to directly compare relative profiles.

Referring to figures 7-9, we see a great degree of profile similarity by comparing the glycosylated and non-glycosylated fraction to the un-altered serum profile. With the exception of slight deviations, we see that the shape of the profiles remain consistent, indicating that autoantibodies are in fact glycosylated. Due to the fact that we used different dilutions, it is difficult to directly compare RFU values. We know that longitudinal serum samples taken 9 years apart show fidelity not only in the shape of the profile, but rather even in their RFU or relative titers of aABs. We've addressed this by normalizing our raw RFUs respective to their dilutions, and looking at the percent glycosylation, which is further discussed below. However, regardless of the RFUs and aAB titers, the similarity in profile shape indicates that most aABs are not only glycosylated, but that the glycosylation mechanism affects them roughly the same way.

The presence of a glycan on the Fab region creates steric hindrance that could interfere with binding [4]. Since glycosylated antibodies are not able to bind to their targets with both of their Fab arms, they are unable to activate downstream immune functions. The presence of reactivity with the arrays confirms that univalent aABs are able to bind their protein targets in spite of the fact that they are functionally univalent.

We speculate that aAB glycosylation plays a role in modulating their immune function. Previous studies indicate that antibody glycosylation prevents activation of downstream sequellae such as recruiting other components of the immune system. Since the function of aABs are yet to be completely understood, it is difficult to say how glycosylation affects them. However, the presence of reactivity indicates that glycosylation does not prevent aABs from binding their targets. Therefore, glycosylation must play a modulatory role.

We next looked at the extent of glycosylation for each individual aAB that binds to its cognate protein target on the array. Since the RFU corresponds to the relative titer of aABs, we first normalized the glycosylated and non-glycosylated fractions to each other, and then calculated the corresponding percentages. aABs demonstrated the full range of glycosylation, with some being 0 to 100% glycosylated. However, the extent of glycosylation changed with each sample, with most of the aABs being 20-29% glycosylated at 20 weeks gestation (4067 aABs), then almost evenly distributed between 30-49% glycosylated at 37 weeks gestation (4981 aABs), followed by a sharp decrease post-pregnancy to 10-19% (6518 aABs). This is particularly interesting because even though the overall level of glycosylation did not change from pregnancy to post-pregnancy, we see a big difference in the extent of glycosylation in individual aABs.

The post-pregnancy reversion back to having mostly non-glycosylated aAB species hints at an immunomodulatory role that may be involved in creating an immune

tolerant environment for the fetus. One possible way to explain this phenomenon is from the perspective of exposure of the fetus to aABs at a sensitive time. It has previously been documented that the maternal transfer of IgG to the fetus begins early in the second trimester, and continues into the third trimester when most of the antibodies are transferred [18]. Continual fetal development will inevitably lead to exposure of many auto-antigens, especially those unique to the paternal contribution, which can be a potential target to aABs. Though we've proposed that the role of aABs is clearance of debris, in fetal development, exposure of self-antigens to aABs may have a detrimental effect. The debris generation in fetal development is going to be greater than average, simply due to the incredible amount of cell division, and organ growth and tissue renovation that needs to take place for a fetus to develop. Untimely exposure to aABs could interfere with this development and have detrimental effects. In previous studies of glycosylated antibodies in pregnancy, it was believed that antibodies that would recognize paternal antigens would get glycosylated in order to prevent fetal rejection by the mother's immune system [5, 7, 9, 19] and since half of the fetal antigens are presumably of maternal origin, maternal aABs could potentially bind to those antigens. With that in mind, it would make sense to increase aAB glycosylation during pregnancy. At 7 months post-pregnancy, most antibodies (6518) are only 10-19% glycosylated. If the 7 month post-pregnancy state of glycosylation represents a healthy non-pregnant state (i.e. baseline profile) this indicates that a low level of aAB glycosylation plays an everyday role in immune-modulation of aABs. During early pregnancy (P3), we see that a greater number of aABs (8239) shows broader distribution of glycosylation ranging from 10-39%. This number shifts further

in favor of glycosylation in late pregnancy, with the majority of aAB (7758) being 30-69% glycosylated. This together indicates a ramped up effort to mitigate their downstream sequellae post binding to fetal antigens. With this in mind, much further work is needed to not only look into the identity of the individual aABs that shift during pregnancy, but to also look into what is the original function of the extensive network of aABs and how glycosylation modulates their downstream functions.

SUPPLEMENTARY FIGURES

Table S1. Spectrophotometer readings from purification of IgG, glycosylated IgG and non-glycosylated IgG from a healthy non-pregnant individual

Protein G HP SpinTrap Column					
Fraction	**Fraction Volume (uL)**	**Dilution Factor**	**OD @ 595nm**	**Protein Concentration (ug/uL)**	**mg of IgG**
Elution 1	400	1:10	0.190	6.333	2.533
Elution 2	400	1:1	0.290	1.933	0.773
Elution 3	400	-	0.113	3.767	1.507
E1/E2 Combined	800	1:1	0.497	3.313	2.651
Pierce Glycoprotein Isolation Kit, ConA					
Flow-Through 1	500	1:1	0.391	2.607	1.303
Flow-Through 2	400	-	0.337	1.123	0.449
Flow-Through 3	400	-	0.153	0.510	0.204
Flow-Through 4	400	-	0.104	0.347	0.139
Flow-Through 5	400	-	0.072	0.240	0.096
Elution 1	200	-	0.086	0.287	0.057
Elution 2	200	-	0.07	0.233	0.047
Elution 3	200	-	0.056	0.187	0.037

Table S1: IgG was purified from 500 uL of serum using a Protein G HP SpinTrap Column according to manufacturer's protocol. The protein concentration of each elution fraction was determined using a spectronic spectrophotometer. The first and second elution fractions from the Protein G column were combined and served as the starting sample for the ConA Column (Pierce Glycoprotein Isolation Kit, ConA). The sample was diluted 4:1 with 5X Binding/Wash Buffer provided in the kit. The protein concentration of each flow-through fraction (corresponding to the non-glycosylated IgG) and elution fraction (corresponding to the glycosylated IgG) was determined as mentioned above.

Figure S1. Purification of IgG, glycosylated IgG and non-glycosylated IgG from human serum obtained from a healthy non-pregnant individual

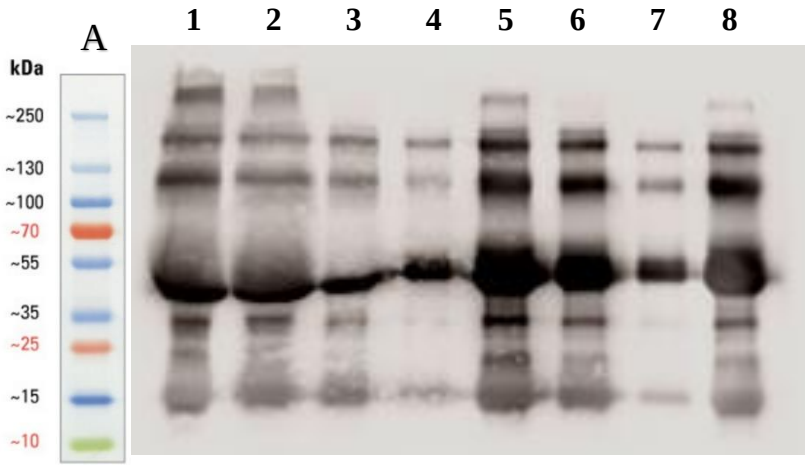

1. **Human Serum**
2. **PG Flow-Through 1**
3. **PG Flow-Through 2**
4. **PG Flow-Through 3**
5. **PG Elution Fraction 1**
6. **PG Elution Fraction 2**
7. **PG Elution Fraction 3**
8. **PG Elution Fraction 1 and 2 Combined**

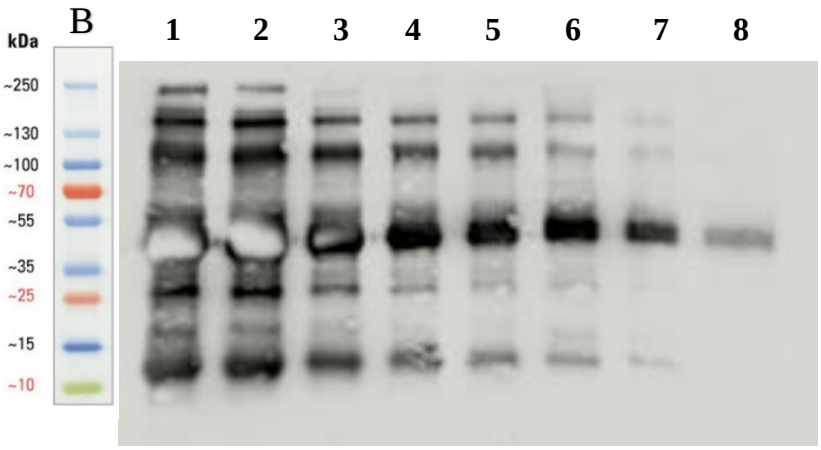

1. **PG Elution Fraction 1 and 2 Combined**
2. **ConA Flow-Through 1**
3. **ConA Flow-Through 2**
4. **ConA Flow-Through 3**
5. **ConA Flow-Through 4**
6. **ConA Elution Fraction 1**
7. **ConA Elution Fraction 2**
8. **ConA Elution Fraction 3**

Figure S1: IgG was purified from 500 uL serum (A1), and the flow-through and elution fractions from the Protein G (PG, A2-8, B1) and ConA Columns (B2-8) were collected and samples were prepared for a western blot using 6X Laemmli buffer. Goat anti-human IgG (H+L) HRP conjugate was used as the primary antibody (1:5000).

Table S2. Spectrophotometer readings from purification of IgG, glycosylated IgG and non-glycosylated IgG from a healthy non-pregnant individual

Protein G HP SpinTrap Column					
Fraction	**Fraction Volume (uL)**	**Dilution Factor**	**OD @ 595nm**	**Protein Concentration (ug/uL)**	**mg of IgG**
Elution 1	400	N/A	N/A	N/A	N/A
Elution 2	400	N/A	N/A	N/A	N/A
Elution 3	400	-	0.106	0.353	0.141
E1/E2 Combined	800	N/A	N/A	N/A	N/A
Pierce Glycoprotein Isolation Kit, ConA					
Flow-Through 1	673	-	0.237	0.790	0.532
Flow-Through 2	400	-	0.044	0.147	0.059
Flow-Through 3	400	-	0.011	0.037	0.015
Flow-Through 4	400	-	0.009	0.030	0.012
Flow-Through 5	400	-	0.005	0.017	0.007
Elution 1	200	-	0.045	0.075	0.015
Elution 2	200	-	0.023	0.038	0.008
Elution 3	200	-	-0.004	0.000	0.000

Table S2: IgG was purified from 100 uL of serum using a Protein G HP SpinTrap Column according to manufacturer's protocol. The protein concentration of each elution fraction was determined using a spectronic spectrophotometer. The first and second elution fractions from the Protein G column were combined and served as the starting sample for the ConA Column (Pierce Glycoprotein Isolation Kit, ConA). The sample was diluted 4:1 with 5X Binding/Wash Buffer provided in the kit. The protein concentration of each flow-through fraction (corresponding to the non-glycosylated IgG) and elution fraction (corresponding to the glycosylated IgG) was determined as mentioned above.

N/A = Not Available

Figure S2. Purification of IgG, glycosylated IgG and non-glycosylated IgG from human serum obtained from a healthy non-pregnant individual

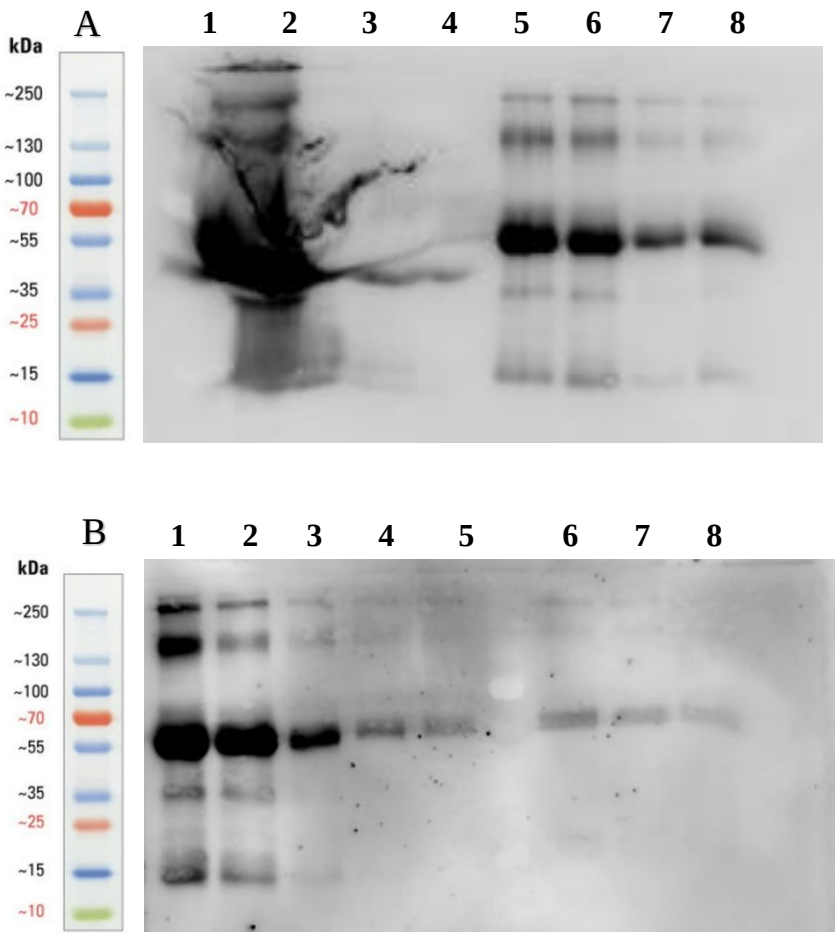

Figure S2: IgG was purified from 100 uL serum (A1), and the flow-through and elution fractions from the Protein G (PG, A2-8, B1) and ConA Columns (B2-8) were collected and samples were prepared for a western blot using 6X Laemmli buffer. Goat anti-human IgG (H+L) HRP conjugate was used as the primary antibody (1:5000).

Figure S3. Purification of IgG, glycosylated IgG and non-glycosylated IgG from human serum obtained from a healthy non-pregnant individual

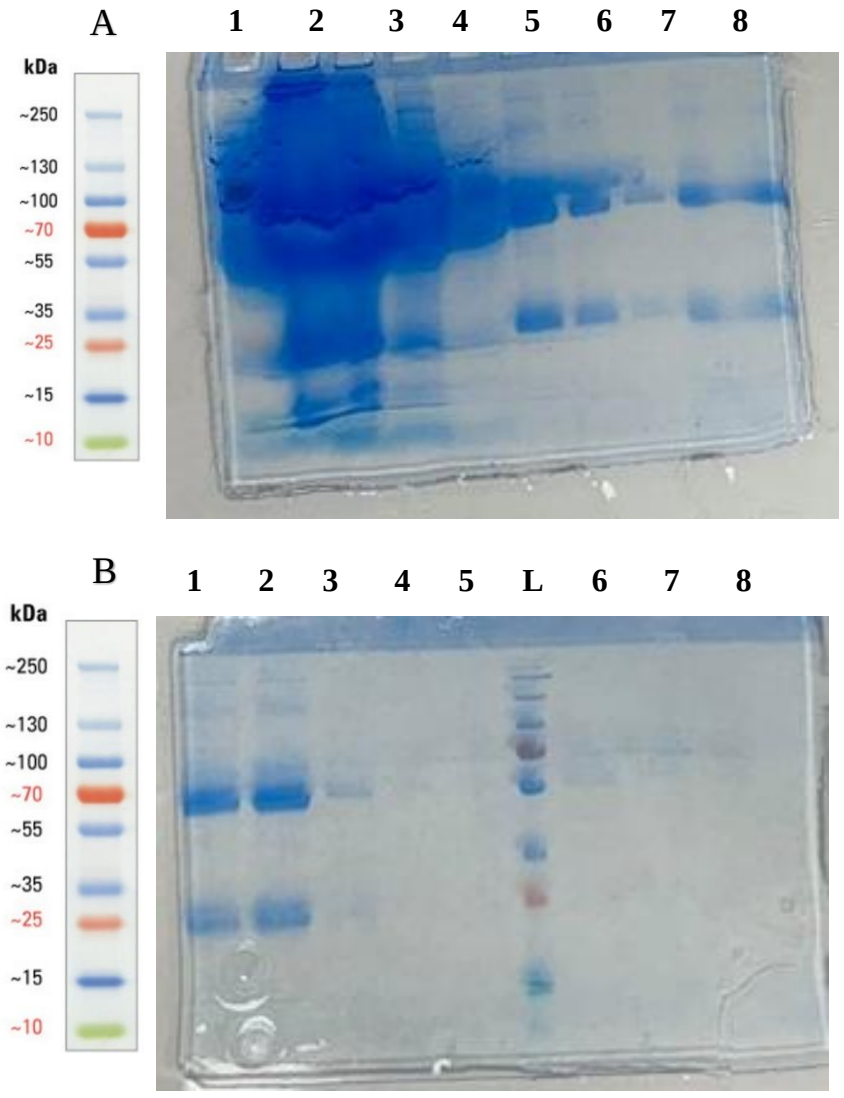

Figure S3: IgG was purified from 100 uL serum (A1), and the flow-through and elution fractions from the Protein G (PG, A2-8, B1) and ConA Columns (B2-8) were collected and samples were run on an SDS-PAGE Gel to be stained using SimplyBlue SafeStain.

Table S3. Spectrophotometer readings from purification of IgG, glycosylated IgG and non-glycosylated IgG from a healthy non-pregnant individual

Protein G HP SpinTrap Column					
Fraction	**Fraction Volume (uL)**	**Dilution Factor**	**OD @ 595nm**	**Protein Concentration (ug/uL)**	**mg of IgG**
Elution 1	400	1:10	0.111	3.700	1.480
Elution 2	400	1:1	0.155	1.033	0.413
Elution 3	400	-	0.101	0.337	0.135
Diluted Serum	337.5	-	0.684*	2.280	0.770
Pierce Glycoprotein Isolation Kit, ConA					
Flow-Through 1	337.5	1:1	0.351	2.340	0.790
Flow-Through 2	400	-	0.089	0.297	0.119
Flow-Through 3	400	-	0.042	0.140	0.056
Flow-Through 4	400	-	0.061	0.203	0.081
Flow-Through 5	400	-	0.030	0.100	0.040
Elution 1	200	-	0.062	0.207	0.041
Elution 2	200	-	0.031	0.103	0.021
Elution 3	200	-	0.017	0.057	0.011

Table S3: IgG was purified from 250 uL of serum using a Protein G HP SpinTrap Column according to manufacturer's protocol. The protein concentration of each elution fraction was determined using a spectronic spectrophotometer. The first elution fraction from the Protein G column served as the starting sample for the ConA Column (Pierce Glycoprotein Isolation Kit, ConA). The sample was diluted 4:1 with 5X Binding/Wash Buffer provided in the kit. The protein concentration of each flow-through fraction (corresponding to the non-glycosylated IgG) and elution fraction (corresponding to the glycosylated IgG) was determined as mentioned above.

*OD readings above 0.6 are considered unreliable. However, we were not able to repeat this measurement because additional sample volume was not available.

Figure S4. Purification of IgG, glycosylated IgG and non-glycosylated IgG from human serum obtained from a healthy non-pregnant individual

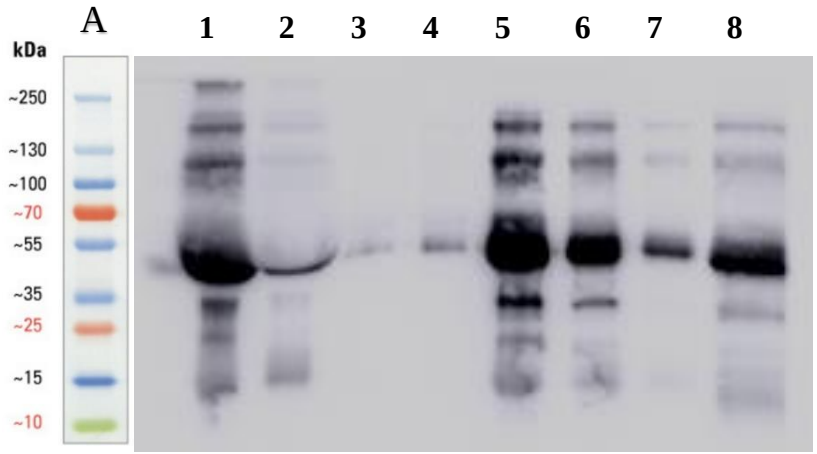

1. **Human Serum**
2. **PG Flow-Through 1**
3. **PG Flow-Through 2**
4. **PG Flow-Through 3**
5. **PG Elution Fraction 1**
6. **PG Elution Fraction 2**
7. **PG Elution Fraction 3**
8. **PG Diluted E1**

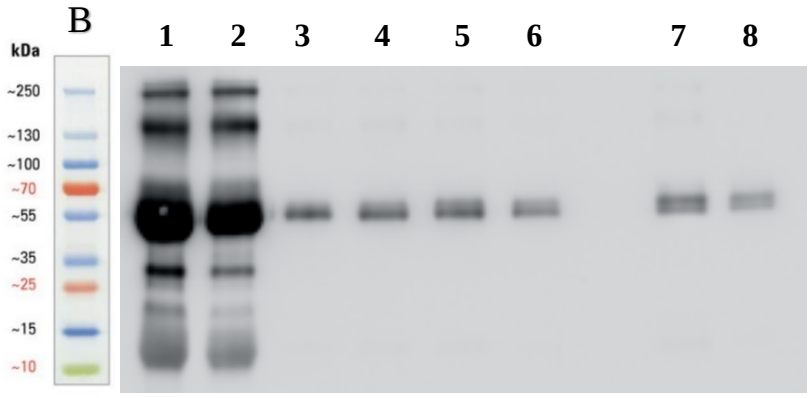

1. **PG Elution Fraction 1**
2. **ConA Flow-Through 1**
3. **ConA Flow-Through 2**
4. **ConA Flow-Through 3**
5. **ConA Flow-Through 4**
6. **ConA Flow-Through 5**
7. **ConA Elution Fraction 1**
8. **ConA Elution Fraction 2**

Figure S4: IgG was purified from 250 uL serum (A1), and the flow-through and elution fractions from the Protein G (PG, A2-8, B1) and ConA Columns (B2-8) were collected and samples were prepared for a western blot using 6X Laemmli buffer. Goat anti-human IgG (H+L) HRP conjugate was used as the primary antibody (1:5000).

Figure S5. Purification of IgG, glycosylated IgG and non-glycosylated IgG from human serum obtained from a healthy non-pregnant individual

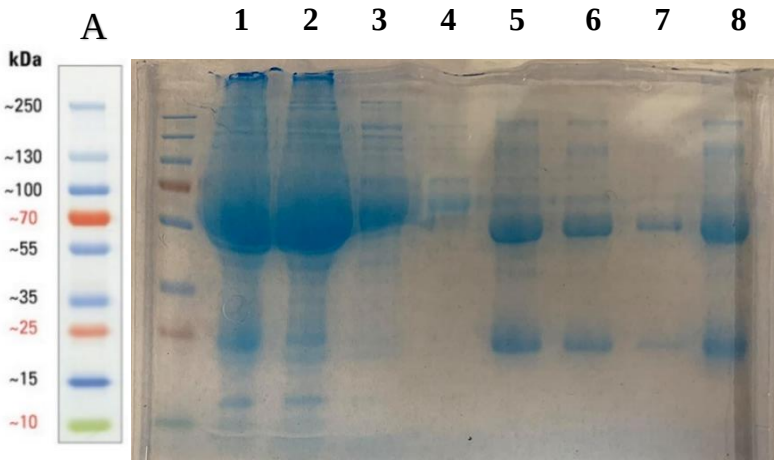

1. **Human Serum**
2. **PG Flow-Through 1**
3. **PG Flow-Through 2**
4. **PG Flow-Through 3**
5. **PG Elution Fraction 1**
6. **PG Elution Fraction 2**
7. **PG Elution Fraction 3**
8. **PG Diluted E1**

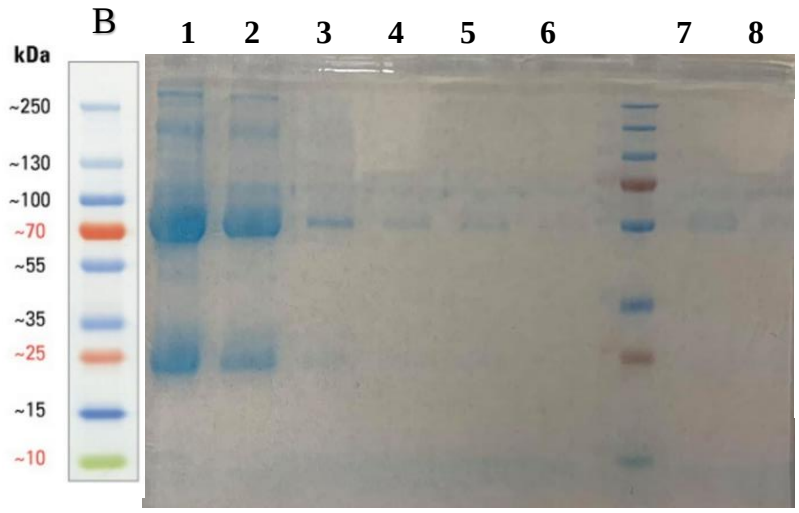

1. **PG Elution Fraction 1**
2. **ConA Flow-Through 1**
3. **ConA Flow-Through 2**
4. **ConA Flow-Through 3**
5. **ConA Flow-Through 4**
6. **ConA Flow-Through 5**
7. **ConA Elution Fraction 1**
8. **ConA Elution Fraction 2**

Table S4. Spectrophotometer readings from purification of IgG, glycosylated IgG and non-glycosylated IgG from a healthy non-pregnant individual using longer ConA elution fraction incubation times

Protein G HP SpinTrap Column					
Fraction	**Fraction Volume (uL)**	**Dilution Factor**	**OD @ 595nm**	**Protein Concentration (ug/uL)**	**mg of IgG**
Elution 1	385	1:10	0.091	3.033	1.168
Elution 2	395	1:1	0.196	1.307	0.516
Pierce Glycoprotein Isolation Kit, ConA					
Flow-Through 1	290	1:1	0.285	1.900	0.551
Flow-Through 2	345	-	0.158	0.527	0.182
Flow-Through 3	425	-	0.078	0.260	0.111
Flow-Through 4	350	-	0.058	0.193	0.068
Flow-Through 5	380	-	0.049	0.163	0.062
Elution 1	180	-	0.116	0.387	0.070
Elution 2	190	-	0.074	0.247	0.047
Elution 3	185	-	0.047	0.157	0.029

Table S4: IgG was purified from 300 uL of serum using a Protein G HP SpinTrap Column according to manufacturer's protocol. The protein concentration of each elution fraction was determined using a spectronic spectrophotometer. The first fraction from the Protein G column served as the starting sample for the ConA Column (Pierce Glycoprotein Isolation Kit, ConA). The sample was diluted 4:1 with 5X Binding/Wash Buffer provided in the kit. The protein concentration of each flow-through fraction (corresponding to the non-glycosylated IgG) and elution fraction (corresponding to the glycosylated IgG) was determined as mentioned above.

Figure S6. Purification of IgG, glycosylated IgG and non-glycosylated IgG from human serum obtained from a healthy non-pregnant individual using longer ConA elution fraction incubation times

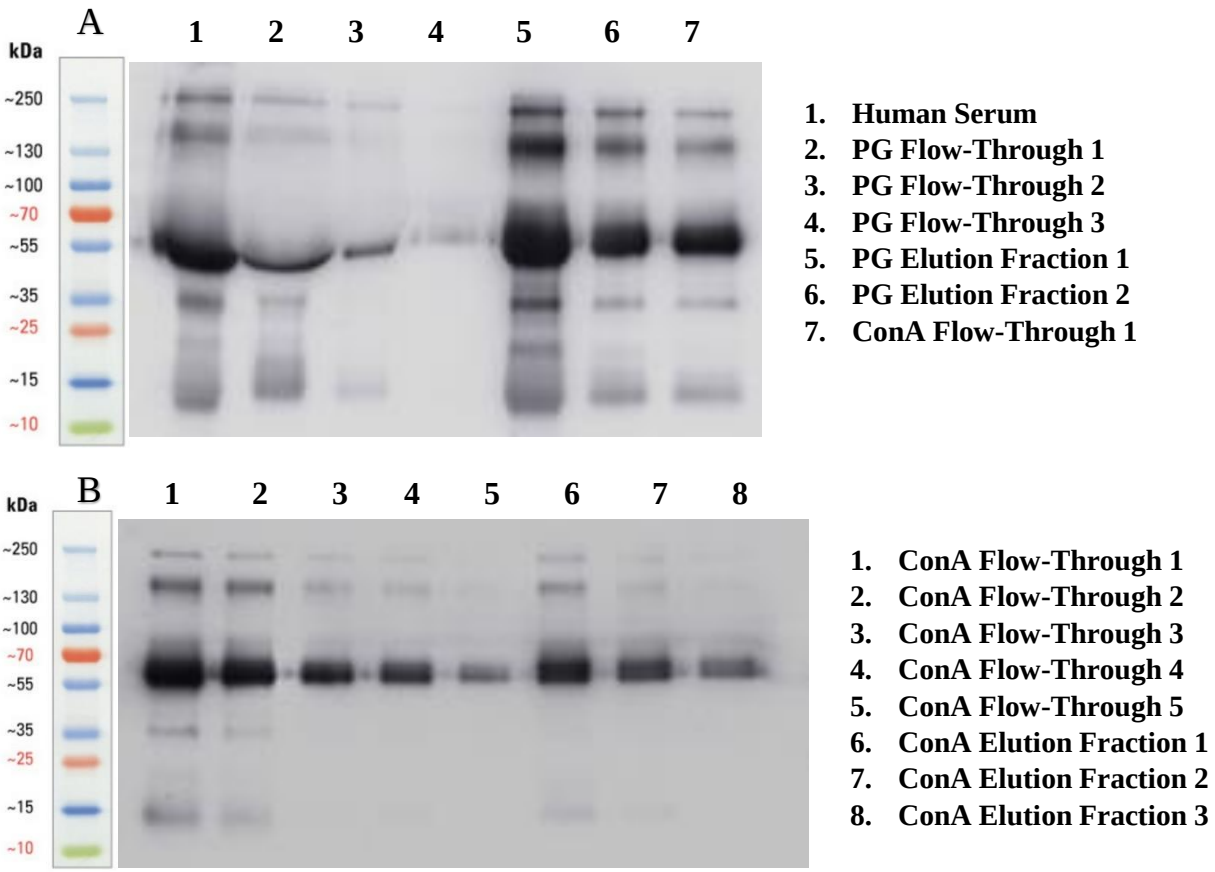

Figure S6: IgG was purified from 300 uL serum (A1), and the flow-through and elution fractions from the Protein G (PG, A2-6) and ConA Columns (A7, B1-8) were collected and samples were prepared for a western blot using 6X Laemmli buffer. Goat anti-human IgG (H+L) HRP conjugate was used as the primary antibody (1:5000).

Figure S7. Purification of IgG, glycosylated IgG and non-glycosylated IgG from human serum obtained from a healthy non-pregnant individual using longer ConA elution fraction incubation times

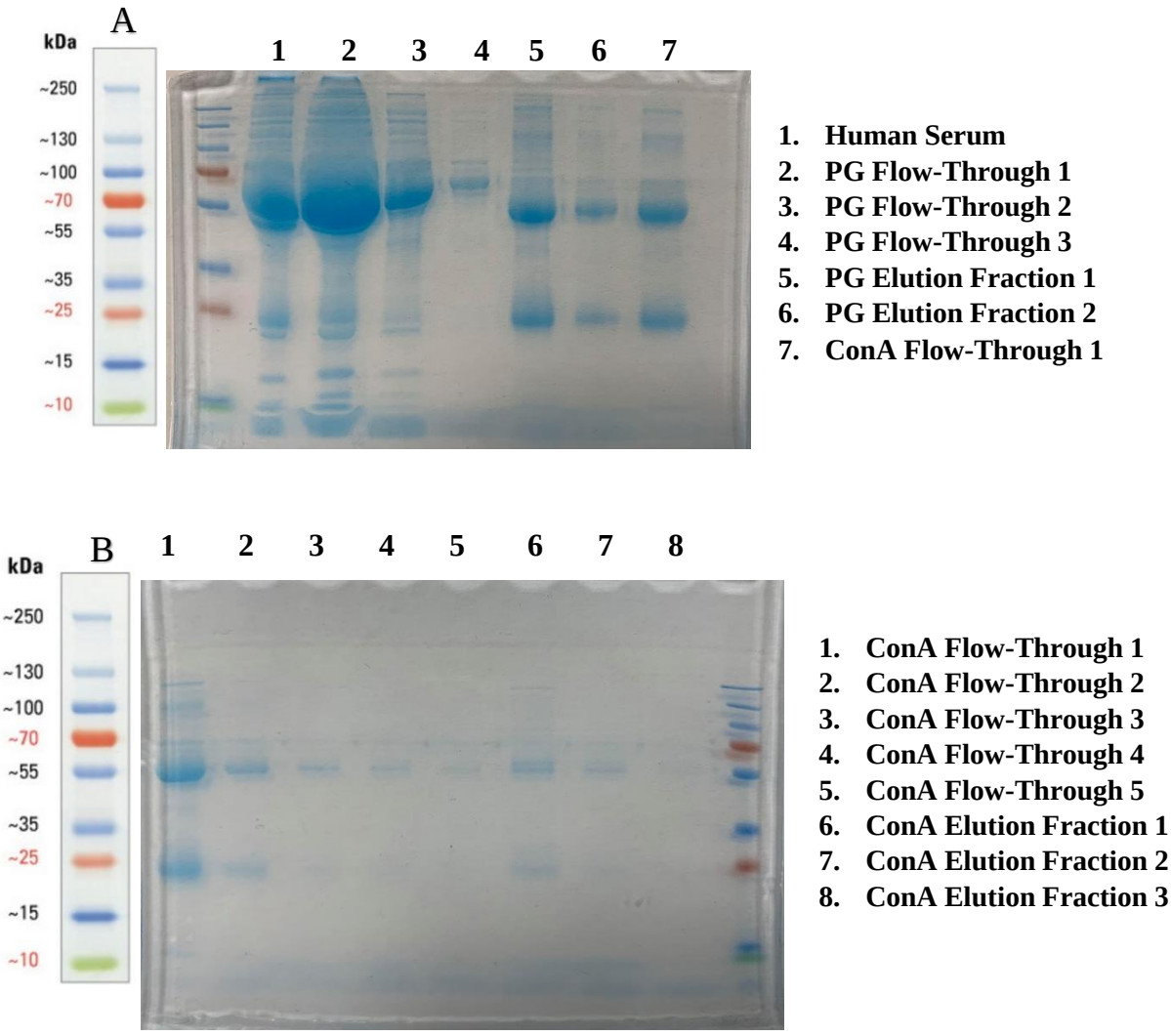

Figure S7: IgG was purified from 300 uL serum (A1), and the flow-through and elution fractions from the Protein G (PG, A2-6) and ConA Columns (A7, B1-8) were collected and samples were run on an SDS-PAGE Gel to be stained using SimplyBlue SafeStain.

REFERENCES

1. van de Bovenkamp, F.S., et al., *The Emerging Importance of IgG Fab Glycosylation in Immunity.* J Immunol, 2016. **196**(4): p. 1435-41.

2. Zenclussen, A.C., et al., *Asymmetric antibodies and pregnancy.* Am J Reprod Immunol, 2001. **45**(5): p. 289-94.

3. Prados, M.B., et al., *Progesterone induces a switch in oligosaccharyltransferase isoform expression: consequences on IgG N-glycosylation.* Immunol Lett, 2011. **137**(1-2): p. 28-37.

4. Kelemen, K., et al., *A progesterone-induced protein increases the synthesis of asymmetric antibodies.* Cell Immunol, 1996. **167**(1): p. 129-34.

5. Barrientos, G., et al., *Low levels of serum asymmetric antibodies as a marker of threatened pregnancy.* J Reprod Immunol, 2009. **79**(2): p. 201-10.

6. Faust, Z., et al., *Progesterone-induced blocking factor inhibits degranulation of natural killer cells.* Am J Reprod Immunol, 1999. **42**(2): p. 71-5.

7. Polgar, B., et al., *Molecular cloning and immunologic characterization of a novel cDNA coding for progesterone-induced blocking factor.* J Immunol, 2003. **171**(11): p. 5956-63.

8. Szekeres-Bartho, J. and T.G. Wegmann, *A progesterone-dependent immunomodulatory protein alters the Th1/Th2 balance.* J Reprod Immunol, 1996. **31**(1-2): p. 81-95.

9. Polgar, B., et al., *Urinary progesterone-induced blocking factor concentration is related to pregnancy outcome.* Biol Reprod, 2004. **71**(5): p. 1699-705.

10. Szekeres-Bartho, J., Z. Faust, and P. Varga, *The expression of a progesterone-induced immunomodulatory protein in pregnancy lymphocytes.* Am J Reprod Immunol, 1995. **34**(6): p. 342-8.

11. Barrett, J.H., et al., *Does rheumatoid arthritis remit during pregnancy and relapse postpartum? Results from a nationwide study in the United Kingdom performed prospectively from late pregnancy.* Arthritis Rheum, 1999. **42**(6): p. 1219-27.

12. Formby, B., *Immunologic response in pregnancy. Its role in endocrine disorders of pregnancy and influence on the course of maternal autoimmune diseases.* Endocrinol Metab Clin North Am, 1995. **24**(1): p. 187-205.

13. de Man, Y.A., et al., *Disease activity of rheumatoid arthritis during pregnancy: results from a nationwide prospective study.* Arthritis Rheum, 2008. **59**(9): p. 1241-8.

14. Laboratories, M.C. *Immunoglobulins (IgG, IgA and IgM), Serum*. 2020 March 16, 2020]; Available from: https://www.mayocliniclabs.com/test-catalog/Clinical+and+Interpretive/8156.

15. Gronwall, C., J. Vas, and G.J. Silverman, *Protective Roles of Natural IgM Antibodies.* Front Immunol, 2012. **3**: p. 66.

16. LabCorp. *Blood Specimens: Chemistry and Hematology*. 2020 March 16, 2020]; Available from: https://www.labcorp.com/resource/blood-specimens-chemistry-and-hematology.

17. Huang, T., et al., *Fractionation of Fab glycosylated immunoglobulin G with concanavalin A chromatography unveils new structural properties of the molecule.* Oncotarget, 2016. **7**(21): p. 31166-76.

18. Simister, N.E., *Placental transport of immunoglobulin G.* Vaccine, 2003. **21**(24): p. 3365-9.

19. Szekeres-Bartho, J., *The Role of Progesterone in Feto-Maternal Immunological Cross Talk.* Med Princ Pract, 2018. **27**(4): p. 301-307.

ATTRIBUTES

Figure 1. Protein G and ConA column chromatography and sample preparation performed by Rahil Kheirkhah. Western blot completed by Rahil Kheirkhah.

Figure 2. Protein G and ConA column chromatography and sample preparation performed by Rahil Kheirkhah. Coomassie Simply Blue SafeStain completed by Rahil Kheirkhah.

Figure 3. Protein G and ConA column chromatography and sample preparation performed by Rahil Kheirkhah. Western blot completed by Rahil Kheirkhah.

Figure 4. Protein G and ConA column chromatography and sample preparation performed by Rahil Kheirkhah. Coomassie Simply Blue SafeStain completed by Rahil Kheirkhah.

Figure 5. Protein G and ConA column chromatography and sample preparation performed by Rahil Kheirkhah. Western blot completed by Rahil Kheirkhah.

Figure 6. Protein G and ConA column chromatography and sample preparation performed by Rahil Kheirkhah. Coomassie Simply Blue SafeStain completed by Rahil Kheirkhah.

Figure 7. Human protein microarrays were processed by Rahil Kheirkhah and Cassandra DeMarshall, Ph.D. Data extraction and analysis was performed by Rahil Kheirkhah.

Figure 8. Human protein microarrays were processed by Rahil Kheirkhah and Cassandra DeMarshall, Ph.D. Data extraction and analysis was performed by Rahil Kheirkhah.

Figure 9. Human protein microarrays were processed by Rahil Kheirkhah and Cassandra DeMarshall, Ph.D. Data extraction and analysis was performed by Rahil Kheirkhah.

Figure 10. Human protein microarrays were processed by Rahil Kheirkhah and Cassandra DeMarshall, Ph.D. Data extraction and analysis was performed by Rahil Kheirkhah.

Figure S1. Protein G and ConA column chromatography and sample preparation performed by Rahil Kheirkhah. Western blot completed by Rahil Kheirkhah.

Figure S2. Protein G and ConA column chromatography and sample preparation performed by Rahil Kheirkhah. Western blot completed by Rahil Kheirkhah.

Figure S3. Protein G and ConA column chromatography and sample preparation performed by Rahil Kheirkhah. Coomassie Simply Blue SafeStain completed by Rahil Kheirkhah.

Figure S4. Protein G and ConA column chromatography and sample preparation performed by Rahil Kheirkhah. Western blot completed by Rahil Kheirkhah.

Figure S5. Protein G and ConA column chromatography and sample preparation performed by Rahil Kheirkhah. Coomassie Simply Blue SafeStain completed by Rahil Kheirkhah.

Figure S6. Protein G and ConA column chromatography and sample preparation performed by Rahil Kheirkhah. Western blot completed by Rahil Kheirkhah.

Figure S7. Protein G and ConA column chromatography and sample preparation performed by Rahil Kheirkhah. Coomassie Simply Blue SafeStain completed by Rahil Kheirkhah.

CHAPTER VI

PERSPECTIVES

SUMMARY AND FUTURE DIRECTIONS

The presence of self-recognizing antibodies had been associated with a failure in antibody production by the immune system, and more often than not, linked to pathology. However, more recent development in research has created space for the presence of these autoantibodies to have their own role, albeit, not a very well understood one. Extensive previous work from our lab has shown that the presence of thousands of autoantibodies (aABs) in the human sera is typical. We hypothesize that every day "wear and tear" generates cell and tissue debris, and one potential function of aABs is maintaining body-wide homeostasis by clearance of the debris from body fluids, such as blood. In this study, we aimed to further expand on some of the fundamental concepts regarding aABs.

First, using human protein microarrays and plasma and cerebrospinal fluid samples obtained pre-surgically and simultaneously from 46 hip fracture repair patients, we demonstrated that CSF exhibits an extraordinarily complex IgG autoantibody profile composed of thousands of autoantibodies. We show that the pattern of expression levels of individual autoantibodies in CSF closely mimics that in

the blood, regardless of age, gender or the presence or absence of disease. There is also an exceptionally high percentage of overlap in the identity of the aABs expressed in the CSF and serum, further adding strength that these findings are indicative of a blood-based origin for CSF autoantibodies. We also demonstrated that an elevated CSF/plasma autoantibody ratio is more common in elderly hip fracture repair patients that experienced post-operative delirium than in non-delirium subjects, thus highlighting the crucial role that blood-brain and/or blood-CSF barrier compromise may play in the development of post-operative delirium.

Using five longitudinal serum samples obtained from one healthy individual over a span of nine years, we found that blood autoantibody profiles are remarkably stable over a long period of time, and that autoantibody profiles in both blood and CSF show features that are common among different individuals as well as individual-specific. With this, we introduced the concept of baseline aAB profiles. We hypothesized that in the absence of pathology, aAB profiles of healthy individuals remains stable. This stable profile is referred to as the "baseline aAB profile" and is composed of two conceptual subsets of aABs: a larger subset with levels that are comparable among multiple individuals and a much smaller subset with levels significantly higher or lower than the norm, thus making these aAB "stand out" as peculiar to this individual (i.e., contributing to an individual "autoantibody fingerprint"). Taken together, this suggests the presence of an "aAB setpoint" for each individual that is linked to the current status of the body. Deviation from this baseline or set point could be triggered by a number of events and body stressors, such as

surgery, infections, menstruation, pregnancy, sudden weight loss and other short- and long-term pathologies. In fact, previous work has used disease-specific deviations from the baseline to identify biomarkers for early disease detection.

Next, we explored the effects of pregnancy of baseline aAB profiles, as an example non-disease body-associated stressors. The question remaining to be answered was two-fold: does a physiological stressor affect the baseline aAB profile, and if so, does the aAB profile recover once this physiological stressor is removed. We saw that in the presence of pregnancy, there is an initial global reduction in the titers of the aABs, however, the shape of the aAB profile still mimics that of the baseline profile. By 7 months post-pregnancy (post-removal of the stressor), the relative titers of aABs appear to be restored to original levels. This return to original pre-pregnant (pre-stressor) levels further supports the hypothesis and aAB profiles have a "set-point" which they try to adhere to. Therefore, we show that in response to a stressor, aAB profiles undergo changes, however, following removal of the stressor, aAB profiles can return to their baseline levels. Even though this stands true for most of the aABs composing the profile, there is a small subset of aABs that maintain an imprint of the stress-induced profile, even after the stressor is removed.

Lastly, we looked into the prevalence of distribution of glycosylation in aABs using longitudinal serum samples taken from a pregnant patient. First, we were able to confirm that aABs are in fact Fab glycosylated, retain antigen binding capacity and are able to bind to the protein targets on human protein microarrays, and that almost all

aABs are glycosylated. Looking at longitudinal overall glycosylation, we did not see an overall increase in the total percent of antibodies that were glycosylated, however, we did observe a shift in the extent of glycosylation in individual aABs throughout pregnancy. Most of the aABs were only 10-19% glycosylated at 7 months post-pregnancy. During pregnancy, we saw a broader distribution of individual aAB glycosylation, with most of them being 10-39% glycosylated in early pregnancy and 30-69% glycosylated in late pregnancy. We speculate that the increase in aAB glycosylation in due to its immune-regulatory role in order to prevent detrimental effects in fetal development, however much extra work is needed to look into specific aAB targets that shifted their glycosylation throughout pregnancy and fully understand why.

The initial work we have done in this thesis, looking at glycosylation patterns of aABs, serves to only open the door to a slew of new projects that can be done. First, we would like to continue the current work using the other three pregnant samples that are available to us. By mapping the pre-pregnant aAB glycosylated profile, we will be able to look more specifically how pregnancy affects the changes in glycosylation patterns that we see. Furthermore, we need to include the data for the 16 weeks gestation and 28 weeks gestation samples for a more comprehensive picture of how pregnancy changes the distribution of glycosylated aABs.

Furthermore, we have longitudinal samples taken from a psychosis patient who experiences relief of her symptoms during pregnancy. By using the protocol

established in this thesis we'll be able to establish her glycosylated aAB profile throughout her pregnancy, and by comparing her profile to our healthy pregnant patient, we'll potentially be able to elucidate changes that can be implicated in psychosis pathology.